SERI/STR-231-3136
UC Category: 61
DE87001192

Fuel Grade Ethanol by Solvent Extraction

Final Subcontract Report

D. W. Tedder
Georgia Institute of Technology
Atlanta, GA

April 1987

SERI Technical Monitor:
J. D. Wright

Prepared under Subcontract No. XX-4-04076-01

Solar Energy Research Institute
A Division of Midwest Research Institute

1617 Cole Boulevard
Golden, Colorado 80401-3393

Prepared for the
U.S. Department of Energy
Contract No. DE-AC02-83CH10093

Printed in the United States of America
Available from:
National Technical Information Service
U.S. Department of Commerce
5285 Port Royal Road
Springfield, VA 22161

Price: Microfiche A01
Printed Copy A08

Codes are used for pricing all publications. The code is determined by the number of pages in the publication. Information pertaining to the pricing codes can be found in the current issue of the following publications, which are generally available in most libraries: *Energy Research Abstracts, (ERA): Government Reports Announcements* and Index (*GRA* and I); *Scientific and Technical Abstract Reports (STAR):* and publication. NTIS-PR-360 available from NTIS at the above address.

TABLE OF CONTENTS

LIST OF TABLES

LIST OF FIGURES

CHAPTER 1

EXECUTIVE SUMMARY
(D. W. Tedder)

This report summarizes final results for ethanol recovery by solvent extraction and extractive distillation. Earlier reports and theses describing various aspects of this work include:

D. W. Tedder (ed), Fuel-Grade Ethanol Recovery by Solvent Extraction: Final Report, Georgia Institute of Technology, Atlanta, GA (August 1984).

D. W. Tedder (ed), Fuel-Grade Ethanol Recovery by Solvent Extraction: Technical Progress Report for Period September 15, 1981 through September 15, 1982, Georgia Institute of Technology, Atlanta, GA (September 1982).

D. W. Tedder (ed), Fuel-Grade Ethanol Recovery by Solvent Extraction: Technical Progress Report for Period September 15, 1980 through September 15, 1981, Georgia Institute of Technology, Atlanta, GA (September 1981).

M. Anselme. Immobilized Yeast Extractor for Ethanol Production, M.S. Thesis, School of Chemical Engineering, Georgia Institute of Technology, Atlanta, GA (June 1985).

W. Y. Tawfik, Design of Optimal Fuel-Grade Ethanol Recovery System Using Solvent Extraction, Ph.D. Thesis, School of Chemical Engineering, Georgia Institute of Technology, Atlanta, GA (1986).

L. M. Sroka, Membrane Use in Ethanol Recovery Processes, M.S. Thesis, School of Chemical Engineering, Georgia Institute of Technology, Atlanta, GA (August 1984).

N. Griffin, Vapor-Liquid Equilibria of Selected Ethanol Systems, M.S. Thesis, School of Chemical Engineering, Georgia Institute of Technology, Atlanta, GA (December 1983).

K. B. Garg, Design of Liquid-Liquid Extractants for the Recovery of Fuel-Grade Ethanol, M.S. Thesis, School of Chemical Engineering, Georgia Institute of Technology, Atlanta, GA (March 1982).

W. Y. Tawfik, Efficiency of Ethanol Extraction from Aqueous Mixtures, M.S. Thesis, School of Chemical Engineering, Georgia Institute of Technology, Atlanta, GA (1982).

D. R. Sommerville, Diffusion of Ethanol in Organic Solvents, M.S. Thesis, School of Chemical Engineering, Georgia Institute of Technology, Atlanta, GA (April 1985).

L. H. Krosnowski, The Measurement of the Diffusion Coefficients of Ethanol in Organic Solvents, M.S. Thesis, School of Chemical Engineering, Georgia Institute of Technology, Atlanta, GA (June 1983).

A. J. Eckles, Modeling of Ethanol Extraction in the Karr Reciprocating Plate Column, M.S. Thesis, School of Chemical Engineering, Georgia Institute of Technology, Atlanta, GA (1984).

The present report discusses the comparative economics of distillation versus ethanol recovery by solvent extraction (Chapter 2).

Chapters 3 and 4 summarize experimental methods and procedures. Equilibrium data is presented in Chapters 6-7 and Appendices A and B. Empirical correlations are also presented in Chapters 6-7. Much of this data was presented in earlier reports, but it is recapitulated here for reader convenience.

Preliminary results on immobilized cell fermentation in upflow reactors are summarized in Chapter 5. Chapter 8 presents the results of pervaporation studies in solvent regeneration. Chapter 9 summarizes the results of mass transfer studies in reciprocating plate columns for liquid/liquid systems of interest. Additional experimental data for the reciprocating plate column are summarized in Appendix C.

Chapter 10 summarizes the economic optimization analyses for the SEED process (Solvent Extraction and Extractive Distillation). It was learned through the optimization that solvent selectivity in the SEED process is less important economically than solvent loading. That is, the optimal solvent composition was 100% tridecyl alcohol. Future studies should, therefore, attempt to identify other high boiling solvents with similar properties, but higher loadings and lower selectivities.

The conclusion of this work can be summarized as follows. Ethanol dehydration and recovery dilute fermentates is feasible using liquid/liquid extraction and extractive distillation. Compared to distillation, the economics are more attractive for more dilute feeds (e.g. less than 5 wt% ethanol initially). However, an economic bias in favor of SEED appears to exist even for 10 wt% feeds.

It is of particular interest to consider the group extraction of ethanol and acetic acid followed by conversion to a mixture of ethanol and ethyl acetate. The latter species is a more valuable commodity and group extraction of inhibitory species is one feature of liquid/liquid extraction that is not easily accomodated using distillation. Upflow immobilized reactors offer the possibility of achieving high substrate conversion while also maintaining low metabolite concentrations. However, many questions remain to be answered with such a concept.

Although the use of the SEED process for the recovery of ethanol enhances the economics of gasahol production using fermentation, the benefits do not appear sufficient to enable market entry at this time. Basically, the feedstock costs dominate the economics. A producer needs feed material without cost. Alternatively, the value of ethanol must rise to about $2.00/gal on the commodities market before significant production via the fermentation route will become attractive.

However, Solvent Extraction and Extractive Distillation (SEED) is technically feasible. The solvent must have a vapor pressure that is significantly less than water or ethanol. Then the extract can be dehydrated in an extractive distillation column (EDC) and the dry product recovered using a subsequent solvent regeneration column (SRC). The process in energy efficient because relatively little water or solvent is distilled, and ethanol is only evaporated once. Sensible heat requirements are minimized through heat exchanger matching.

CHAPTER 2

ECONOMIC ANALYSIS AND DESIGN SUMMARY: THE SEED PROCESS VERSUS DISTILLATION
(D. W. Tedder)
2.1 Design Basis

The research effort focused on the use of solvent extraction and extractive distillation together (the SEED Process) to achieve the design goals. A laboratory system consisting of a 1 inch diameter Karr Reciprocating Plate column and two glass bubble cap columns was constructed and tested. The two bubble cap columns were also tested while using a 16 stage mini mixer-settler rather than the reciprocating plate column for the liquid/liquid cascade.

The reciprocating plate column consisted of 92 stainless steel reciprocating plates with an active contact height of 244 cm. The glass column inner diameter is 2.54 cm, Model KC 1-8 sold by the Chem Pro Corp., New Jersey.

The two bubble cap columns had 7.6 cm diameters. The extractive distillation column included three bubble cap trays above the feed and three below. The solvent regeneration column consisted of four bubble cap trays below the feed and two below. Each tray had one bubble cap with liquid flowing across the tray.

In all cases, total solvent recycle was achieved and steady state was approached. Beer extract was produced and dehydrated by extractive distillation through the selective removal of coextracted water. The dehydrated extract was then passed to a solvent regeneration bubble cap column for ethanol recovery. Regenerated solvent was also recycled continuously to the top of the extractive distillation column.

Liquids were transported between the units using either laboratory scale metering pumps from FMI Inc., Oyster Bay, MA or a low-frequency bellows pump sold by Fischer. The latter pump was used to return cooled solvent from the solvent regeneration column to atmospheric pressure without cavitation. (Commercial units will likely require the use of a barometric leg at that point.)

Initial tests with the solvent 1 + 1 by volume tridecyl alcohol and Isopar-M were completed. Ethanol was extracted from a sucrose beer containing about 5 wt% ethanol. The feasibility of the EDC concept was proven since it was possible to maintain the ethanol concentrations below 1 wt% in the EDC distillate.

Subsequent tests used ethanol/water mixtures containing from 3 to 9 wt% ethanol and either the reciprocating plate column or the mini mixer-settler bank. The solvent consisted either of pure

tridecyl alcohol or tridecyl alcohol/Isopar-M mixtures. Product recovered from the EDC distillate typically contained 1 to 20 wt% ethanol. Product recovered from the SRC column ranged from 85 to 98 wt% ethanol.

In order to achieve the desired results, the feed temperatures for both the EDC and SRC columns must be carefully controlled. Solvent foaming problems can be controlled by starting up the EDC and SCR columns with total solvent recycle without sending extract to the EDC. It helps to have the solvent at the correct temperature on each stage in the EDC column before extract is introduced.

2.2 Computer Simulation

Detailed equilibrium stage calculations based upon experimental equilibrium data, UNIQUAC and UNIFAC models, and the SimSci PROCESS flowsheet model, indicate that the basic concept is correct. Moreover, the model predicts that a 99 mole % recovery of ethanol can be achieved from beers as dilute as 0.5 wt% ethanol. Conditions in the EDC and SRC columns must be adjusted, however, with the beer quality to achieve a 99 mole % ethanol product. Solvent carryover, a problem in the lab, is controllable using a partial condenser in the SRC column.

2.3 Economic Comparisons

Cost analysis was completed in which three beers (5.15%, 1.9%, and 0.57 wt%) were treated using the SEED process. Figure 2.1 shows the conceptual SEED flowsheet. Comparisons were then made with the Berkeley optimized distillation (1) concept using their net energy balances, cooling water, and theoretical tray estimates. Azeotropic distillation costs were modelled using the data provided by Black(2). All cases assumed a 99% ethanol recovery and purity(mole basis).

Using the LBL concept, heat is introduced into the beer stripper and passed to the beer concentrator by matching the stripper condenser with the concentrator reboiler. Hence, the concentrator operates at reduced pressures. By heat exchanger matching, the energy requirements for the azeotropic distillation are satisfied from the stripper duty.

Two fuel prices were used for natural gas, $4.64 and $6.47/MBTU, based upon a recent study by Breuer (3). Capital investment was estimated using correlations derived from Guthrie (4). Although a premium fuel was assumed, the resulting internal stream prices ($6.39 and $8.51/MBTU) are comparable with estimates by Breuer for coal and only slightly affect the resulting conclusions.

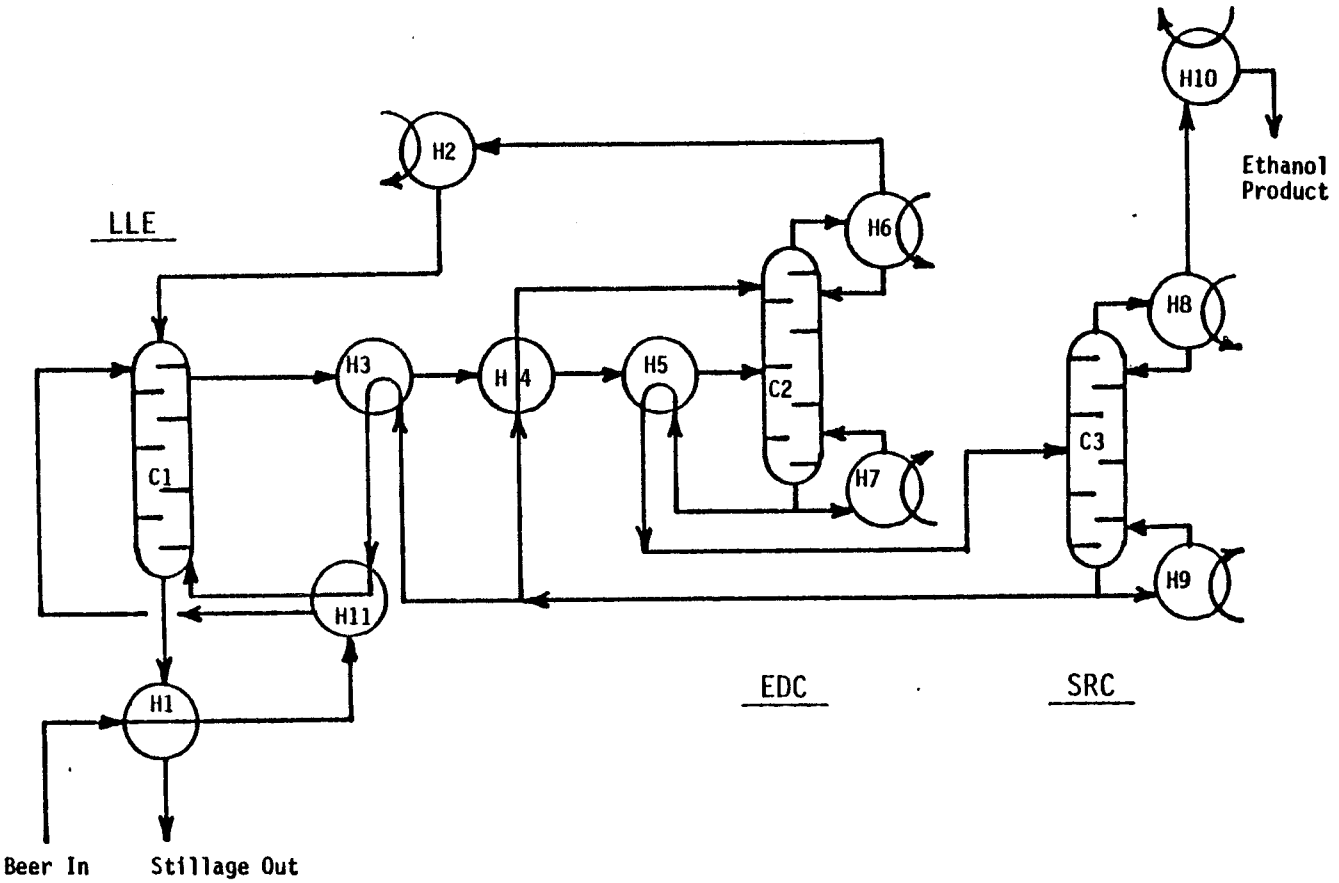

Fig. 2.1 Ethanol Recovery from 0.57 wt% beer using Solvent Extraction/Extractive Distillation with heat exchanger matching. Corresponds to cases 5E and 6E

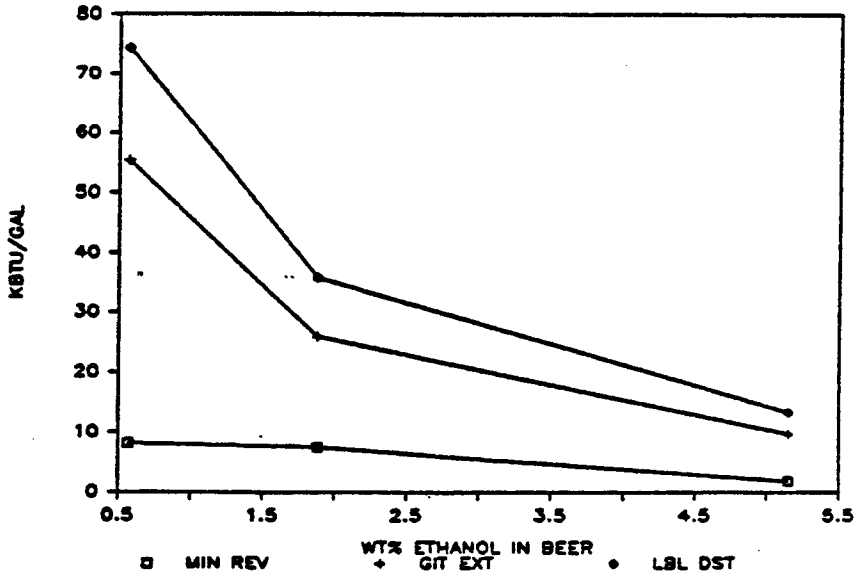

Fig. 2.2 Estimated energy requirements for ethanol recovery by GIT Solvent Extraction and Optimized Distillation from low-grade beers.

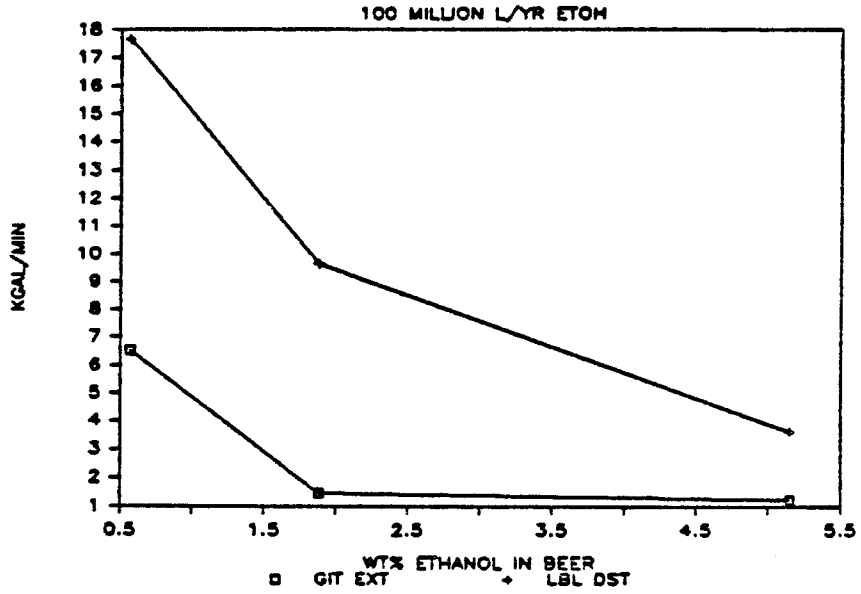

Fig.2.3 Estimated cooling water requirements for ethanol recovery by GIT Solvent Extraction and Optimized Distillation from low-grade beers.

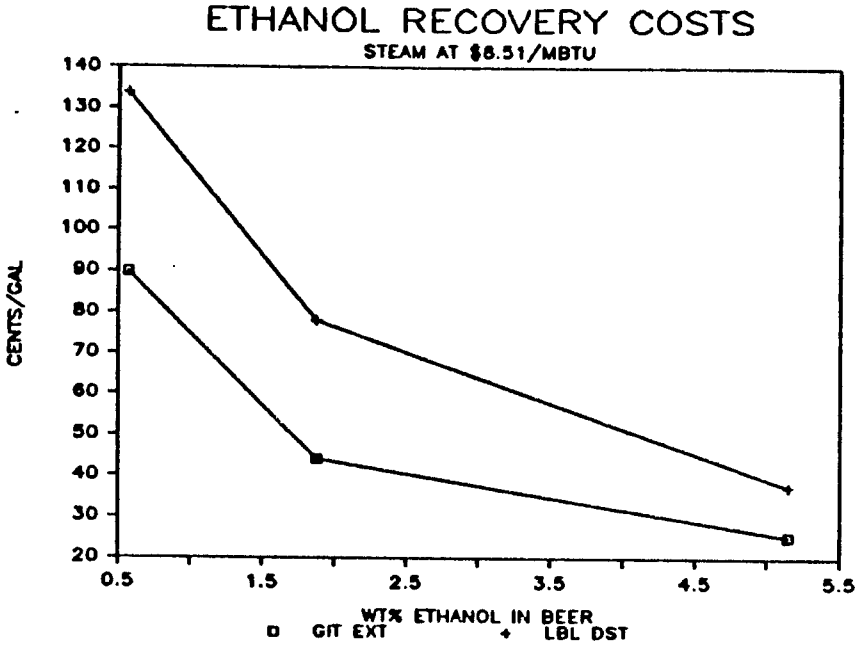

Fig. 2.4 Estimated ethanol recovery costs from low-grade beers using GIT Solvent Extraction and Optimized Distillation.

Table 2.1 Major equipment items and costs for the GIT Solvent Extraction Process.

Ethanol Extraction Cost Estimate Case: 3E
by D. W. Tedder M&S: 781.7 July 1984
04-Nov-84 Note: 99%Recov,99%Pure,from 1.88wt%beer
Basis: 100 million L Ethanol/yr
Hours/yr: 7920 3336 gal/hr operating 330 days/yr
Table Estimated Equipment Costs

Item	Descript	Size Units	Size	Mat Fac	Pres Fac	FOB Cost ($1000)	Module Cost ($1000)
	Battery Limits Equipment						
Columns	(C1)Extract	ft	45	3.67	1	$761.5	$1,446.5
	(C2)Ext Dst	ft	46	1	1	$78.2	$284.9
	(C3)SolStrip	ft	46	1	1	$97.5	$351.4
Ht Ex	(H1)Beer Eco	ft2	981.5	3.67	1	$91.6	$179.2
	(H2)Beer Pre	ft2	1462.	3.67	1	$118.7	$232.2
	(H3)Sol.Eco	ft2	2492.	1	1	$45.7	$150.5
	(H4)Sol.Eco	ft2	3123.	1	1	$53.0	$174.3
	(H5)C2 Con	ft2	53.63	1	1	$3.8	$12.4
	(H6)C2 Reb	ft2	2816.	1	1	$49.5	$163.0
	(H7)C3 Con	ft2	645.8	1	1	$19.0	$62.6
	(H8)C3 Reb	ft2	9862.	1	1	$111.8	$368.1
	(H9)Prod Con	ft2	1367.	1	1	$31.0	$101.9
	(H10)Beer Ec	ft2	5596.	3.67	1	$284.0	$555.5
						$1,745	$4,082
Boiler	250 lb	klb/hr	105.3	1	1	$277.6	$508.0
Cooling Tower		gpm	1455.				$167.4
Elec Dist	Gen. Pur	kw	300				$80.5
Water Dis	Gen. Pur	gpm	1000				$104.5
	Offsite Cost Totals:					$278	$860

Table 2.2 Total Capital Investment for Ethanol Case: 3E

Item	FOB Cost ($1000)	Module Cost ($1000)
Battery Limits Equipment	$1,745	$4,082
Offsite Costs	$278	$860
Totals	$2,023	$4,943
Contingency & Fees 18 %		$890
Total Installed Cost (TIC)		$5,833
Working Capital 15 % TIC		$875
Total Capital Investment (TCI)		$6,707

Table 2.3 Manufacturing Costs for Ethanol EXTRACTION

Basis: 100 million L Ethanol/yr		($1000)	($1000)
Fixed Costs			
TCI Finance Charge	5 Years at 12%	$1,860.7	
Taxes & Insurance	5 % of TIC	$291.6	
Maintenance	5 % of TIC	$291.6	
Subtotal:			$2,444.0
Utilities			
Electricity ($0.06/kw-hr)		$142.6	
Natural Gas ($6.47/million BTU)		$5,975.8	
Water ($2.00/1000 gal)		$10.0	
Subtotal:			$6,128.4
Labor (2 workers/shift at $12/worker-hr)			$630.7
Overhead (50 % of Labor and Maintenance)			$461.2
Annual Manufacturing Cost:			$9,664.2
$/L Ethanol:	$0.097		
$/Gal Ethanol:	$0.366		
Ethanol Selling Price (30% ROI before taxes)			
$/L Ethanol:	$0.117		
$/Gal Ethanol:	$0.442		

Table 2.4 Total Capital Investment for Ethanol Case: 3D

Item	FOB Cost ($1000)	Module Cost ($1000)
Battery Limits Equipment	$4,841	$11,156
Offsite Costs	$338	$1,323
Totals	$5,179	$12,479
Contingency & Fees 18 %		$2,246
Total Installed Cost (TIC)		$14,725
Working Capital 15 % TIC		$2,209
Total Capital Investment (TCI)		$16,934

Table 2.5 Manufacturing Costs for Ethanol Distillation

Basis: 100 million L Ethanol/yr		($1000)	($1000)
Fixed Costs			
TCI Finance Charge	5 Years at 12%	$4,697.7	
Taxes & Insurance	5 % of TIC	$736.3	
Maintenance	5 % of TIC	$736.3	
Subtotal:			$6,170.2
Utilities			
Electricity ($0.06/kw-hr)		$142.6	
Natural Gas($6.47/million BTU)		$7,900.4	
Water ($2.00/1000 gal)		$10.0	
Subtotal:			$8,053.0
Labor (2 workers/shift at $12/worker-hr)			$630.7
Overhead (50 % of Labor and Maintenance)			$483.5
Annual Manufacturing Cost:			$15,537.3
$/L Ethanol:	$0.155		
$/Gal Ethanol:	$0.588		
Ethanol Selling Price (30% ROI before taxes)			
$/L Ethanol:	$0.206		
$/Gal Ethanol:	$0.780		

The SEED process energy requirements (see Fig. 2.2) compare favorably with optimized distillation. For the 5%, 2% and 0.5 wt% beers, the estimates are 9,700, 25,900, and 55,000 BTU/gal respective. This corresponds to energy saving of about 3,600, 10,000 and 19,000 BTU/gal respectively when compared to optimized distillation. Since the solvent extraction cases have not been optimized, further improvements can be expected.

Cooling water requirements (see Fig. 2.3) for the SEED process are also much lower than for optimized distillation. The solvent extraction process offers new opportunities for heat exchanger matching and, more importantly, facilitates beer preheat with significantly reduced transfer area requirements.

Cost analysis for the three beer cases (see Fig. 2.4) suggests that solvent extraction becomes more economically attractive as the beer quality decreases. The capital investment requirements are also less than for optimized distillation, especially for lower grade beers. Some of the economic differences are summarized in Tables 2.1-2.5 for the 2 wt% beer case. Estimated ethanol recovery costs ranges from $0.25-$0.90/gal for solvent extraction. Compared to optimized distillation, the estimated savings were about $0.12, $0.34, and $0.44/gal for the three beer cases respectively.

These initial results for ethanol recovery from dilute beers suggest that solvent extraction will eventually displace distillation technology for solute recovery from low-grade fermentates. Additional savings are possible from optimization as discussed in Chapter 10.

2.4 References

1. T. K. Murphy, H. W. Blanch, and C. R. Wilke, Recovery of Fermentation Products from Dilute Aqueous Solution, LBL-17979, Lawrence Berkeley Laboratory (April 1984).

2. C. Black, CEP(September 1980) 78.

3. C. T. Bruer, Chem. Eng. (September 17, 1984) 97.

4. K. M. Guthrie, Modern Cost Engineering Techniques, McGraw-Hill, New York (1970) 80.

CHAPTER 3

EXPERIMENTAL EQUIPMENT AND MATERIALS
(W. Y. Tawfik)

3.1 Concentration Measurements

Equilibrium data were obtained by concentration measurements in both phases. The concentration analyses were made using a gas/liquid chromatograph, a Hewlett Packard type 5710A, with a 4-ft. x 1/8-inch diameter, Porapak Q 80/100 mesh packed column. Helium was used as the carrier gas, obtained from the Alabama Oxygen Co., Inc., Bessmer, Alabama. The gas chromatograph was operated at oven temperature of 150°C and injection port temperature of 250°C with a thermal conductivity detector which was also operated at 250°C. The peaks were integrated using a Hewlett Packard 3390A peak integrator.

The output from the integrator was in the form of area percentages of those sample components which chromatographed. The area percentages were then converted to the corresponding weight percentages using calibration curves that were obtained by analyzing samples of known compositions and plotting the integrated ratio of area percentages versus the ratio of weight percentages. A similar calibration curve was used for analyzing the organic phases using reagent grade propanol from Fischer as a reference peak. In the latter case, this analysis yielded the ethanol and water concentrations in the organic phase as well as the weight fraction solvent. Solvent concentrations in the aqueous phases were also measured using propanol spiking.

3.2 Constant Temperature Bath

The effect of temperature on ethanol and water equilibria was studied using a circulating heating bath model HAAKE-L equipped with a heating element and a heat controller model HAAKE-D1. The bath is operated with temperature accuracy of ±0.1°C. The heated samples were carried on glass bottles with capacity of 15 cc. An equilibration time of about 30 minutes was needed to achieve uniform temperatures in the samples. For insuring good temperature measurements, reference bottles containing samples similar to the ones being tested were used to measure temperatures inside the sample.

Another type of heating bath was used to provide heated aqueous feed and organic solvent to the insulated extraction column in order to operate it at higher temperatures. This bath consisted of a small rectangular glass tank with a capacity of approximately five and a half gallons. The temperature in the bath was regulated by a Model 73 Immersion Circulator, obtained

from Fisher Scientific Company. The control of temperature was to ±0.01°C.

3.3 Karr Reciprocating Plate Extraction Column

This column consists of 92 stainless steel perforated plates mounted on a central shaft which can be reciprocated by means of a drive mechanism located above the column. The main portion of the column is a borosilicate glass pipe. The frequency of reciprocation can be varied from 0-400 strokes per minute (Fig. 3.1). The amplitude is also variable.

The model that was used is the KC 1-8 purchased from the Chem Pro Corp., New Jersey. It has an overall height of 152 inches, a diameter of 1 inch, a plate stack height of 96 inches, a base length of 24 inches, a base width of 15 inches and a plate spacing of 2 inches. This column was wrapped with heating tape purchased from Fisher Scientific for temperature control. Solvents and aqueous feeds entering the column were preheated as required.

3.4 Temperature Measurements

A type K thermocouple (nickel chromium/nickel aluminum) was used to measure the operating temperatures of both the mixer-settler and the reciprocating plate column. The thermocouple was connected to a digital multimeter type Simpson 460 Series 4, made by Simpson Electronic Co., Elgin, Illinois, which has a nominal accuracy of ±0.2 MV. The reference thermocouple junction was maintained at a temperature of 0°C.

3.5 Pumping

Positive displacement pumps, purchased from Fluid Metering, Inc., Oyster Bay, were used to provide a uniform flow of aqueous feed and organic solvent to the extractors. These flow rates range from 0-120 ml per minute. Tygon tubing with 1/4-inch outside diameter was used for piping.

3.6 R.P.M. Measurements

The rotational frequencies of the centrifuges and the mixers were measured using a tachometer Model C-871 made by Power Instruments, Inc.

3.7 Vapor-Liquid Apparatus

3.7.1 Setup 1.

The liquid-vapor equilibrium chamber consisted of three principal devices: glassware for distilling with total reflux, an acetone/dry ice cooling system, and a pressure regulated vacuum system. Figure 3.2 illustrates the general layout of the apparatus.

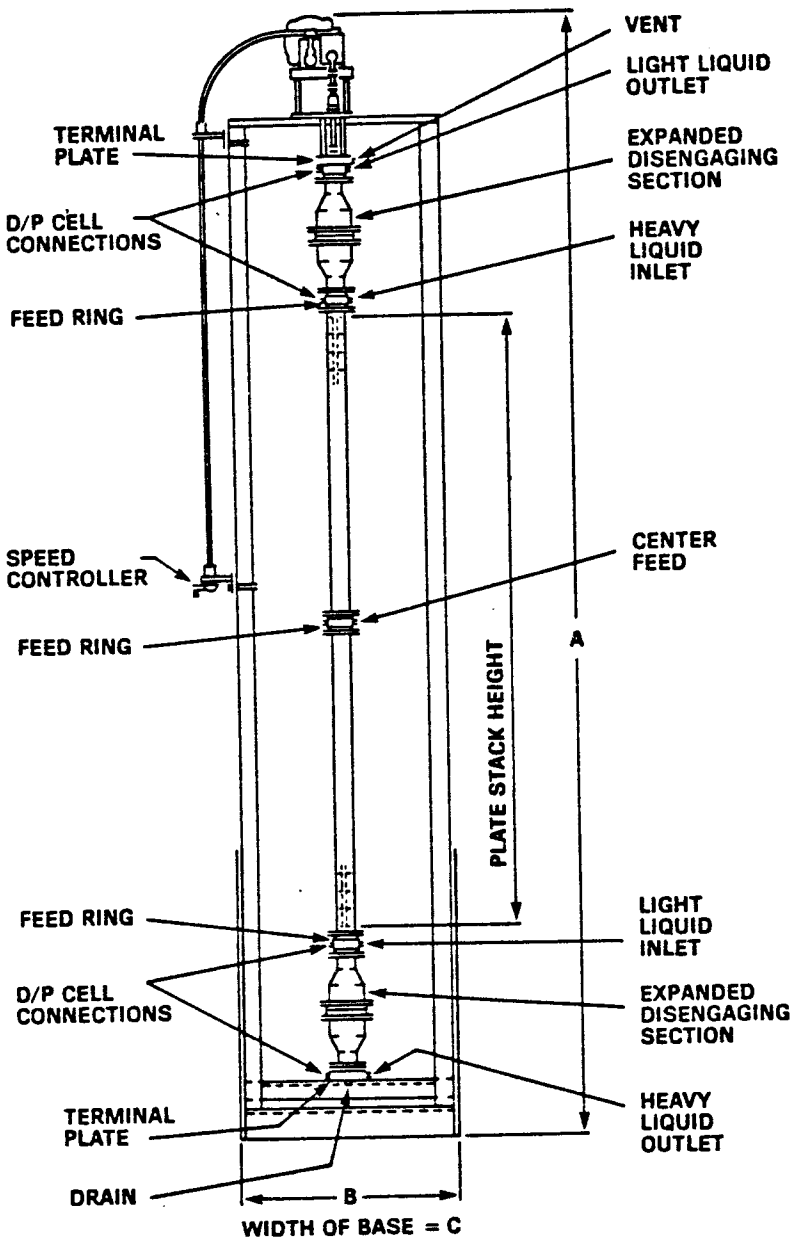

Fig. 3.1 Reciprocating plate column.

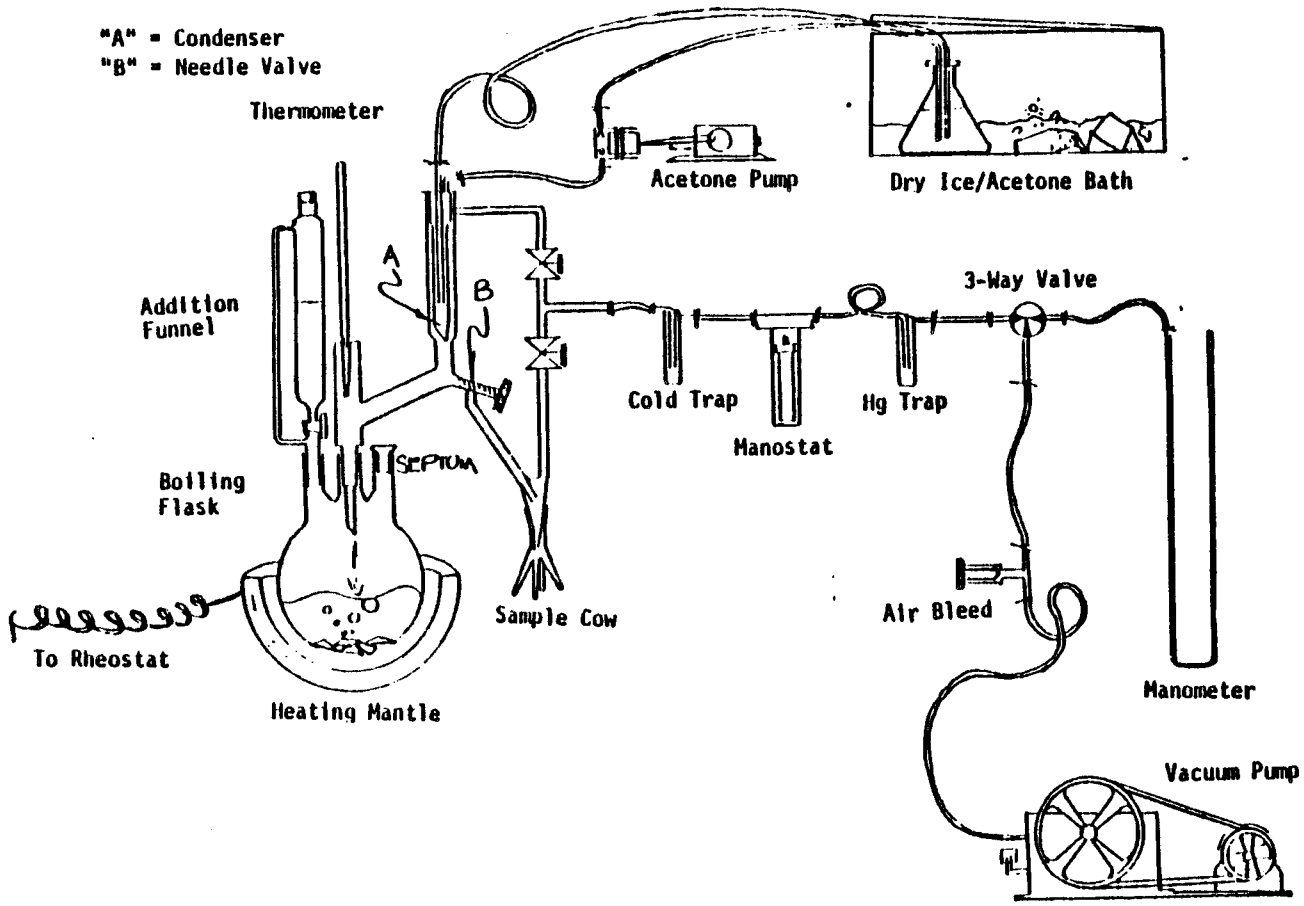

Fig. 3.2 VLE apparatus (Setup 1)

For a given liquid phase composition and system pressure, both the vapor phase composition and the system temperature are fixed.

The distillation glassware and heater consisted of a heating mantle with rheostat (0-110V), a 500-ml boiling flask, a distillation head with finger condenser, a side-mounted needle value for sampling refluxed condensate, a sampling cow with four 5-ml fingers, and vacuum attachments. A thermometer (typically -10°C to 250°C) was also used. Ideally, the 500 ml boiling flask should be three-necked, supporting the use of a septum for withdrawing liquid samples without breaking the vacuum, the thermometer, and an additional funnel for introducing the various components. More importantly, the system was insulated from the boiling flask to condenser to prevent premature condensation of the vapors.

The acetone cooling system included a positive displacement cooling pump (F.M.I.), a dry ice/acetone bath, and connections to the condenser.

The vacuum system included a cold trap, a Gilmont C-2200-D Manostat, a mercury trap, manometer, three-way valve, air bleed needle valve, and a suitable high-vacuum pump.

3.7.2 Setup 2.

For more complicated systems, the previous set-up failed to insure constant pressures for isobaric experimental data. A more sophisticated device (Fig. 3.3) was used to achieve better accuracy.

The equilibrium cell was a Stage-Muller dynamic equilibrium still, manufactured by Fischer Labor und Verfahrenstechnik, West Germany. Good circulation for both liquid and vapor phases was achieved by means of Cottrell pumps, which insured good contact of the liquid and vapor phases with the temperature sensing element.

Thermal insulation for the vapor phase was provided by a silver-plated vacuum jacket surrounding the equilibrium chamber, preventing partial condensation of the vapor phase. Simultaneous sampling for liquid and vapor phases in equilibrium was done through two magnetic sampling valves. The system pressure was maintained constant using a Fischer VKH 100 pressure controller. The features of this still were described in detail by Stage and Fischer's (1, 2).

3.8 Organic Solvents

The following solvents were used as received from their respective vendors:

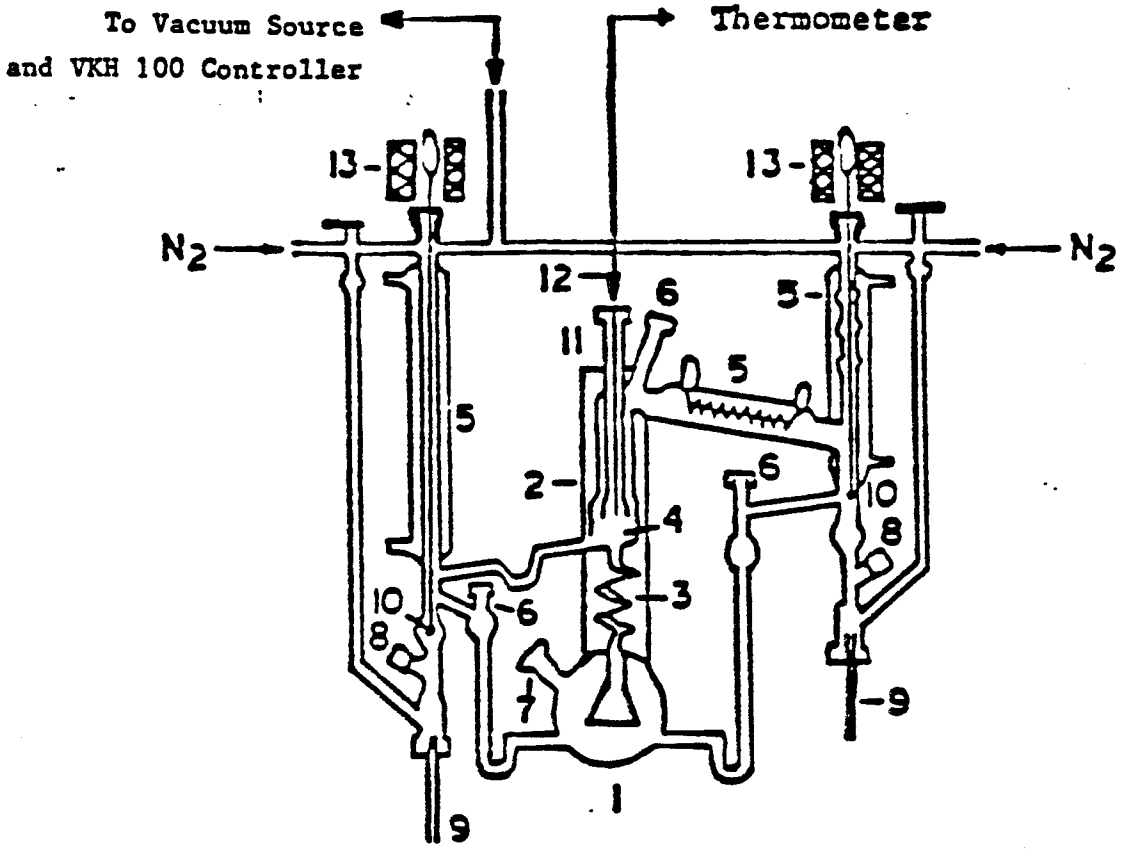

1. Boiling Flask
2. Vacuum Jacket
3. Cottrell Pump
4. Equilibrium Chamber
5. Condensers
6. Injection Ports
7. Filling Spout and Thermometer Well
8. Teflon Valves
9. Sample Tubes
10. Glass Ball Valves
11. Equilibrium Thermometer Well
12. Equilibrium Thermometer
13. Solenoid Devices (Actuates 10)

Fig. 3.3 VLE apparatus (setup 2, Othmer still)

2 Ethyl-1-hexanol (2EHOH). This technical grade organic solvent has a boiling range of 183 - 185°C and was purchased from the Fisher Scientific Company, New Jersey.

2,6 Dimenthyl-4-heptanone (DMH). This practical grade organic has an initial boiling point of 169°C and was purchased from the Fisher Scientific Company, New Jersey.

Isopar-L. This is a heavy narrow-cut, isoparaffinic solvent composed of C_{12} mixtures of branched alkanes. It has a specific gravity of 0.767 at 15.6°C, a viscosity of 1.99 c.p. at 25°C and a boiling range of 177 - 197°C. The solvent is a refinery product obtained from Exxon Refining.

Isopar-M. This is a heavy isoparafinic narrow refinery cut, composed mainly of mixtures of C_{12} and C_{13}, with a boiling point range of 207° to 254°C and specific gravity of 0.78 at 25°C. The solvent is a product of Exxon.

Methyl Ester CE-1218. This is a Proctor and Gamble product with saponification value of 238 and specific gravity of 0.866 at 25°C. The solvent contained 55% C_{12}, 22% C_{14}, 10% C_{16}, and 13% C_{18}.

Norpar-12. This is a narrow-cut, normal parrafinic solvent composed primarily of C_{11} and C_{12} mixtures of alkanes. It has a specific gravity of 0.751 at 15.6°C, a viscosity of 1.26 c.p. at 25°C, and a boiling range of 188 - 219°C. The solvent is a refinery product obtained from Exxon.

Tridecyl Alcohol. This is a distilled product, consisting of isomeric primarily alcohols, predominately C_{13}. It has a specific gravity of 0.838 at 20°C, a viscosity of 18.9 c.p. at 25°C and a boiling range of 253 - 266°C.

Tri-n-butyl phosphate. This is a technical grade solvent from Fisher. It has a normal boiling point of 289°C with decomposition and a specific gravity of 0.976 at 25°C.

The aqueous solutions were prepared by mixing different quantities of absolute reagent grade ethanol (99.5% pure) with distilled water. Gas chromatography was used to determine the weight percentages of ethanol in the aqueous solutions. Apparatuses were calibrated and checked for accuracy using the ethanol/water binary system and literature data (3).

3.9 References

1. H. Stage and W.G. Fischer, "Improved LABODEST Circulation Apparatus for Measurement of Vapor-Liquid Equilibria", G.I.T. Special Periodical, vol. 11, (1968).

2. H. Stage and W.G. Fischer, "Experimental Experience with

and Improved LABODEST Circulation Apparatus", J. Chem. Eng., vol. 7, (1973).

3. J.A. Larkin and R.C. Pemberton, Thermodynamic Properties of Mixtures of Water and Ethanol, Division of Chemical Standards, England, (1976).

CHAPTER 4

EXPERIMENTAL METHODS AND RESULTS
(W. Y. Tawfik)

4.1 Vapor-Liquid Equilibrium Measurements

4.1.1 Vapor Pressure Measurement.

About 100 ml of the pure liquid were placed in the boiling flask. Heat was provided using a heating mantel. Continuous stirring was provided using a magnetic stirrer to insure homogeneous temperature in the liquid phase. When Setup 2 (Chapter 3) was used, good circulation was provided using the Cottrell pumps for both phases in equilibrium. When Setup 1 (Chapter 3) was used, the system was operated at total reflux, providing more time to achieve thermal equilibrium. While the use of the manostat resulted in some pressure fluctuations, the VKH 100 pressure controller in Setup 2 minimized the pressure disturbance to acceptable levels (±0.1 mm Hg). The cooling media for the vapor condenser was acetone and dry ice. Equilibrium was achieved when the monitored temperatures remained constant for 30 minutes at the given pressure. The previous procedure was repeated at different pressures and the temperatures and the corresponding vapor pressures were recorded. The experimental vapor pressure data for ethanol and seven different solvents are summarized in Appendix A (Tables A1 through A8).

4.1.2 Isobaric Binary VLE Measurements.

It was found by experience that the optimized procedure should start with 100 ml of the less volatile component of the binary to avoid thermal instabilities. Incremental amounts of the more volatile component were added to the boiling flask, and good mixing provided before heating the system to insure homogeneous mixtures. The previous procedure was repeated at the given pressure for each liquid composition; however, more time (about 45 minutes) was needed to achieve thermal equilibrium. Simultaneous samples of liquid and vapor were then drawn, and the temperature recorded at the given pressure. Composition analysis was carried out using the HP gas chromatograph as described earlier.

The previous procedure was repeated until the entire composition range of the binary system was covered. The test system used for both setups was the ethanol-water binary system. Good agreement with the literature data of Larkin and Pembertom (36) was found for this test system. The experimental values for the isobaric binary VLE systems of interest are summarized in Appendix A (Tables A9 through A11).

4.2 Liquid/Liquid Equilibrium Measurements

Initial studies (1 through 12) were concerned with gathering equilibrium data about ethanol-water-organic solvent systems using different techniques such as tie-line measurements, solubility curve titrations, batch equilibrations and solvent stripping tests. The experimental data obtained by these experiments classified the organic solvents into two broad categories. Drying solvents have higher selectivities for extracting ethanol from water, but their ethanol distribution coefficients are relatively low. These solvents usually are refinery products, composed mainly from mixtures of heavy molecular weight alkanes such as Isopar-L and Norpar-12. Recovery solvents have higher ethanol distribution coefficients, but their selectivities for ethanol are lower. These solvents are systems like branched alcohols and ketones, such as 2-ethyl-1-hexanol and 2.6-dimethyl-4-heptanone.

In this work, the effects of temperature on the equilibrium were also examined using some of the systems which had been studied earlier by Tedder, et al. (13) and Tawfik (14), at room temperature. These temperature studies resulted from a need to reduce the tendency of some solvents to form a stable emulsion with the aqueous phase. Higher temperatures did not help much in solving the emulsion problem; however, in analyzing some of the organic and the aqueous phases of the heated samples, it was observed that both ethanol distribution coefficients and the solvent selectivities had been increased.

4.3 Tie Line and Distribution Coefficient Determinations

Tie lines and distribution coefficients for any specific solvent were determined by equilibrating a known weight of aqueous solution of ethanol and water (A_i) with a known weight of the given pure solvent (O_i). The concentrations of ethanol in the aqueous phase before and after equilibration with the solvent (x_{ei}, x_e, respectively) were determined by GC analysis. In these cases, the GC analysis was based on the area percentages for the integrated peaks of the ethanol and water species only (i.e., on a solvent-free basis). These area percentages were then converted to the corresponding weight fractions using a calibration curve. However, for a complete organic phase analysis one of the following two techniques were used depending upon the nature of the solvent.

4.3.1 Graphical Method.

First the system was titrated volumetrically. Starting with a known weight of either solvent or water, successive additions of the remaining two species were titrated into the mixture to repeatedly form and remove the liquid/liquid cloud. Using the titrant volumes and pure species densities, the mutual solubility curve was then constructed. The initial aqueous composition was plotted on a ternary diagram with the mutual solubility curve. After equilibrating known weights of aqueous and solvent mixtures, the aqueous composition after mixing was plotted on a ternary

diagram with the mutual solubility curve. Gas chromatography gave the precise ethanol/water weight ratio in the equilibrated aqueous phase. Connecting the two points by a straight line resulted in an intersection with the mutual solubility curve and the equilibrium aqueous composition and yielded one tie line for the system. The intersection between the tie line and the organic phase side of the solubility curve yielded the equilibrium organic compositions (y_e, y_w, y_s).

This method was suitable for relatively wet systems like 2-ethyl hexanol and dimethyl heptanone because of the ease in determination of the water weight fraction in the organic phase from the solubility curve (Figs. 4.1, 4.2). On the other hand, for relatively dry systems like Norpar-12 and Isopar-L (Figs. 4.3, 4.4) in which the organic phase side of the solubility curve almost coincides with the solvent ethanol edge of the ternary diagram, it was difficult to accurately measure the water concentration in the organic phase. In these latter cases the following analytical technique was used. This method is described in detail elsewhere (4-8).

4.3.2 Analytical Method.

This method is based on solving the mass balance equations for the equilibrium phases using the GC analysis of the phase before and after equilibration. In the absence of the solubility curve, one assumption is necessary; namely, that the solubility of the solvent in the aqueous phase within the range of interest is negligible, i.e.

$$x_s = 0 \tag{4.1}$$

Alternatively, the two phases may be analyzed by the GC using propanol spiking to estimate x_s and y_s. However, assuming component mass balance for ethanol and water, the component mass balance equations yield:

$$z_e F - x_e A = y_e O \tag{4.2}$$

$$z_w F - x_w A = y_w O \tag{4.3}$$

where:

z_i = weight fraction of component i in the feed

x_i = weight fraction of component i in the equilibrated aqueous phase

y_i = weight fraction of component i in the equilibrated organic phase

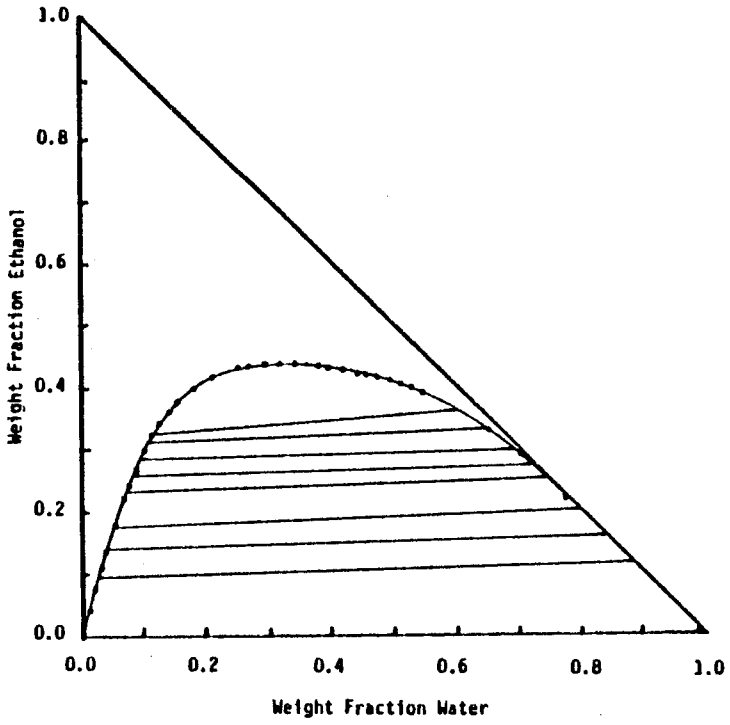

Fig. 4.1 Mutual solubility curve for the system: ethanol, water, and the solvent 2-ethylhexanol.

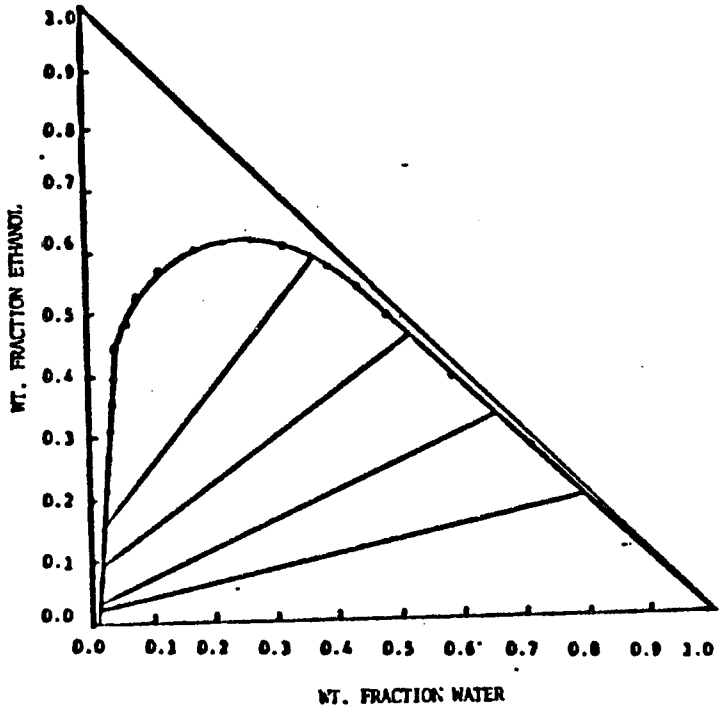

Fig. 4.2 Mutual Solubility Curve and Selected Tie Lines for the system Ethanol-Water-Dimethyl Heptanone

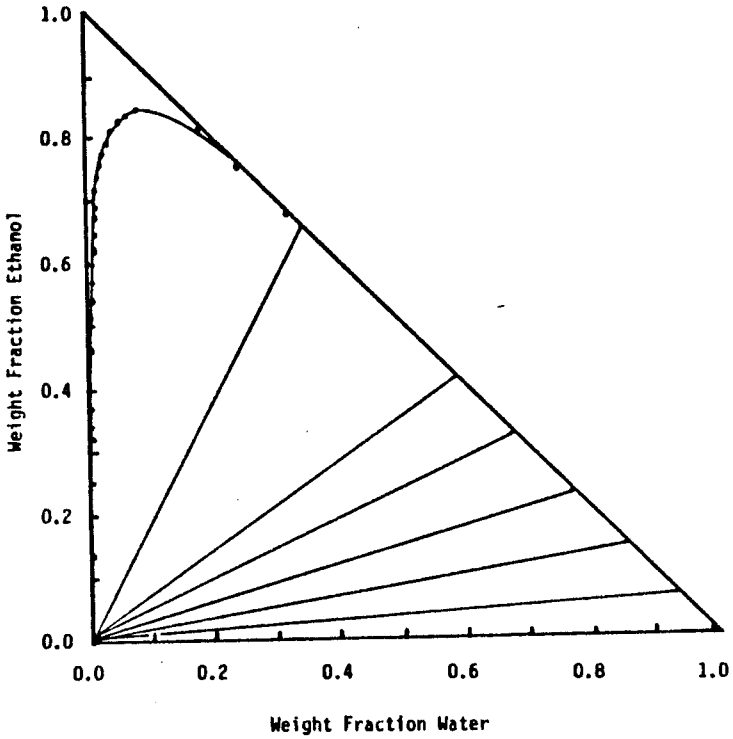

Fig. 4.3 Mutual solubility curve for the system: ethanol, water, and the solvent NORPAR-12.

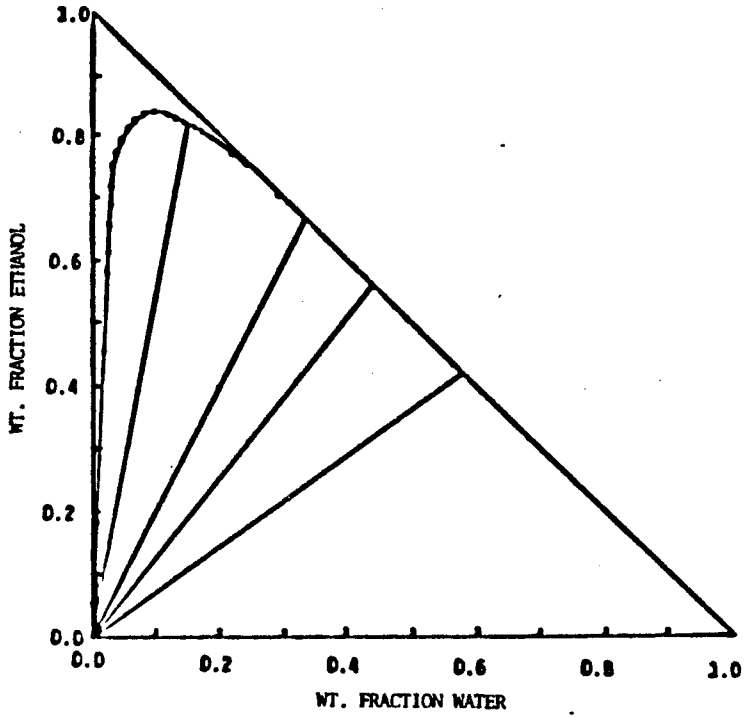

Fig. 4.4 Mutual Solubility Curve and Selected Tie Lines for the System Ethanol-Water-Isopar-L

A = equilibrated aqueous phase weight, gm

O = equilibrated organic phase weight, gm

F = O + A = weight of aqueous and organic phases, gm

Dividing Eqn. 4.2 by 4.3 gives:

$$(z_e F - x_e A) / (z_w F - x_w A) = y_e / y_w \quad (4.4)$$

since

$$(y_e / y_w) = (Y_e / Y_w) \text{ (on a solvent-free basis)} \quad (4.5)$$

where Y_i = weight fraction of component i in the organic phase in solvent free basis.

Rearranging Eqn. 4.4 and solving for A:

$$A = F[(Y_e/Y_w)\, z_w - z_e] / [(Y_e/Y_w)\, x_w - x_e] \quad (4.6)$$

and:

$$O = F - F[(Y_e/Y_w)\, z_w - z_e] / [(Y_e/Y_w)\, x_w - x_e] \quad (4.7)$$

Rearranging Eqns. 4.2 and 4.3 :

$$y_e = (z_e * F - x_e * A)/O \quad (4.8)$$

$$y_w = (z_w * F - x_w * A)/O \quad (4.9)$$

$$y_s = 1 - y_e - y_w \quad (4.10)$$

$$D_e = y_e / x_e \quad (4.11)$$

$$D_w = y_w / x_w \quad (4.12)$$

$$S = D_e / D_w \quad (4.13)$$

where:

D_i = distribution coefficient of component i in weight basis

S = selectivity of component i in weight basis

4.4 The Effect of Temperature and Dextrose on the Distribution Coefficients

The same procedures described above for tie-line determination were repeated for the same solvents at higher temperatures rather than at room temperature using a constant temperature bath. An equilibration time of 30 minutes was provided for the test samples to achieve equilibrium. To insure

accurate measurements, similar reference samples were placed in the same bath and a mercury thermometer was used to measure their temperatures.

The resulting distribution coefficients were correlated initially with the temperatures at the given initial aqueous feed concentrations in the form of:

$$\ln D_i = a' + b'/T \qquad (4.14)$$

This type of correlation was not quite suitable to express the effect of temperature on the distribution coefficients since any change in their values must be accompanied with a change in the ethanol concentrations in the equilibrated aqueous phase and, clearly, that a general correlation must have the distribution coefficients as a function of both variables. Tables B1 through B4 (Appendix B) summarize the measured distribution coefficients for ethanol and water using 2-ethyl-hexanol, Isopar-L, dimethylheptanone, and 20% TDOH in Norpar-12 as solvents, respectively, at different temperatures.

The correlation that was chosen has the form:

$$\ln D_i = a^* + b^* x_e + c^*/T \qquad (4.15)$$

in which a^*, b^* and c^* are constants for the given components and solvents over the range of interest.

Actual fermentation broth was found to have residuals of sugars (mainly sucrose). Moreover, it was found that sucrose has a significant effect on the distribution coefficients for both ethanol and water. The effect resulted in higher ethanol recovery and drier product for a given solvent and is large enough to justify, in some cases, the maintenance of higher levels of sucrose in the aqueous phases through the process. Dextrose was used to test the effect of sugar on the experimental distribution coefficient for ethanol and water. In the presence of dextrose, the experimental values of the distribution coefficients for both ethanol and water are summarized in Tables B5 through B7 (Appendix B) for three different solvents. On the other hand, the distribution coefficient dependence on the ethanol weight fraction was no longer linear, and the best correlation was found to be:

$$\ln D_i = a_0 + a_1 x_e^2 + a_2 x_e + a_3 x_D + a_4 x_D^2 + a_5 \varphi_m + a_6/T \qquad (4.16)$$

where:

x_i = weight fraction of component i in the equilibrated aqueous phase

φ_m = volume fraction of modifier in the solvent

T = temperature, °K

The resultant parameters for this correlation are summarized in the next chapter.

4.5 Countercurrent Extraction Using a Reciprocating Plate Column

This column is a continous extraction device which can be used for countercurrent extraction as described by Karr (15) in detail. The aqueous feed solution was metered into the column via the nozzle above the reciprocating plates. Similarly, the extracting solvent enters the column at a controlled rate via the nozzel below the extractor plates. Before the final adjustment of the reciprocating speed is made, the interface is established at approximately the midpoint of the upper disengaging section. Thus, nearly the entire column will be filled with the organic phase and only a few inches of the aqueous phase will be present at the bottom of the column. The interface is established by setting the control valve in the bottom discharge line through which the aqueous phase exits from the column. Subsequently, a final adjustment of the reciprocation speed of the plates is made. The reciprocation speed should be such that in the vicinity of the plates the average diameter of the dispersed phase droplets is one millimeter or less.

The interfacial area between the continuous and dispersed phase is the principle factor controlling the rate of mass transfer between them. However, the time needed to achieve steady state conditions is also a function of the total feed flow rates and the reciprocating speed. Usually, at least one and a half hours were needed to achieve steady state under the present operating conditions. Analysis of the final extract and raffinate compositions was done using gas chromotography.

The experimental data for 22 runs is summarized in Table C1 (Appendix C) for ethanol-water-Isopar-M systems.

Additional data for a 3-ft column and 1-in column obtained from Karr (16) and Karr and Lo (15, 17) are summarized in Appendix C.

4.6 Continuous Extraction/Extractive Distillation Tests

Tests were carried out using the Karr column for extraction and a custom-fabricated pyrex column for solvent regeneration. Solvent was continuously regenerated and recycled to the Karr column. The solvent regeneration column in this case was about 2 inches in diameter and 3 feet tall. It was equipped with a glass wool demister pad and condenser assembly at the top.

Extraction tests using dilute ethanol mixtures were carried out using either the Karr column or the mixer-settler bank to provide extract. Extract was then processed theough a coalescer, an extract preheater, and passed into an extractive distillation

column consisting of 6 bubble cap trays (3 above and 3 below the feed). Regenerated solvent was continuously pumped to the top of this column (about 3 feet tall) which was equipped with a condenser assembly and a 1-liter triple neck reboiler which was jacketed with a heating mantel. Dehydrated extract was passed by pressure differential from the bottom of the extractive distillation column into the solvent regeneration column. A stainless steel valve in the line was adjusted to achieve steady flowrates. The latter column also consisted of 6 bubble cap trays (2 above and 4 below the feed). It had a condenser assembly and heating mantel similar to the extractive distillation column.

Solvent transfer from the bottom of the solvent regeneration column back to atmospheric pressure was accomplished using a low frequency bellows pump obtained from Fisher. Prior to recovering the solvent, it was necessary to cool it using an ice bath to prevent damage to the bellows pump. It was also found convenient to provide feedback control loops. In particular, the Karr column was operated with on/off control on the liquid/liquid interface at the bottom of the column (i.e. organic continuous).

The temperatures of the extractive distillation column feeds were controlled using a heating mantel, triple neck flask and on/off controllers connected to Variacs. Finally, the pressures in the extractive distillation and solvent regeneration columns were controlled using two additional on/off feedback controllers. Pressures in the extractive distillation and solvent regeneration columns were maintained at reduced values by a common vacuum pump. In all cases, the controllers used conductivity probes which were simply clamped to the parameter of interest (i.e., either an interface let, a mercury thermometer, or a mercury manometer). These techniques were found to be highly effective and could maintain the process to within 1°C and 2mm Hg.

4.7 References

1. D.W. Tedder, C.L. Liotta, F.M. Williams and M. Spanbauer, Fuel-Grade Ethanol Recovery by Solvent Extraction: Technical Progress Report for the Period September 15, 1980 thru March 31, 1981, School of Chemical Engineering, Georgia Institute of Technology, Atlanta, GA (April, 1981).

2. D.W. Tedder and C.L. Liotta, Fuel-Grade Ethanol Recovery by Solvent Extraction, Schools of Chemical Engineering and Chemistry, Georgia Institute of Technology, Atlanta, GA (June 30, 1979).

3. D.W. Tedder, et al., Fuel-Grade Ethanol Recovery by Solvent Extraction: Technical Progress Report for the Period September 15, 1981, Georgia Institute of Technology, Atlanta, GA (October 1981).

4. D.F. Othmer, R.F. White, and E. Trueger, "Liquid-Liquid Extraction Data", Industrial and Engineering Chemistry, vol. 33, no. 10, (1941), pg. 1240.

5. A.V. Brancker, T.G. Hunter, "Tie Lines in Two-Liquid Phase Systems", Ind. and Eng. Chemistry, vol. 32, no. 1, (1940), pg. 35.

6. I. Bachman, "Tie Lines in Ternary Liquid Systems", Ind. and Eng. Chemistry, vol. 32, no. 1, (1940), pg. 35.

7. J.L. Schweepe and J.R. Lorah, "Ternary System Ethyl Alcohol-n-Heptane-Water at 30°", Ind. and Eng. Chemistry, vol. 46, no. 11, (1941), pg. 2391.

8. C.M. Qualline and Van Winkle, "Ternary Liquid Systems", Ind. and Eng. Chemistry, vol. 44, no. 2, (1952), pg. 1668.

9. D.F. Othmer and P.E. Tobias, "Liquid-Liquid Extraction Data", Ind. and Eng. Chemistry, vol. 34, no. 6, (1942), pg. 696.

10. J.W. Roddy and C.F. Coleman, "Distribution and Miscibility Limits in the System Ethanol-Water-TBP", Oak Ridge National Laboratory, (1981).

11. J.W. Roddy, "Distribution of Ethanol Water Mixtures to Organic Liquids", Ind. Eng. Chem. Process Des. Dev., vol. 20, (1981), pps. 104-108.

12. J.W. Roddy and C.F. Coleman, "Distribution of Ethanol-Water Mixtures to Normal Alkanes from C_6 to C_{16}", Ind. Eng. Chem. Fundam., vol. 20, (1981), pps. 250-254.

13. D.W. Tedder, et al., Fuel Grade Ethanol Recovery by Solvent Extraction, Technical Progress Report, Georgia Institute of Technology, (October 1982).

14. W.Y. Tawfik, "Efficiency of Ethanol Extraction from Aqueous Mixtures", Thesis, Georgia Institute of Technology, (1982).

15. T.C. Lo and A.E. Karr, "Development of a Laboratory Scale Reciprocating Plate Extraction Column", Ind. Eng. Chem. Proc. Des. Dev., vol. 11, no. 4, (1972).

16. D.S. Abrams and J.M. Prausnitz, AIChE J., vol. 21, (1975), pg. 116.

17. A.E. Karr and T.C. Lo, "Performance and Scale Up of Reciprocating Plate Extraction Column", Proc. of ISEC, Society of Chem. Ind., London, vol. 218, (1971).

CHARACTERISTICS OF IMMOBILIZED YEAST REACTORS PRODUCING ETHANOL FROM GLUCOSE

(M.J. Anselme and D.W. Tedder)

5.1 Summary

The evolutionary performance of upflow reactors are affected by the cell immobilization matrix and the matrix particle size distribution. Higher productivities are obtained using a low-density brick with a particle size of about 400 to 1400 μ. A medium condition favoring growth quickly leads to large biomass gradients within the reactors and, eventually, reductions in average productivities due to bed plugging. These systems can be accurately modeled using Monod kinetics when dispersion and the biomass gradient are considered. The productivity was apparently not controlled by substrate diffusion in these cases.

5.2 Introduction

Bioreactor design can, in principle, be used to increase productivities, achieve higher conversions, and reduce fermentation costs. Many studies (1-28) have focused on ethanol production from sugar, for example, using a variety of designs. Table 5.1 summarizes reported maximum productivities. A continuous stirred tank reactor (CSTR) without cell recycle represents a lower value reported while a vacuum CSTR with cell recycle is an upper value. Reported values for immobilized cell reactors (packed beds) fall in between.

Immobilized cell reactors offer the possibility of higher cell concentrations than are easily maintained in CSTRs. Typical reported values are summarized in Table 5.2 either in terms of cell dry weight/unit weight of carrier or estimated cells/unit weight of carrier. These values should reflect average properties for the reactors, but not necessarily the available cell concentrations. That is, growing colonies may become isolated through bed plugging during operation and cell activity is more difficult to measure directly than in CSTR.

Also, such reactors are typically operated to maintain cell growth and, therefore, the active cell population on the immobilized carrier increases during initial operation until the bed is effectively saturated. At that point cell debris can often be observed and plugging begins to cause a decrease in average productivities. A measure of such effects is provided in the long term bed stability. Literature values are summarized in Table 5.3.

TABLE 5.1 SUMMARY OF REPORTED LITERATURE PRODUCTIVITIES

Reactor Type	Maximum Productivity Given In the Article (G/L/Hr)	Ref.
Continuous stirred tank without cell recycle	7.0	20
Continuous stirred tank with cell recycle	29.0, 18.3	20
Batch reactor (free cells)	2.2	20
Vacuum Fermentor with cell recycle	82.0	20
Packed bed of birch wood chips	55.80*	5
Packed bed of beech wood chips	21.8*	17
Horizontal packed bed of pectin gel beads	40.0*	20
Packed bed of carrageenan gel beads	43.8*	31
Packed bed of Ca alginate gel beads	50.0*	10
Stirred tank with Ca alginate gel beads	15.0	10
Fluidized bed of Ca alginate gel beads	20.0	19
Packed Ca alginate beads reinforced with polymer	26.77	9
Packed gelatin beads crosslinked with glutaraldehyde	15.9*	28
Packed bed of photocrosslinkable resin beads	11.0	18
Three stage fluidized bed of Al alginate gel beads	8.4	18

* Means that the productivity is based on liquid volume as opposed to total reactor volume.

TABLE 5.2 LITERATURE REVIEW OF CARRIERS' CELL LOADING

Carrier	Loading With Unit		Ref.
Pouzzolane (brick)	3.6	g Of Cell Dw/Kg Of carrier	11
Dowex 50 W X 8 (resin)	5.0	"	11
Beech wood chips	188.0	"	17
Ceramic	16.2	"	17
Cordierite, 3 microns (average pore size)	2.1×10^7	cells/g of carrier	14
Cordierite, 10 microns	43×10^6	"	14
Frited glass, 3.5 mic.	2.7×10^6	"	14
Fritted glass, 3.5 mic.	7.0×10^6	"	14
Fritted glass, 40 mic.	4.9×10^6	"	14
Zirconia ceramic 19 microns	23×10^6	"	14
Borosilicate glass non porous	1.9×10^6	"	14
Polyvinyl chloride	8.5	G of Cell Dw/L of Carrier	11
Polyvinyl chloride mixed with wood	12.4	"	11
Polyvinyl chloride flakes	5.3	"	11
Raschig ring (5-7 mm od)	7.25	"	6
Raschig ring (8-10 mm od)	8.7	"	6
Porous bricket (Rover France)	12.3	"	6
Carrier A (patented)	20.7	"	6
Carrier B (patented)	18.5	"	6
Birch wood chips	26.1	G of Cell Dw/L of Reactor	5
Ca alginate beads (estimated)	150.0	"	19
Continuous stirred tank	12.0	"	20
Continuous stirred tank with cell recycle	50.0	"	20
Vacuum fermentor with cell recycle	124.0	"	20

Cell immobilization is generally achieved by either encapsulation (e.g. Ca alginate beads) or by attachment to a surface (e.g. beech wood chips). In this study, calcium alginate beads were used as a calibration tool to check experimental methods, and the primary emphasis was given to characterizing surfaces for cell immobilization. In the case of highly porous matrices (e.g. low density bricks), cells could attach either to the outer edges of bed particles or within the pores of these particles.

This paper first describes a carrier screening test for surface immobilized yeast reactors producing ethanol from glucose. The carrier which yielded the best reactor performance was then studied to determine the effect of the carrier particle size. Subsequently, the reactor with the best carrier at the optimum particle size was studied to determine the cell concentration gradient. With these results, the performance was modelled as a plug flow reactor with dispersion by integrating the appropriate equations.

5.3 Materials and Methods

5.3.1 The Fermentation Apparatus

The fermentation vessels used in the work were simple jacketed glass cylinders. The inside diameter of the glass tubing was nominally 18 mm, and the single section reactors were all approximately 30 cm high. A four section reactor was also built to measure dry cell weight as a function of reactor height. In this reactor, each jacketed section was 18 mm in diameter and 8 cm high.

The reactors were supplied with feed using a four head peristalic pump. The pump was 1-100 rpm variable speed Masterflex model number 7520-30, the four heads were Masterflex model number 7013-20, all from the Cole Parmer Instrument Co. This system allowed the operation of four upflow reactors simultaneously at approximately the same rates. The reactors were kept at 30^{o}C by circulating water from a constant temperature bath through the reactors' jackets.

5.3.2 Organism, Medium and Fermentation Conditions

The organism used was Saccharomyces cerevisiae, ATCC 4126.
The liquid medium used throughout this work was:
--100 g/l of glucose
(D glucose anhydrous from Aldrich Chemical Co.)
--7.5 g/l of yeast extract
(from BBL Microbiology System)
--7.5 g/l of peptone
(from Fluka Cie, Switzerland)

The pH of the medium was adjusted to 4 with concentrated sulfuric acid (6M).

5.3.3 Surface Immobilization Carriers

Screening procedures were developed to choose between alternative immobilization matrices and to measure the effect of particle size distribution. In these tests, several matrices (see Table 5.4) were examined using the procedures outlined below. Carriers giving better performance as measured in terms of average productivities were subjected to additional testing and characterization.

Figure 5.1 shows the pore size distribution for the brick (data provided by Corning Glass Corp.) and pine. Table 5.5 summarizes the characteristics of reactors 2,3,4,5,6,7 and 8 in which various packings were used.

TABLE 5.3 LITERATURE REVIEW OF LONG TERM REACTOR PERFORMANCE STABILITY

Reactor Type	Stability Period (days)	Ref.
Fluidized bed of Al alginate beads	90	18
Packed bed of photocrosslinkable resin beads	90	18
Packed bed of Ca alginate beads	20	10
Horizontal packed bed of pectin gel	20	20
Packed bed of agar beads treated with polyacrylamide	60	9
Fluidized Ca alginate beads regenerated continuously	166	19
Packed bed of patented carrier (surface immobilization)	75	6
Vacuum fermenter with cell recycle	11	20

TABLE 5.4 SURFACE IMMOBILIZATION CARRIERS TESTED

MATRIX	SIZE	CHARACTERISTICS
Molecular Sieves	2 mm (8-12 mesh)	Activated type 4A from Baker
Boileezers	4 mm particles	Type B-365 from Fisher
Amberlite Resin	3 mm particles	Type IRC 50 from Resinous Products and Chemicals
Cotton	20 μ fibers	
Wool	20 μ fibers	from New Zealand
Fire Brick	Varied particles	13.1 μ pores from Johns Manville
White Pine	8 mm particles	3 μ pores

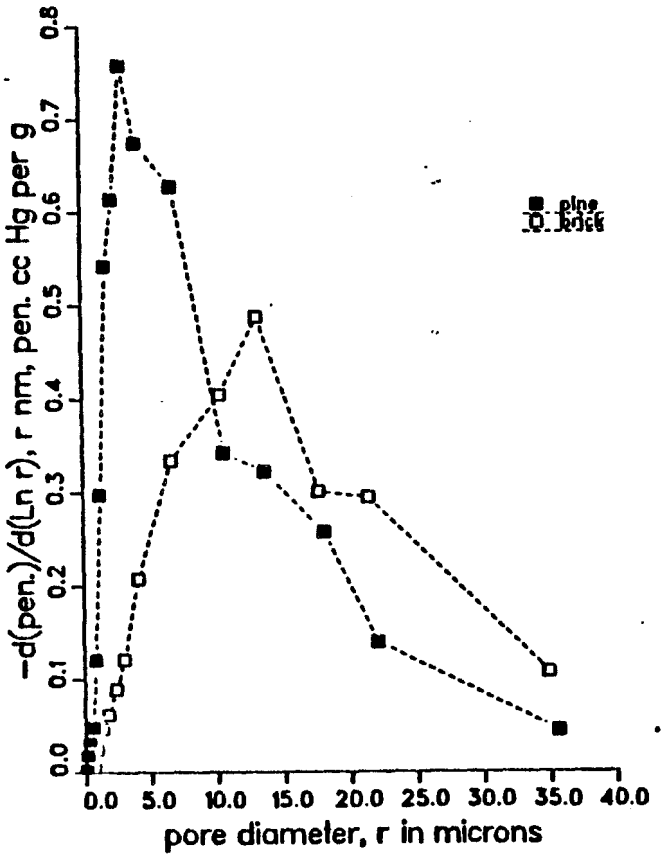

Figure 5.1 Pore Size Distribution of the Brick and Pine Wood

TABLE 5.5 CHARACTERISTICS OF THE REACTORS

Reactor #	Total Volume (Ml)	Packing Nature	Packing Size (Microns)	Mass of Pac. (G)	Liq. Vol. (Ml)	Void Frac. (%)
1	67.4	Ca alginate beads	3000	48.10	24.25	36.00
2	67.0	brick	1981 3962	17.49	62.60	89.40
3	64.0	molecular sieve	Mesh 11-12	47.07	42.85	66.90
4	65.4	boileezers	4000	63.17	40.07	61.3
5	66.0	resin	3000	32.44	36.11	54.70
6	63.0	cotton	diam. 20	3.8	61.50	97.60
7	67.0	wool	diam. 20	3.8	65.50	97.60
8	65.0	white pine	8000	16.16	38.00	58.50
9	69.0	brick	250 425	28.76	54.70	79.28
10	64.0	brick	1397 1981	19.19	56.42	88.16
11	65.4	brick	425 1397	23.04	57.66	88.16
12	66.0	brick	3962 5613	16.36	59.51	90.17
13	66.5	brick	425 1397	24.6	58.69	88.25
14	68.8	brick	425 1397	26.23	60.68	88.20

To show the effect of particle size on the performance of a surface immobilization reactor, the brick was crushed and sieved into five size categories. Each size was then packed in a separate bed. The characteristics of the beds are reported in Table 5.5 A series of U.S. standard sieves of 250, 425, 1397, 1981, 3962 and 5613 microns of opening were used to sieve the crushed brick.

5.3.4 Immobilization Procedure

5.3.4.1 Preparation of the Surface Immobilization Carriers

Once the reactors were packed by pouring the carrier into the glass tubes, absolute ethanol was passed upflow through them for one hour with the feed pump. This technique was used to get rid of any colonies of living organisms and also to clean the carriers of any ethanol soluble impurities. After the ethanol wash, tap water (which pH has been set to 4 with sulfuric acid) was passed upflow through the reactors. In this way the carriers desorbed the ethanol and allowed a more efficient cell immobilization. Experiments showed that if the reactors were not rinsed with water after the ethanol wash, live cell would not be immobilized on the carrier during the insemination period.

After these precautions were taken, a two day old yeast culture was passed upflow through the reactors in closed circuit for 12 hours. During this time, the yeast culture tank was gently stirred to prevent yeast deposition and the pump was set at 11 rpm. This rate represents an average flowrate of 0.4 ml/min.

5.3.4.2 Cellular Growth on the Carriers

After the insemination period for the surface immobilization reactors, the reactors were fed with sterilized medium. Air was sparged for five minutes every hour using the feed line itself.

Prior to use, the medium was sterilized at 120°C for twenty minutes in an autoclave to prevent any biological acitivity in the feed tank that would perturb the actual sugar concentration in the inlet flow of the reactors. However, sterilization of the feed was not sufficient to assure aseptic conditions in the reactors because the insemination procedure had not been done under aseptic conditions.

5.3.5 Residence Time Distribution

To study the residence time distribution, reactor 14 (see Table 5.5) was used. After the inseminations, the feed pump was set at 11 rpm (0.358 ml/min) which corresponds to 3.2 hrs of residence time based on total volume. The reactor was sparged for five minutes every ten hours with the feed pump at 100 rpm. When complete conversion of the glucose was achieved, the reactor was rinsed and the reactor response to a step change in ethanol concentration was measured in the effluent. The ethanol weight percent in the outlet of the reactor was recorded versus time. The data was then analyzed using standard procedures (30) to compute axial dispersion.

5.3.6 Analytical Procedures

5.3.6.1 Ethanol Concentration Measurement

The ethanol content was determined by gas chromatography. The gas chromatograph was a model 5710 A from Hewlett Packard. The column was six feet long, packed with Poropak Q mesh size 80/100 from Supelco. The carrier gas was helium at a flowrate of 2.43 ml/s, the injection port and the detector of the chromatograph were 250°C.

5.3.6.2 Measurement of Immobilized Cell Dry Weight

The following procedures were used to determine the dry weight of the cells immobilized in a reactor, or in each of the four modules that make up the fermentor designed for the cell density profile determination (see characteristics of the chambers in Table 5.6). First one stopped pumping fermentation medium and began pumping fresh water at the same flowrate. The superficial velocity being the same as during fermentation, no additional cell washout was observed. When essentially pure water began to flow from the reactor (after two residence times, approximately) the contents of the reactor, or of each chamber, were poured in beakers. The beakers were then placed in an oven at 60°C for three days. After three days of drying, the packing were weighed. By difference with the weight of the carrier before it was packed in the reactor, one determined the dry weight of cells immobilized on the carrier. To be sure that the packing was really dry, it was put a fourth day in the oven and weighted again to make sure that the weight did not change.

TABLE 5.6 CHARACTERISTICS OF THE FOUR CHAMBER REACTOR

	Total Vol. (Ml)	Mass of Carrier (G)	Liq. Vol. (Ml)	Void Fraction (%)
Chamber #1 (bottom)	14.4	4.8	12.7	88.0
Chamber #2	15.0	5.48	13.2	88.0
Chamber #3	15.2	4.87	13.4	88.0
Chamber #4 (top)	15.6 ---	5.4 ---	13.7 ---	88.0 ---
whole reac.	60.2	20.55	53.0	88.0

Note: The four chamber reactor was packed with the brick. The brick particle size was between 425 and 1397 mic.

5.4 Results and Discussion

5.4.1 Carrier Screening for Surface Immobilization

In order to find a surface immobilization carrier which will improve the reactor performance, reactors 2,3,4,5,7, and 8 were operated. The ethanol content of the outlet medium and the CO2 production rate were recorded versus time during reactor operation. Except for the sparging periods the feed pump was set at 8 rpm; however, only reactors 2,3,4, and 5 were sparged with air. Air was sparged in these reactors after each sampling for five minutes with the feed pump at 100 rpm (4.55 ml/h). During the sparging time no medium was fed in the reactors.

The ethanol concentration in the outlet versus time for the various reactors are reported in Figure 5.2 and Table 5.7. The productivities in Table 5.7 are on a total reactor volume basis.

From the results which are obtained for residence times close enough to allow comparison, it appears that reactor 2 (firebrick) has the best performance. It is the only reactor to reach total glucose conversion (94%) of theoretical) at a residence time of approximately 4.5 Hrs.

5.4.2 Particle Size Influence on the Reactor Performance

5.4.2.1 RESULTS

The reactors 2, 9, 10, 11 and 12 were inseminated and then the cells were grown using the medium with the pump at 8 rpm. Air was sparged using the feed pump for five minutes at 100 rpm after each sampling. This corresponds approximately to five minutes of sparging every twenty hours. After each sparging period, the ethanol concentration in the outlet increased until it reached a maximum. This maximum ethanol concentration is characteristic of each reactor for the residence time corresponding to 8 rpm.

Once the maximum theoretical ethanol concentration was reached the pump was set 11 rpm. After the ethanol concentration stabilized this process was repeated at feedrates of 14 and 17 rpm.

This procedure resulted in a slowly drifting system where the biomass gradually accumulated on the bed as can be inferred from examination of Figures 5.3 and 5.4. Because growth conditions were maintained in the reactor, the overall average productivity (Fig. 5.4) gradually increased until the adverse effects of plugging began to predominate. In each instance, however, a gradual increase in productivity resulted until a maximum was achieved.

TABLE 5.7 ANALYSIS OF REACTOR 3, 4, 5, 6, 7 AND 8 FOR CARRIER SCREENING

Time (Hrs)	CO2 (MicL/S)	ETOH Area %	Feed (Ml/Mn)	Res. Time (Hrs)	ETOH Wt %	Produc. (G/L/Hr)
Reactor #2, brick 1981-3962 microns						
0.00	0.00	0.00	0.24	4.75	0.00	0.00
22.50	57.00	2.58	0.24	4.75	3.44	7.25
43.67	54.80	3.18	0.24	4.75	4.25	8.94
56.67	59.90	3.01	0.24	4.75	4.02	8.46
69.75	62.10	3.56	0.24	4.75	4.75	10.00
91.30	54.10	3.63	0.24	4.75	4.84	10.19
Reactor #3, molecular sieve						
22.50	4.70	0.39	0.24	4.54	0.52	1.15
43.67	5.30	0.39	0.24	4.54	0.52	1.16
56.67	8.96	0.69	0.24	4.54	0.91	2.01
69.75	10.10	0.79	0.24	4.54	1.05	2.32
91.50	12.10	0.95	0.24	4.54	1.26	2.78
Reactor #4, boileezers						
22.50	9.60	0.40	0.24	4.64	0.54	1.16
43.67	12.80	0.54	0.24	4.64	0.72	1.56
56.67	20.10	1.22	0.24	4.64	1.62	3.50
69.75	23.10	1.52	0.24	4.64	2.03	4.37
91.50	24.30	1.81	0.24	4.64	2.41	5.20
Reactor #5, resin						
22.50	10.00	0.00	0.24	4.64	0.00	0.00
43.67	13.40	0.71	0.24	4.64	0.94	2.03
56.67	21.70	2.00	0.24	4.64	2.67	5.75
69.75	19.60	1.52	0.24	4.64	2.02	4.36
91.50	16.80	1.55	0.24	4.64	2.07	4.47
Reactor #6, cotton						
19.0	10.5	1.22	0.26	4.04	1.63	4.03
43.5	11.2	1.21	0.26	4.04	1.62	4.00
52.57	10.6	1.15	0.26	4.04	1.54	3.80
Reactor #7, wool						
19.0	6.58	0.98	0.25	4.41	1.31	2.97
43.5	6.51	1.00	0.25	4.41	1.34	3.03
52.5	6.20	0.91	0.25	4.41	1.22	2.76
Reactor #8, white pine						
19.0	13.40	1.50	0.28	3.89	2.00	5.14
43.5	11.11	1.25	0.28	3.89	1.67	3.86
52.4	11.10	1.23	0.28	3.89	1.64	3.86

The maximum ethanol concentrations observed in the outlet corresponding to each residence time (on a total volume basis) are reported for various particle size in Table 5.8. These data are characteristic of the packing type and the particle size distribution. Figure 5.5 shows the maximum productivites versus the various residence times for the different brick reactors. A datum using calcium alginate beads (2) is also shown.

5.4.2.2 Interpretation

Table 5.8 and Figure 5.5 suggest several comments. First, the size of the brick particles has an important influence on the reactor's performance.

This observation can be interpreted in the following way. The yeast cells are more numerous near the surface of the particle than deep in the pores (electron micrographs also support this observation (31)) and this cell density gradient in the pores can be due to several factors. First, the pores natural tortuosity or the pore plugging by cell growth can make it harder for yeast cells to grow deep in the pores. Secondly, a glucose or oxygen concentration gradient in the pores due to the metabolization by the cells immobilized in the pores can slow down the cell growth rate near the pore mouth. Any, or a combination of, these phenomena would limit the useable volume for cell immobilization in the particle.

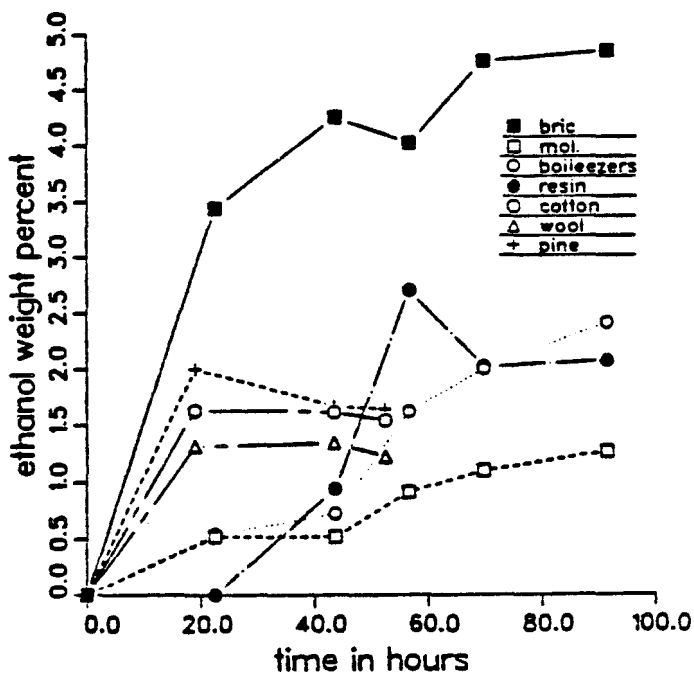

Fig. 5.2 Carrier screening

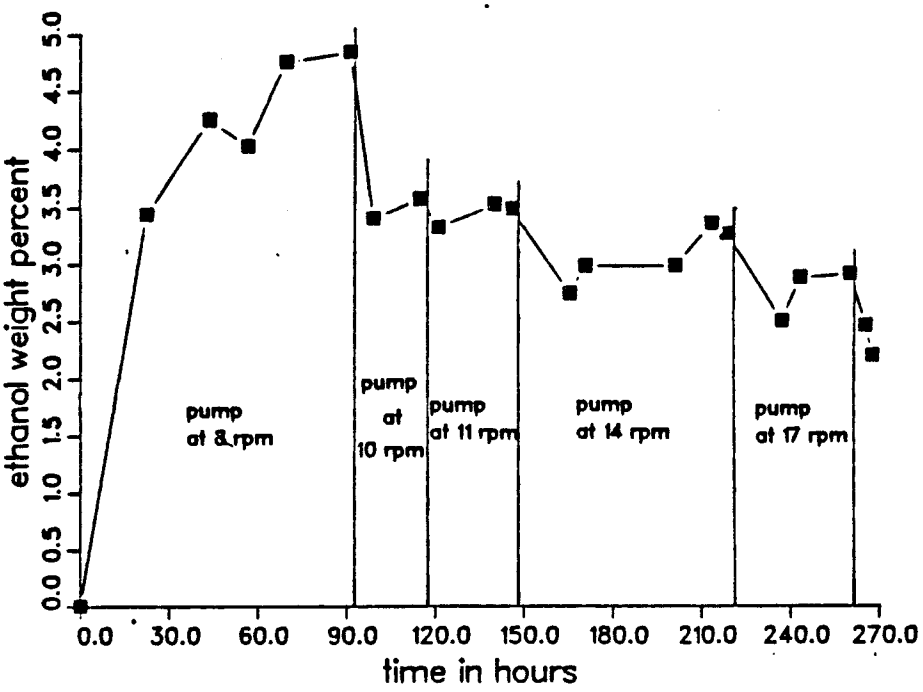

Fig. 5.3 Ethanol versus time for reactor 2 (1981-3962 micron brick pellets)

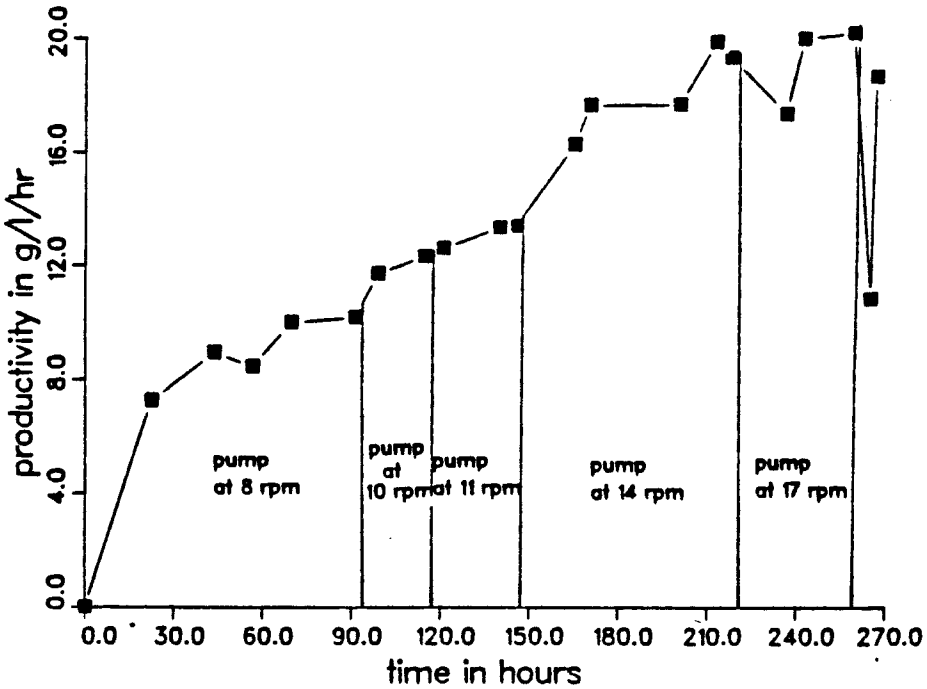

Fig. 5.4 Productivity of reactor 2 versus time.

If, however, the influence of the particle size is due primarily to a limitation of the cell penetration in the particle, then why would a reactor packed with 337 micron diameter particles (reactor 9) have an overall productivity lower than the one of a reactor packed with 911 micron diameter particles (reactor 11)? This result can be due to the fact that the interstitial gas holdup tends to increase with decreasing particle size. Thus, the effective liquid residence times are actually decreased for very small particle size distributions due to this effect.

One can also think of macroscopic limitation to the access of glucose to some particles by channeling that would tend to decrease the performance of the reactor when the particle size diminishes. A positive and a negative influence of the diminishing particle size explains the presence of an optimum particle size which represents the best trade off situation.

Figure 5.5 indicates that the ethanol weight percent in the outlet flow of reactor 11 (optimum particle size) is better than the performance of the calcium alginate encapsulation reactor (Reactor 1 and Figure 5.6) which was operated to verify the accuracy of the experimental techniques. The productivity at complete glucose conversion of reactor 11, 23.2 g/l/hr, compares well with literature data (2) for the encapsulated reactor.

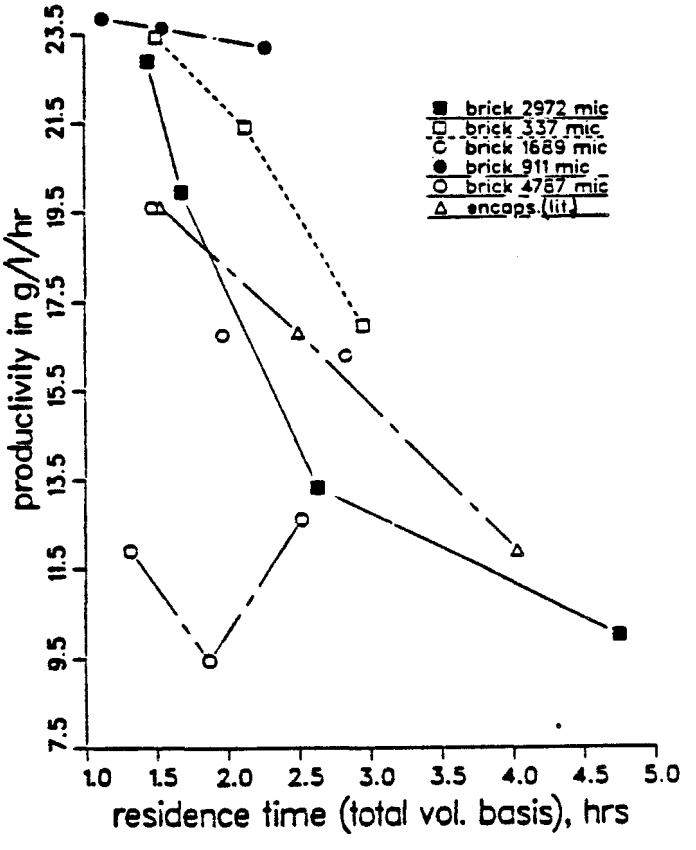

Figure 5.5 Maximal Productivity vs Residence Time for Various Pellet Size

5.4.3 Determination of Cell Dry Weight in the Reactors

5.4.3.1 Overall Cell Dry Weight in the Reactors

The reactors using brick as a carrier (2, 9, 10, 11 and 12) were shut down after thirteen day runs (i.e. the time elapsed from the end of the insemination period until shut down). The dry weight of the cells was then determined. The results are reported in Table 5.9 and they compare well with the published results in Table 5.2. However, they represent average dry cell concentrations that are not uniformly distributed in the reactor as is shown below.

5.4.3.2 Cell Density Profile in the Reactors

The four chamber reactor was used to determine the cell density profile in the reactor. It was packed with the brick, the particle size varies between 425 and 1397 microns as in reactor 11. After insemination, the feed pump was set at 11 rpm and air was sparged every ten hours using the feed pump at 100 rpm. Eleven rpm corresponds to a liquid flowrate of 0.375 ml/hrs and thereby to a residence time of 2.675 Hrs.

After five days, the ethanol area percent given by the gas chromatograph was 3.7% which corresponds to 49.3 ethanol weight percent (96% of theoretical). This confirms the performance of reactor 11 (see Fig. 5.6). After the shutoff and rinsing of the reactor, the dry weight of cells in each reactor chamber was measured. The results are reported in Table 5.10. These results show that for comparable performances the four chamber reactor and reactor 11 have very different overall dry weight of cells immobilized per unit volume of reactor. This result also suggests that after 13 days an significant amount of unavailable (or inactive) biomass is accumulated in reactor 11.

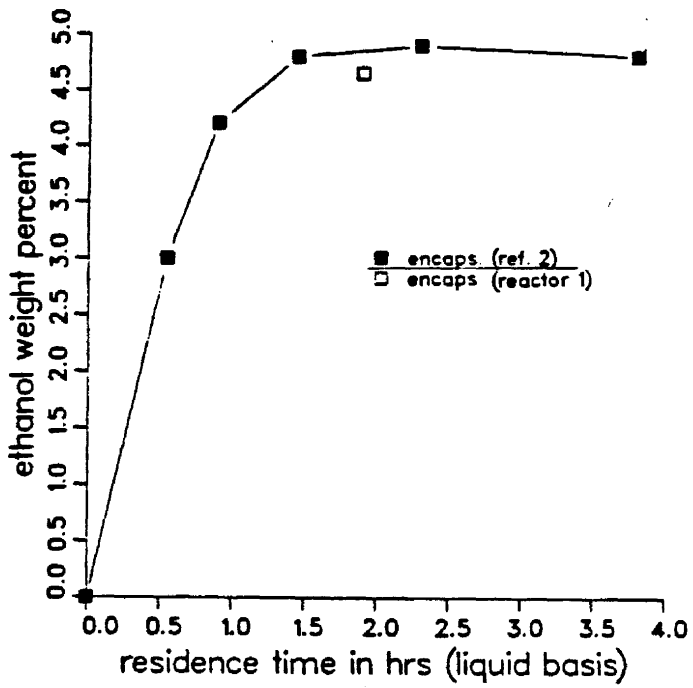

Fig. 5.6 Comparison of encapsulation reactor with published results

TABLE 5.8 PERFORMANCES OF REACTOR 2, 9, 10, 11 AND 12

Pump Rpm	Flowrate (Ml/Mn)	Res. Time (Hrs)	ETOH (Area %)	ETOH (Wt %)	Prod. G/(L-Hrs)
Reactor #2, brick 1981-3962 microns					
8	0.235	4.752	3.570	4.759	10.015
11	0.424	2.634	2.630	3.508	13.321
14	0.662	1.680	2.510	3.348	19.931
17	0.774	1.443	2.475	3.302	22.885
Reactor #9, brick 250-425 microns					
11	0.378	2.954	3.759	5.010	16.959
14	0.524	2.131	3.419	4.558	21.389
17	0.725	1.540	2.705	3.608	23.425
Reactor #10, brick 1397-1981 microns					
11	0.377	2.829	3.453	4.603	16.270
14	5.42	1.968	2.470	3.295	16.743
17	0.725	1.471	2.160	2.882	19.589
Reactor #11, brick 425-1397 microns					
11	0.502	2.271	3.778	5.035	23.189
14	0.706	1.544	2.735	3.648	23.628
17	0.968	1.126	2.013	2.689	23.854
Reactor #12, brick 3962-5613 microns					
11	0.436	2.523	2.382	3.178	12.596
14	0.588	1.871	1.326	1.770	9.461
17	0.835	1.317	1.173	1.566	11.885

The results also show that there was large variation in the amount of cells immobilized with the height of the reactor. This variation is important enough to invalidate the assumption sometimes made (10) that the cell density is constant along the reactor length. This phenomenon is probably due to the fact that because of glucose consumption there is a glucose gradient in the reactor which favors growth in the bottom of the reactor. Added to this factor, the bottom of the reactor consumes the dissolved oxygen and makes growth possible even if no air is sparged. However, the dissolved oxygen concentrations are lower at the top of the reactor. Figure 5.7 shows the dry weight of cells per unit volume of reactor as a function of the position in the reactor. The position in the reactor is given by the volume between the bottom of the reactor and the considered position. The center of the four segments of Figure 5.7 were used as data points to develop a three parameter equation fitting the data. The three parameters are determined using the nonlinear least square method. The fitting equation is:

$$M_{DW} = 110.9e^{-0.0984V} + 4.44 \qquad (5.1)$$

where M_{DW} is in g/L and V is in ml.

The calculated values of M_{DW} versus V are shown in Figure 5.7. Equation 5.1 was used below in the development of a kinetic model.

5.4.4 Residence Time Distribution

From the analysis of the response to the ethanol concentration step, the axial Peclet number of the reactor was calculated (30,31). This number was found to be 24.69 which is too large to consider the reactor as perfect plug flow.

TABLE 5.9 AVERAGE CELL DRY WEIGHT IN REACTORS USING BRICK AS A CARRIER AFTER A 13 DAY RUN.

Reactor #	Total Vol(Ml)	Mass Of Brick (G)	Dw of Cell (G)	Dw/Mass Of Car. (G/G Of Carrier)	Dw/Vol. Of Reac. (G/L Of Reactor)
2	67.0	17.49	2.03	0.12	30.30
9	69.0	28.76	2.22	0.08	32.17
10	64.0	19.19	3.81	0.20	59.53
11	65.4	23.04	5.98	0.26	91.44
12	66.0	16.36	2.92	0.18	44.24

TABLE 5.10 DRY WEIGHT OF CELL IN THE FOUR CHAMBER REACTOR

Chamber #	Total (Vol(Ml)	Mass Of Brick (G)	Liq. Vol. (Ml)	Cell Dw(G)	Dw/Mass Of Car.	Dw/Vol Of Reac. (g/l)
#1 (bottom)	14.4	4.80	12.16	0.85	0.177	59.03
#2	15.0	5.48	12.89	0.26	0.047	17.33
#3	15.2	4.87	12.53	0.11	0.026	7.24
#4 (top)	15.6	5.40	14.07	0.08	0.015	5.12
whole reactor	60.2	20.55	51.65	1.30	0.063	21.59

Note: The data for the whole four chamber reactor are computed in the following manner:

--the total volume is the sume of the volume of the chambers
--the mass of carrier is the sum of the mass of carrier in each chamber
--the liquid volume is the sum of the liquid volume of each chamber
--the void fraction is the ratio of the liquid volume by the total volume (both for the whole reactor)

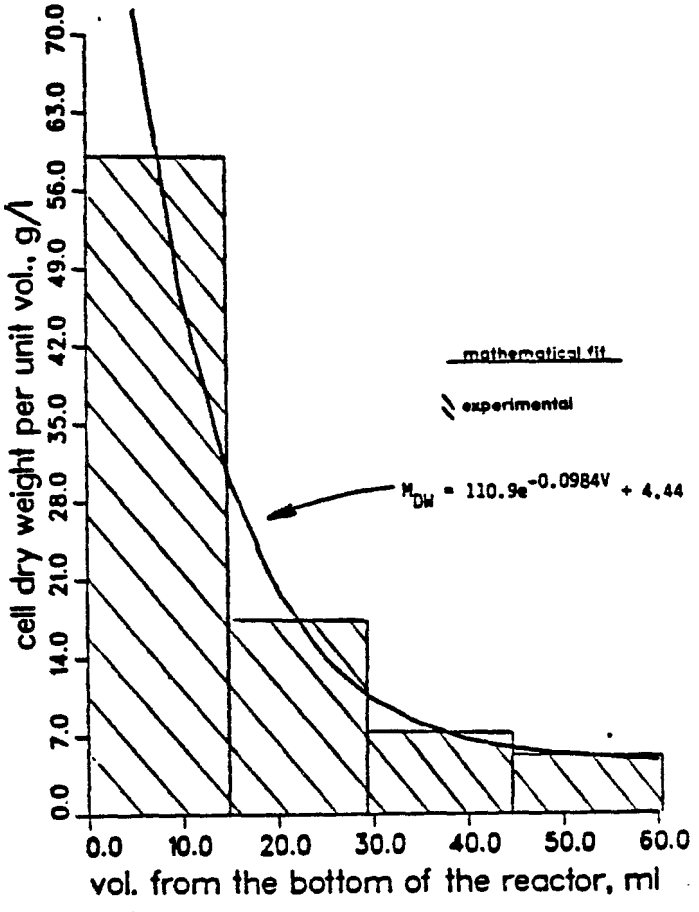

Figure 5.7 Cell Dry Weight Profile in the Four Chamber Reactor

5.4.4 Kinetic Model

A kinetic model was developed to fit the three maximum performance data points of reactor 11. To develop this model the following assumptions were made:

- Hypothesis 1: the cell loading profile of reactor 11 is proportional to the cell loading profile of the four chamber reactor. The proportionality coefficient is the ratio of the average cell dry weight in reactor 11 by the average cell dry weight in the four chamber reactor.

- Hypothesis 2: The active cell loading profile does not depend on the residence time at which the data was taken.

- Hypothesis 3: Each data point corresponds to nearly steady state operation. That is the maximal ethanol weight percent the ethanol concentration profile in the reactor does not depend on time.

- Hypothesis 4: Y_1 the ethanol yield (i.e. the ratio of the mass of ethanol produced to the mass of glucose consumed), is considered constant along the reactor and equal to its average value which can be calculated using the ethanol concentration at the reactor outlet and the glucose concentration at the reactor inlet.

- Hypothesis 5: The Peclet number is constant over the range of experimentally varied linear velocities.

With these assumptions a differential material balance on ethanol can be written leading to:

$$D_z \frac{d^2P}{dZ^2} - \left(\frac{Q}{A\varepsilon}\right)\frac{dP}{dz} + (\mu)\ (R_p) = 0 \qquad (5.2)$$

where
- D_z = the axial dispersion coefficient, in m^2/s
- z = the variable height in the reactor, in m
- P = the ethanol concentration at height z, in kg/m^3
- Q = the volumetric flowrate of the liquid, in m^3/s
- A = the overall cross section of the reactor, in m^2,
- ε = the void fraction of the reactor

M_{DW} = the dry weight of the cell per unit volume of reactor at height z, in kg of cell dry weight/m^3 of reactor,

Rp = the rate of ethanol production, in kg/(s-kg dry weight)

The cell dry weight in reactor 11 was estimated from the cell density profile in the four chamber reactor using Hypothesis one. This approach gives:

$$M_{DW} = 469.9e^{-9.061AZ} + 18.81 \qquad (5.3)$$

where z = the height, in m, of the considered position in reactor 11

A = the average cross section area of reactor 11

D_W = the mass of cell dry weight in reactor 11, in kg/m3,

Then the differential equation was integrated between z=0 and Z (0.3 m) for each set of experimental conditions. For each of these integrations, M_{DW} versus z remains unchanged (Hypothesis 2).

The axial dispersion D_Z was investigated using two alternative hypotheses. In the case of laminar flow with molecular diffusion (32):

$$D_Z = \mathcal{D} + \frac{(U\ d_t)^2}{192\mathcal{D}} \qquad (5.4)$$

where $\mathcal{D}$ is estimated from the experimental pulse test data for the reactor.

Alternatively, over small changes in the linear velocity of the reactor bed, one might expect the axial Peclet number (UL/D_Z) to be nearly constant. In this case (Hypothesis 5):

$$D_Z = D_{Zo}\left(\frac{U}{Uo}\right) \qquad (5.5)$$

In each instance, alternative assumptions concerning the rate limiting reaction step were examined. The models were then tested using the criteria:

$$SSE = \min_{\beta}\left\{\sum_{j=1}^{nobs}(P-\hat{P})^2\ \Big|_{z=0}\right\} \qquad (5.6)$$

where P and $\hat{P}$ were the experimental and predicted sugar concentrations at the reactor inlet. Hence, for each assumed parameter value, numerical integration of the reactor was completed for all data point to compute the sum of the squared errors (SSE). The parameter value was then adjusted to minimize the residual deviations.

Integrations were completed using the experimentally measured ethanol concentration in the ractor effluent as one boundary condition and

$$\left.\frac{\partial P}{\partial Z}\right|_{Z=0.3m} = 0 \qquad (5.6)$$

as the second boundary condition. In other words, the second condition assumes that the free cell activity is negligible (4) at the reactor outlet. Experimentally, conditions were maintained well below the cell slough off velocity.

The integration of Equation 5.2 was completed for two different expressions for Rp and while considering or neglecting the second order term of the differential equation. Rp was first assumed to be of the Monod form with exponential ethanol inhibition.

$$Rp = (R_{LC})M_{DW}e^{-k_1 P}\frac{\mu_{max}C_G}{K_2 + C_G} \qquad (5.7)$$

where R_{LC} is the ratio of available to total cells per unit volume of bed. (on a dry weight basis)
μ_{max} is the specific ethanol productivity, in kg of ethanol/(s-kg of cell dry weight),
k_1 is the second Monod parameter; 0.0167 m^3/kg (Ref. 10),
k_2 is the third Monod parameter; 1 kg/m^2
C_G is the glucose concentration, in kg/m^2.

Using hypothesis four, C_G is given by Eq. 5.8:

$$C_G = C_{GP} - P/Y_1 \qquad (5.8)$$

where C_{GO} = the glucose concentration in the feed; 100 kg/m^3
P = the ethanol concentration at height z, in kg/m^3
Y_1 = the yield at the top of the reactor (Hyp. 4); 0.5035 kg of ethanol produced/kg of glucose consumed

Then Rp was assumed to be of the Monod form without ethanol inhibition.

$$R_P = (R_{LC})M_{DW}\,\mu_{max}\frac{C_G}{k_2 + C_G} \qquad (5.9)$$

Finally Rp was assumed to be controlled by sugar diffusion. In this case the cell gradient is not considered

$$R_p = k_3 C_G \qquad (5.10)$$

For each of these expressions (except the last one), one found by trial and error the value of $(R_{LC}\mu_{max})$ that minimizes the sum of the squares of the residual errors while predicting the ethanol concentration at z=0 given by each set of three integrations. The results are given in Table 5.11.

It is important to note that the equation is nonhomogeneous and numerically unstable if integrated from z=0 to z=0.3 m. However it converges quickly when integrated from z=0.3 to z=0.m.

By dropping the dispersion term, the significance of the second order term was determined. Table 5.11 indicates the sum of the squared errors for each of the cases studied.

TABLE 5.11 APPARENT FIT OF ALTERNATIVE REACTOR MODELS

MODEL	CASE	$(R_{CL}\ \mu_{max})$	SSE
$D_Z \frac{d^2P}{dz^2} - \left(\frac{Q}{Ae}\right)\frac{dP}{dz} + (R_{CL}\mu_{max})M_{DW}e^{-k_1P}\left(\frac{C_G}{k_2+C_G}\right) = 0$			
$D_Z = \mathcal{D} + \frac{(Ud_t)^2}{192\mathcal{D}}$	1	0.0006	138
$D_Z = D_{Zo}\left(\frac{U}{U_o}\right)$	2	0.00055	98
$D_Z \frac{d^2P}{dZ^2} - \left(\frac{Q}{Ae}\right)\frac{dP}{dz} + (R_{CL}\mu_{max})M_{DW}\left(\frac{C_G}{k_2+C_G}\right) = 0$			
$D_Z = \mathcal{D} + \frac{(\mu d_t)^2}{192\mathcal{D}}$	3	0.000356	12.08
$D_Z = D_{Zo}\left(\frac{U}{U_o}\right)$	4	0.000356	0.37
$\left(\frac{Q}{Ae}\right)\frac{dP}{dZ} + (R_{CL}\mu_{max})M_{DW}\left(\frac{C_G}{k_2+C_G}\right) = 0$	5	0.00102	8.04
$D_Z \frac{d^2P}{dZ^2} - \left(\frac{Q}{AE}\right)\frac{dP}{dZ} + (R_{CL}\mu_{max})\ C_G = 0$			
$D_Z = D_{Zo}\left(\frac{u}{u_o}\right)$	6	0.00014	2400

The results in (i.e. the SSE magnitudes) Table 5.11 suggest that a Monod type kinetic expression with no ethanol inhibition fits the data the best. They also suggest that the conversion rate is not limited by substrate diffusion. Reference 2 (using the same yeast strain) also reports reaction kinetics with no ethanol inhibition as long as the ethanol concentration is below 8%. Moreover, the assumption that the Peclet number is conserved appears more valid than laminar flow with molecular diffusion.

Using a specific productivity $\mu max=0.75$ g/(gs (2), the kinetic model suggest that only 40.4% of the cells immobilized in reactor 11 were available (or active) ($R_{CL}=0.403$). Also, the dispersion term improves the data fit significiantly.

5.5 Conclusions

The experimental results suggests that the particle size of a surface immobilization carrier greatly influences the performance of the carrier and that it is possible to use a simple procedure to determine the best particle size. They also suggest that it is possible to find a carrier with performances that compare favorably to encapsulation reactors. However, controlling the cell population appears highly important. Initially, growth is desirable, but cell gradients results probably due to oxygen and glucose gradients within the upflow reactor. Subsequently, continued cell growth leads to bed plugging and productivity losses. Under the conditions of this study, immobilized cell reactors are not stable for extended periods. Hence additional work in culture stabilization is required.

The cell density profile determination shows a very important cell density gradient in the reactor which could be used in further studies to improve the fermenter design, allowing a better use of the fermenter space and preventing early plugging.

The mathematical modelling suggests that the dispersion term characterizing the backmixing of the fermenter cannot be neglected and that the rate limiting step in these experiments was that of substrate metabolization. (i.e. Monod type without inhibition). Although the hypotheses used in this analysis were not entirely valid (e.g. the biomass concentrations were slowly drifting), the nonlinear least squares analysis suggests that it is possible to gain insight into the fundamental behavior of such systems using this approach.

5.6 References

1. M. Kierstan and Bucke, "The Immobilization of Microbial Cells, Subcellular Organelles, and Enzymes in Calcium Alginate Gels". Biotech. Bioen. Vol. 19, page 387-397 (1977).

2. T.H. Lee, J.C. Ahn and Dewey D.Y. Ryu "Performance of an Immobilized Yeast Reactor System for Ethanol Production". Enzyme Microb. Techol., 1983, Vol. 5, January.

3. M. Nagashima, M. Azima, S. Noguchi, K. Inuzuka and H. Samejima, "Continuous Ethanol Fermentation Using Immobilized Yeast Cells". (1983).

4. M. Moo-Young, J. Lamptey and C.W. Robinson "Immobilization of Yeast Cells on Various Supports for Ethanol Production". Biotechnology Letters, Vol. 2, number 12 (541-548).

5. S. Furusaki, M. Seki, K. Fukumura, "Reaction Characteristics of an Immobilized Yeast Producing Ethanol". Biotech. Bioeng., Vol. 25, 2921-2928 (1983).

6. K. Furukawa, E. Heinzle and I.J. Dunn, "Influence of Oxygen on the Growth of Saccharomyces Cerevisiae in Continuous Culture". Biotech. Bioeng., Vol. 25, p. 2293-2317 (1983).

7. A. Navarro, H. Marangoni, I. Magana Plaza, D. Callieri, "Horizontal Reactor For the Continuous Production of Ethanol by Yeasts Immobilized in Pectin". Biotechnology Letters, Vol. 6 number 7 p. 465-470.

8. T.K. Ghose, K.K. Bandyopadhyay, "Rapid Ethanol Fermentation in Immobilized Yeast Cell Reactor". Biotech. Bioeng., Vol. 22, p. 1489-1496 (1980).

9. H.Y. Wang and D.J. Hettwer "Cell Immobilization in K-Carrageenan with Tricalcium Phosphate", Biotech. Bioeng., Vol. 24, p. 1827-1838 (1982).

10. M.A. Gencer, R. Mutarasan "Ethanol Fermentation in a Yeast Immobilized Fermentor", Biotech. Bioeng., Vol. 25, p. 2243-2262 (1983).

11. W.Y. Kuu and J.A. Polack "Improving Immobilized Biocatalysts By Gel Phase Polymerization" Biotech. Bioeng., Vol. 25, p. 1995-2006 (1983).

12. Dewey D.Y. Ryu, Y.J. Kim and J.H. Kim, "Effect of Air Supplement on the Performance of Continuous Ethanol Fermentation System", Biotech Bioeng., Vol. 26, p. 12-16 (1984).

13. H. Tanaka, M. Matsumura, I.A. Veliky, "Diffusion Characteristics of Substrates In Ca-Alginate Gel Beads", Biotech. Bioeng., Vol. 26, p. 53-58 (1984).

14. O.C. Sitton and J.L. Gaddy, "Ethanol Production in a Immobilized-Cell Reactor" Biotech. Bioeng., Vol. 22, p. 1735-1748 91980).

15. P.L. Rogers, Kye Joon Lee and D.E. Tribe, "Kinetics of Alcohol Production By Zymomonas Mobilis at High Sugar Concentrations", School of Biological Technology, University of N.S.W. Sydney Australia. ( ).

16. R.C. Righelato, D.Rose, A.W. Westwood, "Kinetics of Ethanol Production By Yeast in Continuous Culture", Biotechnology Letters, Vol. 3, number 1, p. 3-8 (1981).

17. C. Maignan, J.M. Navarro and G. Durand, "Activite Metabolique de microorganismes Retenus par des Supports Solides", Oecol Plant., 9 (4), 365-382 (1974).

18 M. Wada, J. Kato and I Chibata, "Continuous Production of Ethanol in High Concentration Using Immobilized Growing Yeast Cells", European J. Appl. Microbiol. Biotechnol. 11, 67-71 (1981).

19. B.L. Maiorella, H.W. Blanch, and C.R. Wilke, "Biotechnology Report. Economic Evaluation of Alternative Ethanol Fermentation Processes", Biotech. Bioeng., Vol. 26, September 1984.

20. G. Cysewski and C.R. Wilke, "Process Design and Economic Studies of Alternative Fermentation Methods for the Production of Ethanol", Biotech. Bioeng., Vol. 20, p. 1421-1444 (1978).

21. R.A. Messing, R.A. Oppermann and F.B. Kolot, "Pore Dimensions For Accumulating Biomass. II Microbes that Form Spores and Exhibit Mycelial Growth", Biotech and Bioeng., Vo. 21, p. 59-67 (1979).

22. R.A. Messing and R.A. Opperman, "Pore Dimension For Accumulating Biomass. I. Microbes that Reproduce by Fission or Budding", Biotech. Bioeng., Vol. 21, p. 48-58 (1979).

23. R.A. Messing, "Review. Support Bound Microbial Cells", Applied Biochem. Biotechnol., 6, 167-178 (1981).

24. R.A. Messing, R.A. Opperman and F.B. Kolot "Pore Dimension For Accumulating Biomass", in A.C.S. Symposium Series No. 106, Washington, D.C. (1979).

25. S. Aiba, A. Humphrey and N.F. Millis, Biochemical Engineering, Second Edition, Academic Press, Inc., New York (1973).

26. S. Nagai, "Role of Biotechnology in Bioenergy. Recent Topic of Ethanol, Hydrogen and Methane Production in Japanese Institutes", Energy from Biomass (1984).

27. D.C. Sitton, "Biotechnology and Energy Production Symposium", Gatlinburg, TN.

28. Biotech. Bioeng., Vol. 10, 845 (1968).

29. Peppler and Perlman, Microbial Technology, Second Edition p. 134.

30. Levenspiel, Chemical Reaction Engineering, John Wiley and Sons, New York (1962).

31. Marc J. Anselme, "Immobilized Yeast Reactor for Ethanol Production, MS Thesis, School of Chemical Engineering Georgia Institute of Technology, Atlanta, (1985).

32. J.E. Bailey and D.F. Ollis, Biochemical Engineering Fundamentals, McGraw-Hill, New York, 543, (1977).

CHAPTER 6

LIQUID/LIQUID DATA AND CORRELATIONS
(W.Y. Tawfik)

6.1 Correlations for Liquid/Liquid Equilibrium

6.1.1 2-Parameter Correlation.

Initially, the research effort (1, 2, 3, 4, 5) focused on evaluating both the distribution coefficients and selectivities for the alternative solvents. For a quick evaluation, the tie-line data were obtained initially at a room temperature of about 27°C ±2°C. These single temperature tests provide good initial comparison between the alternative solvents. The distribution coefficients obtained from these tests were then correlated to the ethanol weight fraction in the equilibrated aqueous phase.

$$\ln D_i = a + bx_e \qquad (6.1)$$

where:

D_i = distribution coefficient of component i in weight basis

x_e = weight fraction of ethanol in equilibrated aqueous phase

Parameter estimates were generated for Eqn. 6.1 using linear regression analysis. Table 6.1 summarizes the calculated constants (a) and (b) for 15 different solvents obtained from combinations of five pure solvents together with R^2, the squared correlation coefficient, which is defined as:

$$R^2 = t^2 / (\upsilon + t^2)$$

where:

υ = number of degrees of freedom = $N_{obs} - 2$

t = value for the t-statistic distribution with 95% confidence interval and υ degrees of freedom

The experimental data are summarized elsewhere (5).

The constants of Eqn. 6.1 are specific for the given solvents at a temperature of 27°C ±2°C and they are valid for the values of the equilibrated aqueous concentrations less than the plait point composition. In general the dependence of the water distribution coefficients on the equilibrated aqueous concentration of ethanol is much higher than the ethanol (i.e., b_{ETOH} is less than b_{H2O}). On the other hand, the constant (a) represents the extrapolated value of the logarithm of the distribution coefficient at zero ethanol concentration in the equilibrated aqueous phase and the given temperature.

Table 6.1 The Parameters for the Distribution Coefficient Correlation of Ethanol and Water at 27°C with R^2 the Squared Correlation Coefficient

Solvent[a]	Ethanol			Water		
	a	b	R^2	a	b	R^2
100% 2EHOH	-0.5	1.0	0.56	-4.1	7.3	0.91
100% DMH	-1.7	1.9	0.86	-5.5	6.4	0.99
100%TDOH	-0.72	1.3	0.81	-3.8	4.5	0.97
100% Isopar-L	-7.2	4.5	0.95	-11.8	7.0	0.93
100% Norpar-12	-3.7	0	0.62	-7.9	0	0.71
10% TDOH, 90% Norpar-12	-3.0	1.3	0.64	-6.7	3.7	0.95
20% TDOH, 80% Norpar-12	-2.2	1.5	0.6	-6.0	8.3	0.88
30% TDOH, 70% Norpar-12	-2.1	1.4	0.96	-5.6	7.4	0.7
50% TDOH, 50% Norpar-12	-1.4	1.4	0.61	-5.6	9.1	0.85
50% TDOH, 50% 2EHOH	-0.95	2.5	0.63	-4.0	5.9	0.97
70% TDOH, 30% 2EHOH	-1.1	2.4	0.81	-4.8	7.4	0.98
50% 2EOH, 50% Isopar-L	-1.1	1.25	0.82	-7.1	12.0	0.98
50% Isopar-L, 25% EHOH, 25% TDOH	-0.69	0	0.82	-5.8	6.3	0.93
35% TDOH, 30% Norpar-12, 35% 2EHOH	-1.08	1.35	0.65	-4.6	5.7	0.99
100% Unleaded Gasoline	-2.7	0	0.71	-6.9	6.2	0.95

[a] All the percentages based on volume percentages

Table 6.1 suggests that the solvents containing alcohol or ketone groups exhibit higher values of the constant (a) which means that their ethanol distribution coefficients are higher than those solvents which are composed of mixtures of alkanes even at low ethanol concentrations in the equilibria aqueous phases. On the other hand, alcohols and ketones have much higher values of the distribution coefficients of water than the alkanes. These results agreed with the measured values of the distribution coefficients for ethanol which were obtained from the literature by many investigators (2, 3, 6, 7, 8).

Tables 6.2 and 6.3 summarize the single point test for the distribution coefficients of ethanol measured through this work and other investigators (4, 7, 8) for both recovery solvents and drying solvents. It is clear from Tables 6.2 and 6.3 that the ethanol distribution coefficients for the recovery solvents which contained alcohol or ketone groups had an average value of 0.6 ±0.3, while those for the drying solvents which contained mixtures of alkanes have a maximum value of about 0.06 at the same ethanol concentration in the equilibrated aqueous phases.

Due to the differences between the values of the distribution coefficients for ethanol of the recovery solvents and the drying solvents, it was thought that the blending of a drying solvent with a recovery solvent would improve the ethanol distribution coefficient for the drying solvent. Table 6.4 summarizes the effect of tridecyl alcohol on the equilibrium characteristics of Norpar-12.

Table 6.4 suggests that increasing the percentage of tridecyl alcohol in Norpar-12 yields larger ethanol distribution coefficients. On the other hand, the selectivity of the Norpar-12 is decreased tremendously with increasing percentage of TDOH. Figures 6.1 through 6.4 also show the effect of tridecyl alcohol on the solubility curve of ethanol-water-Norpar-12 systems.

6.1.2 The Effect of Temperature on the Equilibrium Data.

When the tie-line data was obtained at higher temperatures than room temperature, it was clear that the temperature represented another variable that may be exploited. The dependence of the distribution coefficients for ethanol and water on both the temperature and the ethanol concentration on the equilibrated aqueous phase is shown below:

$$\ln D_i = a^* + [b^* x_e] + [c^*/T] \qquad (6.2)$$

where:

x_e = ethanol weight fraction in the equilibrated aqueous phase

T = temperature, °K

Table 6.2 The Measured Distribution Coefficients for Solvents Containing Ketone and Alcohol Groups

Solvent	De at Xe=0.05	De at Xe=0.15	De at Xe=0.3
100% 2-Ethyl hexanol[a]	0.637	0.704	0.819
100% Tridecyl alcohol	0.519	0.592	0.719
100% dimethyl heptanone	0.201	0.243	0.323
50% TDOH 50% 2EHOH	0.438	0.563	0.819
100% 3-Heptanol[b]	0.798	0.870	0.990
100% Di-n-propyl ketone	0.639	0.693	0.784
100% n-amyl alcohol[c]	0.657	0.869	0.999

Table 6.3 The Measured Distribution Coefficients for Alkanes

Solvent	De at Xe=0.3	De at Xe=0.5	De at Xe=0.7
100% Isopar-L[a]	0.003	0.007	0.017
100% Norpar-12	0.008	0.016	0.024
100% Unleaded Gasoline	0.06	0.07	0.18
100% N-Heptane[d]	0.05	0.09	0.14
100% N-Hexane[e]	0.0085	0.02	-
100% N-Octane	0.007	0.013	-
100% N-Decane	0.006	0.01	-
100% Hexa-decane	0.005	0.007	-

[a] data obtained by this work

[b] data obtained by D.F.Othmer(6)

[c] data obtained by Van Winkle (8) in 1952

[d] data obtained by Schweppe (7) in 1954

[e] data obtained by Roddy and Coleman( ) in 1981

The constant a^* represents the natural logarithm of the extrapolated value of the distribution coefficient at zero ethanol concentration in the equilibrated aqueous phase, while the constant b^* represents the measure of dependence on the distribution coefficients on the equilibrium aqueous phase concentration of ethanol.

In general, as the temperature increases, the solvent loading also increases and more ethanol and water are extracted. The temperature has a similar effect on both the recovery and the drying solvents except that the distribution coefficients of water are less sensitive to temperature in the case of the drying solvents. Therefore, their selectivities also increase with the temperature as well as their ethanol loading. Consequently, running the drying cycle extractor at higher temperatures results in a dryer product and higher ethanol recovery.

The experimental data were correlated in the form of Eqn. 6.2. Table 6.5 summarizes the values of the constants a^*, b^* and c^* for these four solvent systems.

Table 6.4 The Effect of Tridecyl Alcohol on the Ethanol Distributor Coefficients and the Selectivity of Norpar 12

Solvent	D_e	D_w	Selectivity
100% Norpar-12[a]	0.024	0.0004	60
10% TDOH 90% Norpar-12	0.056	0.0017	33
20% TDOH 80% Norpar-12	0.129	0.0056	22
30% TDOH 70% Norpar-12	0.141	0.0077	20
50% TDOH 50% Norpar-12	0.283	0.0091	19

[a]All the values were calculated at ethanol weight fraction in the equilibrated aqueous phase of (0.1).

Table 6.5 Empirical Correlations for Ethanol and Water Extraction into Several Organic Solvents

Solvent [b]	Solute	a^*	b^*	c^{*a}	R^2
2-Ethyl hexanol	Ethanol	2.8	1.77	-1063	0.88
	Water	-0.76	6.95	-973	0.95
Isopar-L	Ethanol	1.86	1.44	-1922	0.92
	Water	-5.18	4.89	-1321	0.74
Dimethyl heptanone	Ethanol	8.68	1.61	-3084	0.89
	Water	4.21	5.5	-2880	0.78
20% Tridecyl alcohol in Norpar-12	Ethanol	5.4	3.19	-2310	0.95
	Water	-0.16	4.23	-1549	0.92

[a] The applicable range of Temperature is between 20°C and 85°C

[b] The correlation is applicable up to the plait point

[c] The correlation is applicable up to X_e=0.8

[d] The correlation is applicable up to X_e=0.5

[e] The correlation is applicable up to X_e=0.7

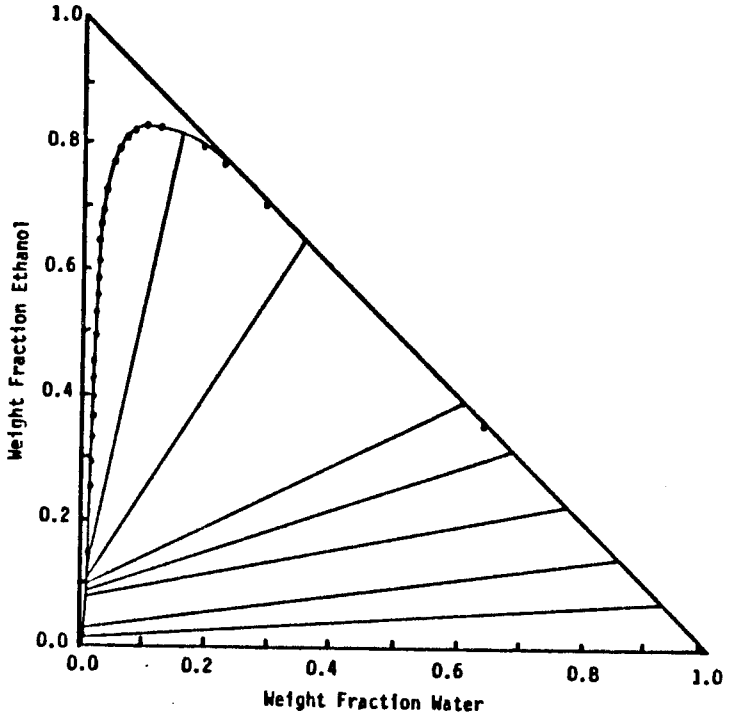

Fig. 6.1 Mutual solubility curve for the system: ethanol, water, and the solvent 10 vol % tridecylalcohol in NORPAR-12.

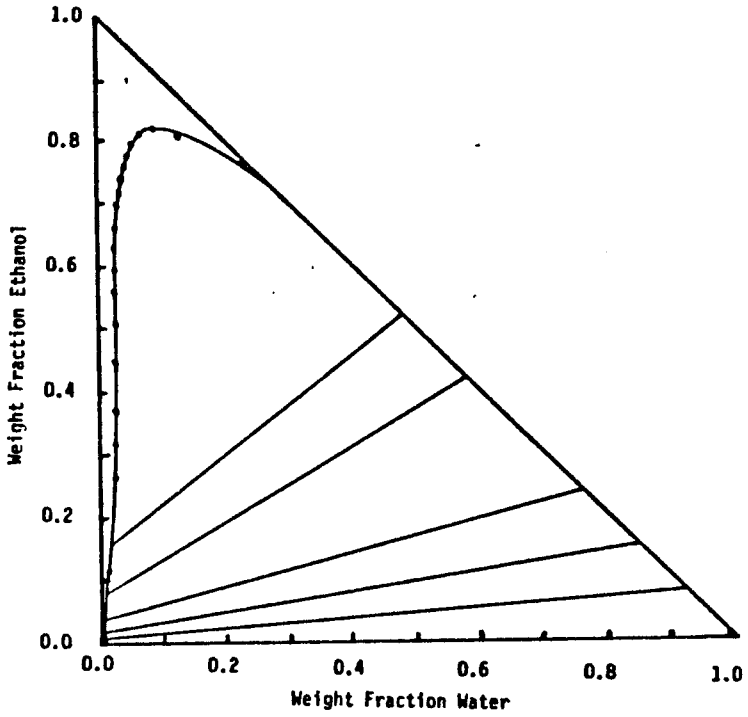

Fig. 6.2 Mutual solubility curve for the system: ethanol, water, and the solvent 20 vol % tridecyl alcohol in NORPAR-12.

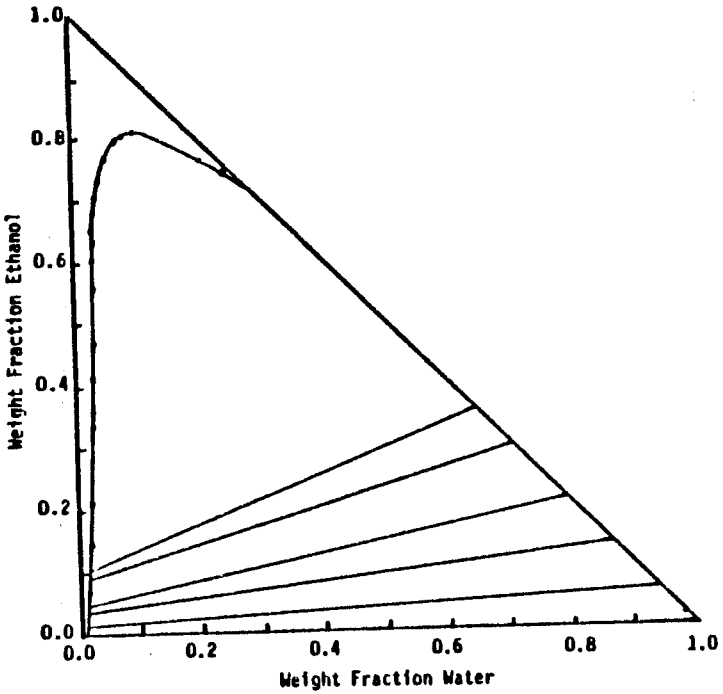

Fig. 6.3 Mutual solubility curve for the system: ethanol, water, and the solvent 30 vol % tridecyl alcohol in Norpar-12

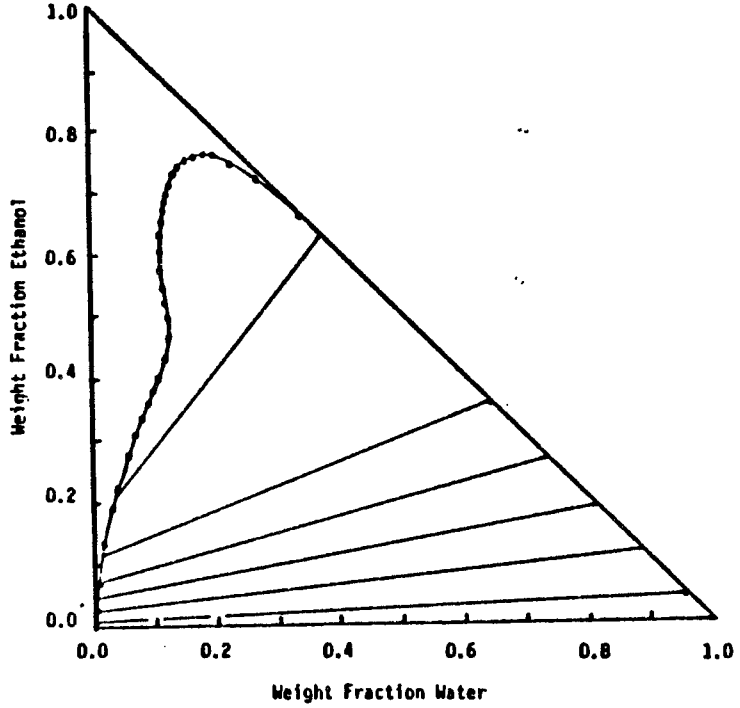

Fig. 6.4 Mutual solubility curve for the system: ethanol, water, and the solvent 50 vol % tridecyl alcohol in NORPAR-12.

6.2 The Effect of Dextrose on Distribution Coefficients

Simultaneous tests were made to determine the effects of temperature, the percentage of modifier, and the percentage of the dextrose on the distribution coefficients and the selectivities. The experimental results suggested an increase in the activity of the water in the aqueous phase occurs due to the presence of the dextrose. This effect was realized for the solvents, TBP in Isopar-M, and this increase resulted in an increase in ethanol distribution coefficients. However, no significant increase in the selectivity was noticed. On the other hand, the dextrose effect was insignificant for some of the dryer solvents such as the methyl ester (CE-1218) comparing to the temperature.

The basic model for the distribution coefficients of ethanol and water is proposed in the following form:

$$D_i = f(X_e, X_D, \varphi_m, 1/T) \quad i = \text{ethanol,water} \tag{6.3}$$

For each solvent the non-linear least square technique (NONLS2) (9) was used to fit the parameters of the models. The check on the statistical significance of the non-linear model was the measure of omitting the variable interactions. The general form of the correlation is found to be:

$$\ln D_i = [a_0] + [a_1 x_e^2] + [a_2 x_e] + [a_3 x_D] + [a_4 x_D^2] + [a_5 \varphi_m] + [a_6/RT] \tag{6.4}$$

where i = ethanol or water and:

D_i = distribution coefficient of component i on weight basis

x_i = weight fraction of component i in the equilibrated aqueous phase

T = temperature, °K

φ_m = volume fraction of modifier

The experimental data in Appendix B were fitted to Eqn. 6.4 using a non-linear least square program to minimize the objective function

$$S_i = \Sigma [D_{ij}(exp) - D_{ij}(calc)]^2$$

where:

i = ethanol, water

$j = 1,2,\ldots,N_{obs.}$

The parameters for Eqn. 6.4 are summarized in Tables 6.6 and 6.7 for the solvents TDOH/Isopar-M, TBP/Isopar-M, and methyl ester, respectively. The variation of the parameter values can be explained by proposing different extraction mechanisms for ethanol and water, and the formation of different complexes. Although the model does not predict the plait point equilibrium composition, it can be used with reasonable accuracy in the practical range of extraction (low ethanol concentration).

6.3 Prediction of the Mutual Solubility Curve Using the UNIQUAC Model

Since all the liquid/liquid systems which are included in this work contain water/ethanol mixtures in addition to different organic solvents, there are very few models available which can predict the equilibrium composition with an acceptable range of accuracy. In general, a good model should describe the nonideality caused by the presence of the polar components (e.g. ethanol and water) and their degree of association.

For any component i, the UNIQUAC liquid activity coefficient is given by:

$$\ln \gamma_i = [\ln(\varphi_i/x_i)] + [(z/2)q_i \ln(\theta_i/\varphi_i] + L_i - [(\varphi_i/x_i)\Sigma x_j L_j] - [q_i' \ln \Sigma\theta_j'\tau_{ji})] + - [q_i'\Sigma\{\theta_i'\tau_{ij}\}/\Sigma\{\theta_k'\tau_{kj}\}] \quad (6.5)$$

where:

$$\varphi_i = (r_i x_i)/\Sigma r_j x_j \quad (6.6)$$

$$\theta_i = (q_i x_i)/\Sigma q_j x_j \quad (6.7)$$

$$\theta_i' = (q_i' x_i)/\Sigma q_j' x_j \quad (6.8)$$

$$L_j = [z/2\,(r_j - q_j)] - (r_j - 1) \quad (6.9)$$

Equation 6.5 requires only the pure component segment and area fractions (φ_i, θ_i) and the binary parameters, which are given by:

$$\tau_{ij} = \exp(-\Delta U_{ij}/RT) \quad (6.10)$$

The data sources for the interaction binary parameter τ_{ij} as cited by Prausnitz (10) are:

1. Vapor-liquid Isotherms (P, y, x)
2. Vapor-liquid Isobars (T, y, x)
3. Total Pressure data (P, x or y)
4. Boiling or dew point data
5. Mutual solubility data
6. Azeotropic data
7. Activity coefficients at infinite dilution.

Table 6.6 The parameter values of Eqn. 4.16 for water

Solvent Parameter	TDOH/ Isopar-M	TBP/ Isopar-M	Methyl Ester CE-1218
a_0	-1.280	-5.810	-5.131
a_1	0.000	0.000	0.000
a_2	3.530	3.880	2.780
a_3	-0.495	1.230	1.390
a_4	0.000	0.000	0.000
a_5	8.660	5.060	0.000
a_6	-3631.300	-652.300	-651.420
Standard Error	0.0029	0.0034	0.0006

Table 6.7 The parameter Values of Eqn. 4.16 for ethanol

Solvent Parameter	TDOH/ Isopar-M	TBP/ Isopar-M	Methyl Ester CE-1218
a_0	2.22	1.602	2.943
a_1	2.50	58.470	-34.137
a_2	-1.03	-19.290	8.144
a_3	1.20	0.985	-9.235
a_4	0.00	0.000	37.170
a_5	0.40	3.780	0.000
a_6	-3198.40	-1994.900	-2863.900
Standard Error	0.282	0.248	0.080

In this work liquid/liquid equilibrium data and isobaric vapor/liquid experimental data were used to estimate the binary interaction parameters τ_{ij}.

The experimental weight fractions of the two liquid phases in equilibrium are summarized in Tables B8 through B10 (Appendix B) for the systems 2-ethyl-hexanol, methyl ester and Isopar-M, respectively.

For a multicomponent liquid-liquid system:

$$x_i \gamma_{xi} = y_i \gamma_{yi} \tag{6.11}$$

where:

x_i = mole fraction of component i in x-phase

γ_{xi} = activity coefficient of component i in x-phase

y_i = mole fraction of component in y-phase

γ_{yi} = activity coefficient of component in y-phase

Then

$$\Sigma \{ x_j \gamma_{xj} / \gamma_{yj} \} = 1 \tag{6.12}$$

For a three-component system, there are always two independent relations and the third dependent one is given by:

$$x_3 \gamma_{x3} / \gamma_{y3} = 1 - [x_1 \gamma_{x1} / \gamma_{y1}] - [x_2 \gamma_{x2} / \gamma_{y2}] \tag{6.13}$$

The non-linear least square algorithm (NONLS2) (9) was used to fit the UNIQUAC binary interaction parameters τ_{ij} in Eqn. 6.5. The objective function was to minimize the sum of squares of the two independent relations in Eqn. 6.12.

$$\text{Min} \Sigma \{ [(x_1 \gamma_{x1}/\gamma_{y1})_{j\,calc} - (x_1 \gamma_{x1}/\gamma_{y1})_{j\,obs}]^2 + [(x_2 \gamma_{x2}/\gamma_{y2})_{j\,calc} - (x_2 \gamma_{x2}/\gamma_{y2})_{j\,obs}]^2 \} \tag{6.14}$$

where $j = 1,2,\ldots,N_{obs}$.

The estimated binary interaction parameters obtained from the liquid/liquid equilibrium data are summarized in Table 6.8.

The UNIQUAC interaction parameters (τ_{ij}) are strong functions of temperature. The relation is given by:

$$\tau_{ij} = \exp [(-\alpha_{ij}/T) - (\beta_{ij}/T^2)] \tag{6.15}$$

However, the parameters α_{ij} and β_{ij} are difficult to estimate from the mutual solubility data since the temperature variation was relatively small in the liquid/liquid experimental data. On the other hand, Table 6.8 exhibited different fitted values for the

Table 6.8 UNIQUAC Parameters

System Parameter	Methyl Ester 20°C	Methyl Ester 65°C	2EHOH 20°C	2EHOH 70°C	Isopar-M 25°C
τ_{12}	1.66894	0.073023	0.1876	0.15057	0.6916
τ_{13}	2.08981	0.76398	1.5677	0.70781	1.40359
τ_{21}	0.024711	0.027557	1.28686	2.48834	0.17337
τ_{23}	0.973E-11	1.49449	0.39089	0.91765	0.37363
τ_{31}	0.718E-3	0.0021565	0.318617	2.80112	0.393E-9
τ_{32}	0.023036	0.0014876	0.189968	0.06166	0.00291
Standard Error	0.001843	0.00587	0.00791	0.00776	0.00150

Component:

1: ETOH

2: H_2O

3: Solvent

same binary interaction parameters in Table 7.3. This variation was due to using the ternary mutual solubility data to fit binary parameters. The investigator recommends using the VLE binary data to obtain the binary parameters.

This study suggested that UNIQUAC interaction parameters are not unique, and their values are strong functions of the type of fit (i.e. the regression variables) and the source of data (e.g. VLE versus LLE).

The use of the UNIQUAC model for LLE design calculation would require iterative calculations. The distribution coefficient correlation was preferred for LLE prediction, because it can be easily implemented in an integrated modular sequential design program, such as RUNOPT.

6.4 References

1. J.W. Roddy and C.F. Coleman, "Distribution and Miscibility Limits in the System Ethanol-Water-TBP", Oak Ridge National Laboratory, (1981).

2. J.W. Roddy, "Distribution of Ethanol Water Mixtures to Organic Liquids", Ind. Eng. Chem. Process Des. Dev., vol. 20, (1981), pps. 104-108.

3. J.W. Roddy and C.F. Coleman, "Distribution of Ethanol-Water Mixtures to Normal Alkanes from C_6 to C_{16}", Ind. Eng. Chem. Fundam., vol. 20, (1981), pps. 250-254.

4. D.W. Tedder, et al., Fuel Grade Ethanol Recovery by Solvent Extraction, Technical Progress Report, Georgia Institute of Technology, (October 1982).

5. W.Y. Tawfik, "Efficiency of Ethanol Extraction from Aqueous Mixtures", M.S. thesis, Georgia Institute of Technology, (1982).

6. D.F. Othmer, R.F. White, and E. Trueger, "Liquid-Liquid Extraction Data", Industrial and Engineering Chemistry, vol. 33, no. 10, (1941), pg. 1240.

7. J.L. Schweepe and J.R. Lorah, "Ternary System Ethyl Alcohol-n-Heptane-Water at 30°", Ind. and Eng. Chemistry, vol. 46, no. 11, (1941), pg. 2391.

8. C.M. Qualline and Van Winkle, "Ternary Liquid Systems", Ind. and Eng. Chemistry, vol. 44, no. 2, (1952), pg. 1668.

9. D.W. Marquardt, "An Algorithm for Least Squares Estimation of Non-Linear Parameters", J. Soc. Ind. Appl. Math., vol. 11, no. 2, (1962), pg. 431.

10. J. Prausnitz et al., Computer Calculations for Multicomponent Vapor Liquid and Liquid Liquid Equilibria, Prentice Hall, (1980).

CHAPTER 7

EXPERIMENTAL RESULTS AND DISCUSSION
(W. Y. Tawfik)

7.1 Vapor-Liquid Equilibrium

The need for a vapor-liquid equilibrium model existed for the simulation of the extractive distillation and the solvent regeneration columns. A literature review (1) indicated that liquid activity coefficient models would be appropriate to predict vapor-liquid equilibrium for the systems of interest to this study. That was due to the presence of highly non-ideal components which have strong hydrogen bonds, and therefore strong interaction effects (solvation, association) were expected. Two liquid activity coefficient models (UNIQUAC and UNIFAC) were highly recommended by the literature for their capability to handle these systems.

7.1.1 Estimation of Antoine Vapor Pressure Parameters.

The Antoine equation was used to predict the vapor pressures for pure components. A non-linear least square program (NONLS2) (2) was used to fit the experimental data to obtain Antoine vapor pressure parameters, which are given by:

$$\ln P^v = A_{vp} - B_{vp}/(T + C_{vp}) \qquad (7.1)$$

where T = temperature, °K.

The optimum Antoine parameters were found by minimizing the objective function:

$$S = \Sigma\{[(P_v^o - P_v^e)_j^2] + [(T^o - T^e)_j^2]\} \qquad (7.2)$$

The parameters for Antoine's vapor pressure equation are summarized in Table 7.1 for the solvents of interest. The experimental data that were used to generate these estimates appear in Appendix A.

For higher molecular weight solvents, the constant C_{vp} had a negative value, causing a problem in the optimization. Therefore, for optimization purposes, the constant C_{vp} was set to zero, and Eqn. 7.1 was then reduced to:

$$\ln P^v = A_{vp} - (B_{vp}/T) \qquad (7.3)$$

where T = temperature, °K.

Isobaric binary VLE datam were then obtained experimentally for selected solvent systems. The binary VLE determination allowed a second screening for the solvents on the basis of their stabilities at high temperatures. Solvents such as tributyl

Table 7.1 Vapor Pressure Correlations for VLE Analysis. All pressures in mm Hg. All temperatures in °K.

Species	A_{vp}	B_{vp}	C_{vp}	Model Standard Deviation
Isopar-M	17.07	5262.1	0.0	± 1.06
Isopar-M	17.33	5494.9	9.8	± 1.13
Tri-n-butyl phosphate	66.91	125254.0	1524.4	±12.82
Tri-n-butyl phosphate	20.58	7759.7	0.0	±14.49
Tridecyl Alcohol	22.37	8259.4	0.0	±11.20
Tridecyl acetate	44.68	52473.3	845.3	±8.31
Diisopropyl ketone	8.05	152.5	-328.5	±29.70
2-ethyl-hexanol	23.06	9179.6	102.8	± 2.10
Methyl ester, CE-1218	9.83	1173.5	-166.5	±17.20

phosphate and the methyl ester (CE-1218) were eliminated because of the tendency to decompose, and form butanol and methanol.

7.2 Thermodynamic Consistency Test

Binary vapor-liquid equilibrium data consist of pressure, temperature, and composition of both phases. Only two of the experimental values (e.g. P, y) are enough to completely characterize the system. The additional experimental information may be used to test the data for thermodynamic consistency.

The most reliable consistency test requires calculation of the vapor phase composition from P-X or T-X data and then comparison of the calculated Y's with the experimentally obtained values (3). The smaller the difference between Y_{exp} and Y_{calc} the more thermodynamically consistent the data. The consistency test used in this work was developed by Abbott and Van Ness (4) and programmed for detailed calculations by Fredenslund et al. (3).

The starting point in the test uses the differential expression of Gibbs free energy for an open homogeneous system. The total Gibbs free energy depends on temperature, pressure, and the number of moles of each component, n_i:

$$d(n_T G) = n_T V dP - n_T S dT + \Sigma G'_i dn_i \quad i = 1,2,...,m \qquad (7.4)$$

where:

dP = differential pressure

dT = differential temperature

G = molar Gibbs free energy

n_i = number of moles of component i

V = molar volume

S = molar entropy

G'_i = partial molar Gibbs free energy of component i.

By definition,

$$n_T = \Sigma n_i \text{ and } G'_i = RT \ln \gamma_i \quad i = 1,2,...,m$$

For a system with two phases in equilibrium, Eqn. 7.4 may be expressed for non-isothermal, non-isobaric systems as follows:

$$\Sigma x_i d \ln \gamma_i - (V^E/RT)_i dP + (H^E/RT^2)_i dT = 0 \quad i = 1,2,...,m \qquad (7.5)$$

where V^E and H^E are the excess volume and enthalpy, respectively.

For isobaric data at low pressures, the Gibbs-Duham equation (Eqn. 7.5) can be reduced to:

$$\Sigma x_i . d \ln \gamma_i = 0 \quad i = 1,2,...,m \tag{7.6}$$

and

$$P = \Sigma y_i P = \Sigma [(x_i \gamma_i F_i) / \Phi_i] \tag{7.7}$$

Applying Eqns. 7.6 and 7.7 to a binary system results in:

$$P = x_1 P_1^S (\Phi_1^S/\Phi_1) \exp\{g + x_2 g' + [V_1(P-P_1^S)/RT]\} + x_2 P_2^S (\Phi_2^S/\Phi_2) \exp\{g - x_1 g' + [V_2(P-P_2^S)/RT]\} \tag{7.8}$$

where:

$$g = G^E/RT$$

$$\ln \gamma_1 = g + x_2 g'$$

$$\ln \gamma_2 = g - x_1 g'$$

$$g' = (dg/dx_1)_s \; g = 0 \text{ for } x_1 \text{ and } x_x = 0$$

and where:

G^E = excess Gibbs free energy

γ_i = liquid activity coefficient of component i

P = total pressure

T = system temperature

The subscript S implies saturation conditions.

The liquid phase activity coefficient is calculated from

$$\gamma_i = (Y_i P \Phi_i) / (x_i f_i^o)$$

Fredenslund et al. (3) expressed $g(x_1)$ through the use of Legendre polynomials by:

$$g = G^E/RT = x_1(1-x_1)\Sigma a_k L_k(x_1) \quad k = 0,1,...,n \tag{7.9}$$

where

$$L_k(x_1) = [(2k-1)(2x_1-1)L_{k-1}(x_1) - (k-1)L_{k-2}(x_1)] / k \tag{7.10}$$

$$L_0(x_1) = 1 \; , \; L_1(x_1) = 2x_1 - 1$$

The procedure is based on fitting Legendre polynomials for $g(x_1)$ to the experimental P-T-x_i data. The results are sets of values for y_i(calc) corresponding to the experimental T-x_i values. The isobaric data are considered consistent if the average difference between y_i(calc) and y_i(exp) is less than 0.015. The choice of 0.015, however, is considered to be arbitrary. In most cases this number corresponds to a reasonable value for the sum of errors in the measured liquid and vapor phase mole fractions for high boiling point components. Fredenslund recommended Legendre polynomials of third order for isobaric data. The results of the consistency tests for the experimental isobaric binary data for ethanol-water-Isopar-M-tridecyl alcohol systems are summarized in Figures 7.1 through 7.4. The Legendre coefficients are summarized in Table 7.2.

According to the previous criteria, Figures 7.1 through 7.4 suggested that the isobaric VLE data are thermodynamically consistent. However, for mixtures with large boiling point difference (e.g. ethanol - TDOH) the experimental error was biased. In general, isobaric experimental data for such mixtures are relatively harder to obtain accurately because of the difficulty of controlling the lower system pressures.

7.3 UNIQUAC Liquid Activity Coefficient Model for VLE

The UNIQUAC model proposed the following forms of the molar excess Gibbs energy:

$$g^E = g^E \text{(combinatorial)} + g^e \text{(residual)} \tag{7.11}$$

For the binary mixtures:

$$g^E\text{(combinatorial)} / RT = [x_1 \ln(\Phi_1/x_1)] + [x_2 \ln(\Phi_2/x_2)] + (z/2)[q_1 x_1 \ln(\theta_1/\Phi_1) + q_2 x_2 \ln(\theta_2/\Phi_2)] \tag{7.12}$$

$$g^E\text{(residual)}/RT = -q_1' x_1 [\ln(\theta_1' + \theta_2' \tau_{21})] - q_2' x_2 [\ln(\theta_2' + \theta_1' \tau_{12})] \tag{7.13}$$

where the coordination number z is set equal to 10 and segment fraction, Φ, area fraction, θ and θ', for any mixture with m components, are given by:

$$\Phi_i = r_i x_i / \Sigma r_i x_i \tag{7.14}$$

$$\theta_i = q_i x_i / \Sigma q_i x_i \tag{7.15}$$

$$\theta_i' = q_i' x_i / \Sigma q_i' x_i \tag{7.16}$$

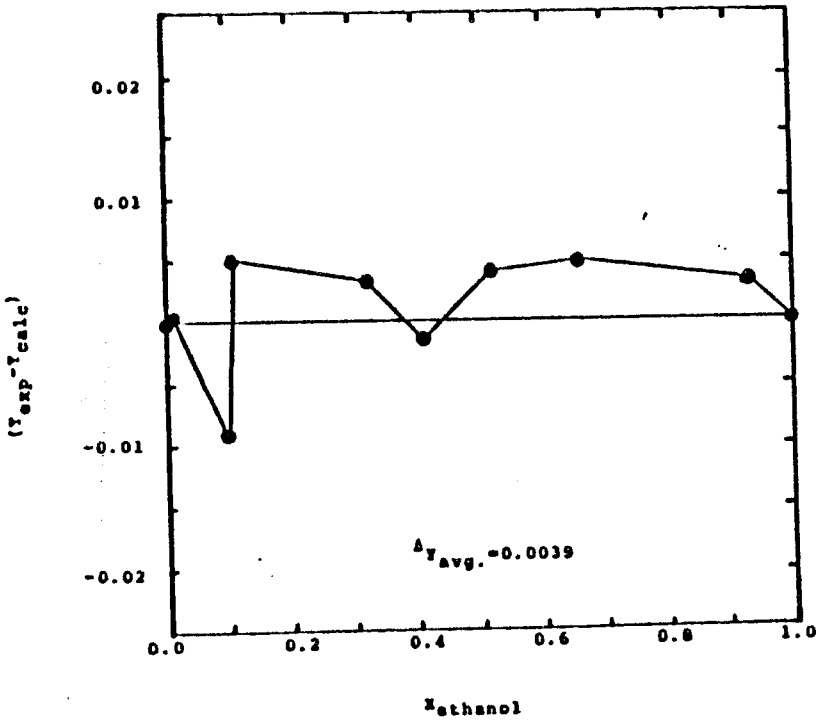

Fig 7.1 Ethanol Water Consistency Test

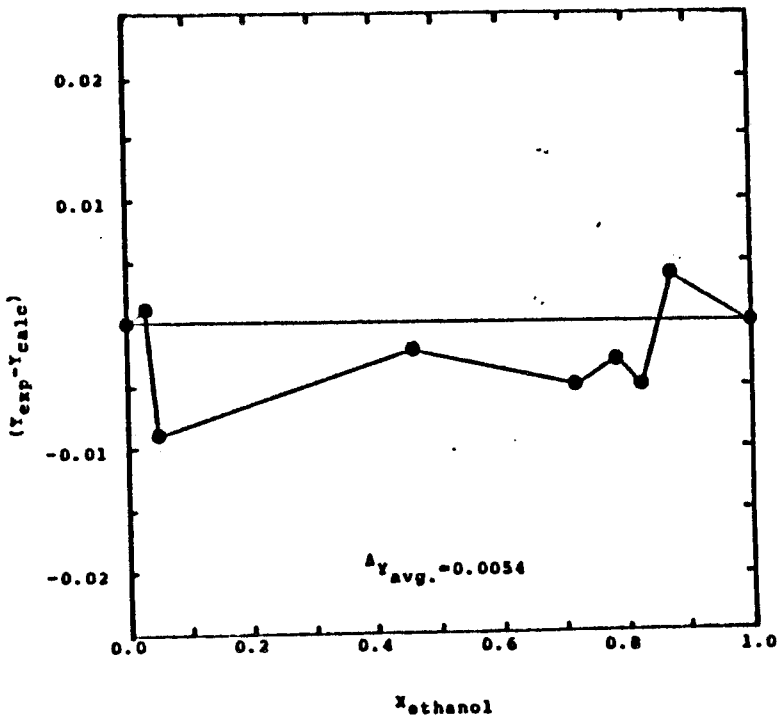

Fig. 7.2 Ethanol-Isopar-M Consistency Test

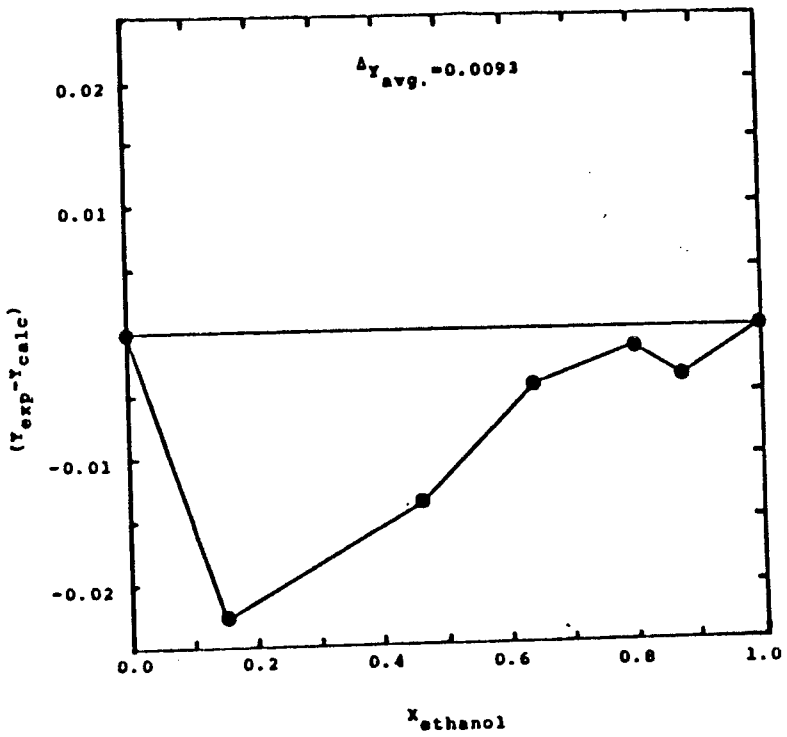

Fig. 7.3 Ethanol-Tridecyl Alcohol Consistency Test

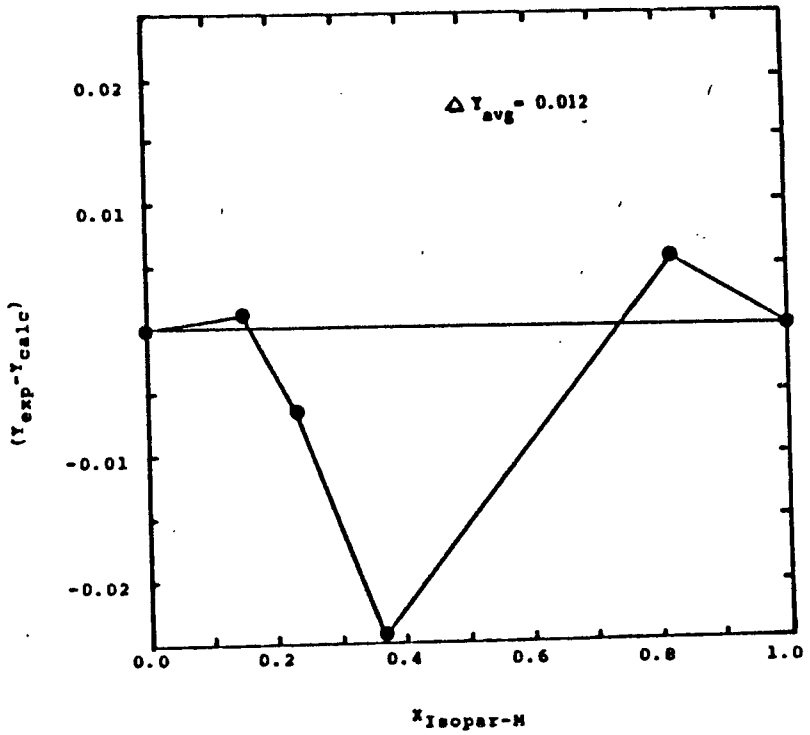

Fig. 7.4 Isopar-M-Tridecyl Alcohol Consistency Test

Table 7.2 Legendre Coefficients

a_k	Ethanol/Water	Ethanol/Isopar-M	Ethanol/TDOH	Isopar-M/TDOH
a_1	1.253	1.891	1.144	3.14
a_2	0.412	0.904	0.020	1.49
a_3	0.013	0.380	2.243	1.225

Table 7.3 UNIQUAC Interaction Parameters Predicted From Binary VLE Systems

Binary System	a_{12}	a_{21}
1-Water 2-ETOH	329.49	-29.43
1-Water* 2-Isopar-M	348.66	762.37
1-Water* 2-TDOH	326.10	342.40
1-ETOH 2-Isopar-M	-117.10	1839.30
1-ETOH 2-TDOH	332.80	35.20
1-Isopar-M 2-TDOH	887.14	-348.89

* values obtained from (50)

$\sigma_x = 0.005$
$\sigma_y = 0.005$
$\sigma_T = 0.5^{\circ}K$
$\sigma_p = 2$ mm Hg

For each binary combination in a multicomponent mixture, there are two adjustable parameters, τ_{12} and τ_{21}. These in turn are given in terms of characteristic energies Δu_{12} and Δu_{21} by:

$$\tau_{12} = \exp(-\Delta u_{12}/RT) = \exp(-a_{12}/T) \quad (7.17)$$

$$\tau_{21} = \exp(-\Delta u_{21}/RT) = \exp(-a_{21}/T) \quad (7.18)$$

The interaction parameters a_{12} and a_{21} are strong functions of temperature in the following form:

$$a_{12} = \alpha_{12} + (\beta_{12}/T) \quad (7.19)$$

$$a_{21} = \alpha_{21} + (\beta_{21}/T) \quad (7.20)$$

The experimental isobaric data for the ethanol, water and selective binaries were used to fit the UNIQUAC interaction parameters a_{12} and a_{21}. A maximum likelihood algorithm by Prausnitz (1) was used to estimate the binary interaction parameters a_{ij} with the non-linear regression on (P, x, y, T) as recommended by the authors. Details of the algorithm are given in reference 1.

The ethanol-water-VLE system has been widely studied by different investigators since it has a special importance for the ethanol dehydration. Furthermore, there is a good agreement among those who studied that system about the efficiency of the UNIQUAC model for predicting the equilibrium compositions for ethanol and water. Table 7.3 summarizes the best fitted UNIQUAC interaction parameters for water-ethanol-Isopar-M-tridecyl alcohol system.

7.4 References

1. J. Prausnitz et al., Computer Calculations for Multicomponent Vapor Liquid and Liquid Liquid Equilibria, Prentice Hall, (1980).

2. D.W. Marquardt, "An Algorithm for Least Squares Estimation of Non-Linear Parameters", J. Soc. Ind. Appl. Math., vol. 11, no. 2, (1962), pg. 431.

3. A. Fredenslund, et al., Vapor Liquid Equilibria Using UNIFAC, Elsvier Scientific Publishing Company, (1977).

4. M. M. Abbott and H. C. Van Ness, "An Extension of Barker's Method for the Reduction of VLE Data," Fluid Phase Equilibria,vol. 1 (1977) pg 3.

CHAPTER 8

THE USE OF PERVAPORATION IN ETHANOL RECOVERY FROM DILUTE AQUEOUS MIXTURES

(L.M. SROKA)

8.1 Summary

Experimental pervaporation data for ethanol/water/solvent systems are presented using commercially available membranes. Economic comparisons with equivalent distillation data are presented. Membrane performance characteristics are described.

8.2 Introduction

Pervaporation is a membrane process which employs a polymer film as a barrier to the transport of one or more components from the liquid feed solution to the vapor permeate. The preferential passing of these components from the feed solution results in the formation of two exit streams of different compositions, thereby causing a separation.

Here the stream which initially enters the membrane unit is referred to as the feed and it may be obtained from many points of an ethanol recovery process. For example, the filtrate from the fermentor, the beer still distillate, or the extact from a solvent extraction system may represent pervaporation feeds.

The stream which leaves the membrane unit after passing through the membrane is referred to as the permeate and the remaining stream as the concentrate. Depending on the characteristics of the membrane, these latter streams may be products or wastes.

In the early 60's Choo (1) and Binning (2) reported experimental data on pervaporation. They provided some separation data and theories pertaining to the mechanisms involved in the transport of components through the membrane. Solubility and diffusivity are mentioned as the controlling factors and many correlations of permeate size, shape, and polarity were presented. These correlations, on the most part were for pure components.

Sweeny and Rose (5) also did early pervaporation experiments with ethanol and n-hexane. Their results suggested that ethanol could be separated from n-hexane with cellulose acetate or polypropylene films.

P. Schissel (6) tested a number of reverse osmosis membranes with ethanol and water solutions that ranged in concentration from 2 to 97 wt% ethanol. Most membranes used in these pervaporation experiments

did not separate the ethanol and water solution appreciably. Two were found that showed a good separation and were tested at many concentrations. The Filmtec FT-30 membrane had a vapor-liquid curve simular in shape to a vacuum distillation of the solution exhibiting small separation or an azeotrope at high concentrations. The UOP RC-100 had a vapor-liquid curve which had a definite azeotrope near 50 wt%.

8.3 PERVAPORATION THEORY

For the process of pervaporation, a solution diffusion mechanism (1-4) is commonly used to explain the phenomena and predict the degree of separation that is possible and the area requirements. This model is based on a poreless membrane which separates the components by their differences in solubility in the membrane and their subsequent diffusion through the membrane. The individual compounds are believed to dissolve into the liquid surface of the membrane, diffuse through the membrane, and then evaporate from the membrane surface which has the vacuum drawn on it. The flux of a compound across the membrane (see Fig. 8.1) is then represented by:

$$J_i = +D_i \frac{C_{im1} - C_{im2}}{\Delta Z} \qquad (8.1)$$

Where J_i is the flux of component i across the membrane, D_i is the diffusion coefficient of i in the membrane, ΔZ is the membrane thickness and C_{im1} and C_{im2} are the concentration of component i in the high and low pressure sides of the membrane. This form of the equation assumes a linear concentration profile in the membrane, isothermal conditions and a diffusion coefficient which is independent of concentration.

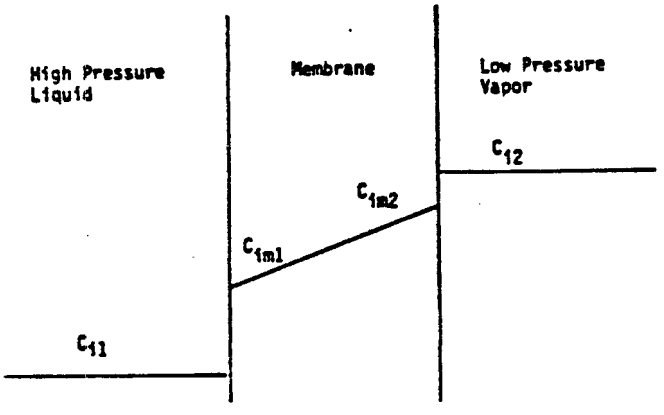

Fig. 8.1 Schematic representation of transport through a nonporous membrane

If the concentration in the membrane is proportional to the bulk concentration of the solutions, then the membrane concentrations in the equation can be replaced by the bulk concentrations and the proportionality factor (Solubility) is given by:

$$C_{im1} = C_{i1}K_i \tag{8.2}$$

Substituting eqn. 8.2 into eqn. 8.1 gives

$$J_i = K_i D_i \frac{C_{i1}-C_{i2}}{\Delta z} \tag{8.3}$$

Let $k_i D_i = P_i$, the permeability coefficient, then one obtains:

$$J_i = P_i \frac{C_{i1}-C_{i2}}{\Delta z} \tag{8.4}$$

The driving force for separation is, therefore, the concentration gradient across the membrane. Vacuum applied to the permeate side of the membrane reduces the concentration of the component in the gas phase so a flux of that component will occur even though, after the vapor is condensed, the concentration of the permeate is greater than the liquid feed concentration.

8.4 EXPERIMENTAL APPARATUS AND MATERIALS

Bench scale pervaporation experiments were performed to determine the selectivity and flux of membranes. An Amicon (401 S) pressure cell with an effective membrane surface area of 6.08 square inches (39.2 cm) was used for these experiments.

To control thermal effects, a HAAKE D1 heating element provided a constant operating temperature. A liquid trap was used to collect permeate along with a condenser which was immersed in liquid nitrogen ($-195.8^{o}C$) or acetone and dry ice ($-75^{o}C$). Figure 8.2 is a schematic of the apparatus configuration.

Membrane permeation data were generated by analyses of the initial feed, the permeate and the remaining concentrate compositions. In all cases, these measurements were made by gas chromatography. The GC used was a Hewlett Packard type 5710A with a 6 foot, poropak Q 80/100 mesh packed column. Instrument grade helium was used as the carrier gas. The GC was operated at an oven temperature of $165^{o}C$ with the injection port and detector at $250^{o}C$. The peaks were integrated using a Hewlett packard 3390A peak integrator. Quantitative analysis was based on the method of internal standards.

Feed solutions were mixed from the following solvents which were used as received from their respective vender. Isopar L is a heavy narrow cut, isoparaffinic solvent mainly composed of a mixture of C12 branched alkanes. It has a specific gravity of 0.767 at 15.6^{o}C, a viscosity of 1.99 cp at 25^{o}C and a boiling range from 188 to 206 ^{o}C. Isopar M is the next heavier isoparaffinic cut available. Both solvents were obtained from Exxon Refining. Reagent grade ethanol and hexane were used along with distilled water.

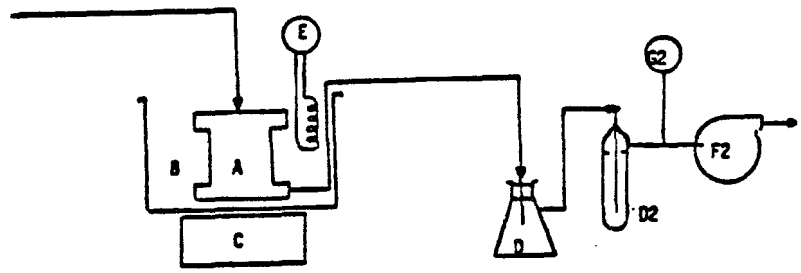

A - Membrane Apparatus
B - Constant Temperature Bath
C - Magnetic Stirrer
D - Liquid Trap
D2 - Condenser
E - Temperature Controller and Indicator
F2 - Vacuum Pump
G2 - Pressure Regulator and Indicator

Figure 8.2 Schematic Representation for the Pervaporation and Ultrafiltration Experimental Apparatus.

8.5 MEMBRANES TESTED

The commercial membranes and the polymer films which were studies are listed in Table 8.1. In most cases, the polymer films were not manufactured for use as a separation medium, but as a barrier to transport.

8.6 DATA ANALYSES

8.6.1 SELECTIVITY

The membrane was assumed to be selective if the concentration differences between the feed and permeate were statistically significant. To determine statistical significance for this small sample group, the "students t-test" methodology was used. The "null hypothesis" was accepted (no separataion) whenever the concentrations of the feed and permeate were statistically equal. The "alternative hypothesis" was accepted (a separation did indeed occur) whenever a statistically significant difference between the feed and permeate was obtained. The confidence level of this test was 95%.

Whether or not the membrane failed the "null hypothesis" test, dimesionless indicators of selectivity were calculated for the membranes. Pervaporation selectivity data are generally expressed in terms of a separation factor, . These parameters were useful for comparisons to data available in the literature. The separation factor, α, is defined as the concentration ratio of

TABLE 8.1
Membranes Studied

Manufacturer, Trade Name	Product Description	
General Electric		
MEM-100	Unbacked Dimethyl Silicone	
MEM-101	Single backed Dimethyl Silicone	
MEM-102	Double backed Dimethyl Silicone	
MEM-213	Single backed Silicone-Polycarbonate	
Rohm & Haas	Cellulose Acetate	0.8 mil
	Polypropylene	2.0 mil
Dow	Polyethylene	2.0 mil
	Polyethylene	1.0 mil
	Cellophane	na

na = not available

ethanol to water in the permeate divided by the ratio of ethanol to water in the feed. The ethanol separation factor was calculated by:

$$\alpha = \frac{\frac{x_p}{(1-x_p)}}{\frac{x_f}{(1-x_f)}} = \frac{x_p}{1-x_p}\,\frac{1-x_f}{x_f} \qquad (8.5)$$

As defined, values differing from unity indicate that a separation was obtained by the membrane.

8.6.2 FLUX

The value for the observed average flux across the membrane was calculated by:

$$J_{ave} = \frac{Q}{At} \qquad (8.6)$$

Where J is the average flux, Q is the amount of permeated collected in t hours, and A is the membrane area.

8.7 EVALUATION CRITERIA

Qualitative criteria were used to determine if a tested membrane and process were practical. The membranes were judged on their selectivity, flux, compatability, and handling properties. A practical process would receive "good" ratings in most catagories. A process would be considered impractical if it received "poor" ratings in either compatibility or selectivity. Other combinations of "good, fair, and poor" would suggest further study. For example, a membrane which had a fair rating in the flux catagory could compensate for the drawback with a good rating in selectivity and compatibility catatories.

8.7.1 SELECTIVITY

Good. The criteria for a "good" rating was that the membrane pass two "student t-tests". The first test determined if a statistically significant change in concentration occurred between the feed and permeate. The second test determined if a statistically significant difference was observed between the permeate concentration and the equilibium vapor concentration.

Fair. The criteria for a "fair" rating was that the mebrane passed a "student t-test" which determined if a statistically significant change in concentration occurred between the feed and permeate.

Poor. The criteria for a "poor" rating was that the membrane failed the "student t-tests".

8.7.2 FLUX

Good. The criteria for a "good" rating was that the membrane exhibited observable fluxes which produced measurable permeate within an hour.
Fair. The criteria for a "fair" rating was that the mebrane exhibited observable fluxes which eventually produced a measurable permeate.
Poor. The criteria for a "poor" rating was that the membrane exhibited no observable flux within two hours.

8.7.3 COMPATIBILITY

Good. The criteria for a "good" rating was that the membrane exhibits no observable changes during and after the compatibility tests. Also, the membrane withstood the conditions employed in the selectivity and flux experiments and could be retested with reproducable results.

Fair. The criteria for a "fair" rating was that the membrane exhibits any of the following properties.

(a) Changes such as discoloration or separation from the backing in the compatibility tests.
(b) Changes in form after the selectivity and flux experiments such as brittleness, discoloration or separation from the backing.
(c) If retested, the results were not reproducable.

Poor. The criteria for a "poor" rating was that the mebrane either swelled to a point where it became gelatinous, or disolved totally in the compatibility tests.

8.7.4 HANDLING

Good. The criteria for a "good rating was that the membrane requires no special care or pretreatment procedures. Also, the physical form of the membrane was self-supporting or was provided with a backing.

Fair. The criteria for a "fair" rating was that the membrane requires precautions to be taken against drying or prewashing with an easily available solvent The membrane was also self-supporting or backed.

Poor. The criteria for a "poor" rating was that the membrane requires complicated pretreatment procedures before use. An unbacked, non-self-supporting membrane also received a poor rating unless it was available in a preassembled unit.

8.8 PERVAPORATION EXPERIMENTAL RESULTS AND DISCUSSION

Pervaporation experiments were completed with ternary mixtures of ethanol, water and Isopar L or binary mixtures of ethanol and solvent as feeds. The results of the pervaporation experiments are summarized in Table 8.2. The separation factors obtained for the cellulose acetate were within the range reported (17-130) by Sweeny and Rose

(5), but the polypropylene did not perform as well as expected. The lower fluxes and separations are presumed to be due to the difference in the quality of the polymer films.

The preferential passing of ethanol and retention of the non polar hexane made the cellulose acetate a prime candidate for removing ethanol from a solvent extract by pervaporation. A "fair" separation was obtained, but it is not as good as the separation obtainable by a simple flash. A flash of the 3% ethanol, 97% Isopar M feed, when operated at 360 mm: Hg and 70°C produces a 90 wt% ethanol product.

A binary feed of ethanol and water was tried to avoid the compatibility problem of the GE membranes with the organic solvents. The pervaporation tests then performed had improved selectivity, a change from "poor" to "fair" and "good" for the GE MEM-213 and MEM-101 respectively. A series of tests employing the GE MEM-101 were performed at different feed compositions and temperatures to further characterize the membrane. The results are summarized in Table 8.3. A run was performed for 26 hours to examine composition variation with time. Four permeate samples were collected, 96%, 93%, 85% and 92% ethanol respectively from a 54.5 wt% feed solution. The samples were composited to get an average permeate of 92 wt% ethanol. The shut down and start up of the appartus is a possible source of the water contamination of the low ethanol sample.

Table 8.2 Results of the General Pervaporation Studies

Membrane	Feed		Permeate		Amount	Time	Pres.	Temp		J
	Etoh	H_2O	Etoh	H_2O	(ml)	(hr)	(mmhg)	°C	α	$\frac{ml}{cm^2 \cdot hr}$
Cellophane	79.0	2.0	----	----	----	1	100	Amb	----	----
Polyethylene	79.0	2.0	----	----	----	1	100	Amb	----	----
Polyethylene	85.1	1.6	86.9	1.7	7	1	180	75	0.96	0.16
GE MEM-213	70.8	0.8	66.8	0.9	5	1	260	Amb	0.94	0.12
GE MEM-213	50.0	50.0	50.0	50.0	100	1.5	260	60	1.0	1.7
GE-MEM-101	70.8	0.8	----	----	----	----	260	60	----	----
GE-MEM-101	53.0	47.0	72.0	28.0	10	6	160	60	2.28	0.04
Cellulose Acetate	44.5	55.5*	94.6	4.4*	0.5	2.5	220	60	26.8	0.005
Polypropylene	42.2	57.8*	15.2	84.8*	0.5	1	220	60	0.24	0.012
Polypropylene	86.0	1.2	71.3	14.6	0.3	6	220	60	0.68	0.001
Cellulose Acetate	50.0	50.0**	96.6	3.4**	0.5	3.5	220	60	28.	0.003
Cellulose Acetate	3.4	96.6**	85.0	15.0**	0.8	8	220	60	161.	0.002
Cellulose Acetate	3.4	96.6**	----	----	----	4	220	60	----	----

*Hexane **Isopar M

Note: Third Component in Ethanol/water/solvent systems Isopar L

Table 8.3 Results of the Pervaporation Studies with the GE MEM-101 Membrane

Membrane	Feed		Permeate		Amount	Time	Pres.	Temp	α	J
	Etoh	H_2O	Etoh	H_2O	(ml)	(hr)	(mmhg)	°C		$\frac{ml}{cm^2 m}$
GE MEM-101	53.0	47.0	72.0	28.0	5	3.5	160	60	2.28	0.036
GE MEM-101	83.6	16.4	86.7	13.3	10	4	160	60	1.27	0.063
GE MEM-101	54.0	46.0	76.0	24.0	10	6	160	60	2.70	0.042
GE MEM-101	97.4	2.6	96.3	3.7	30	4.5	160	60	0.69	0.168
GE MEM-101	52.9	47.1	71.1	28.9	20	----	160	60	2.19	----
GE-MEM-101	94.9	5.1	95.2	4.8	1	1.5	160	50	1.07	0.017
GE-MEM-101	95.7	4.3	96.4	3.6	16	3	160	60	1.20	0.134
GE MEM-101	95.7	4.3	96.4	3.6	5	1	160	60	1.20	0.126
GE MEM-101	94.9	5.1	----	----	---	3	160	40	----	-----
GE MEM-101	8.0	92.0	----	----	----	4	220	60	----	----
GE MEM-101	35.0	65.0	96.4	3.6	0.8	2	220	60	50	0.009
GE MEM-101	35.0	65.0	96.4	3.6	1.0	2.5	220	60	50	0.01
GE MEM-101	8.0	92.0	20.0	80.0	----	----	220	75	2.8	----
GE MEM-101	29.0	71.0	83.0	17.0	4.3	6	220	60	12	0.018
GE-MEM-101	32.0	68.0	93.0	7.0	3.5	6.5	220	60	29	0.014
GE-MEM-101	30.5	69.5	62.5	37.5	6	6	220	60	3.8	0.025
GE MEM-101	54.5	45.5	96.0	4.0	2	2.5	220	60	20	0.02
GE MEM-101	54.5	45.5	92.0	8.0	15	26	220	60	9.6	0.015

The efficiency of the separation of the GE MEM-101 membrane is compared to a vacuum distillation occuring at a similar temperature and pressures in Figure 8.3. The vapor liquid equilibrium data was plotted for the pressure range of 92 to 220 mm Hg at a temperature of 50°C (7). The points for the membrane separation fall above and below this curve. At both low and high ethanol concentrations, it was possible to obtain a 96 wt% ethanol product.

It is possible to rationalize the high percent water in some of the permeate data as being the result of leaks and, therefore, to discount them. After discounting these few points, the composition of the permeate appears to be independent of feed concentration for the range of 30 to 54.5 wt% ethanol at 60°C and a vacuum side pressure of 220 mm Hg.

One theory (8) states that the individual fluxes across the membrane are proportional to the concentration gradient between the vapor and liquid phases. The result of a constant composition permeate tends to contradict this theory unless one considers that the proportionality factor is the product of the solubility of the component in the membrane and the diffusion coefficient through it. When the solubility of the ethanol and water in the membrane is independent of the concentrate composition (for example, when the membrane is saturated) and remains saturated, then the separation obtained is constant over a wide concentration range. The saturation concentration in the membrane then determines the diffusivity of the components through the membrane and the separation obtainable. If the rate of solution of the components into the membrane is slower than the rate at which they diffuse to the vapor side, then the rates that the components dissolve into the membrane matrix (and their steady state concentration) are functions of feed concentration. In this latter case, the relative diffusivity rates through the membrane should vary with the concentration of the components in the feed and the membrane.

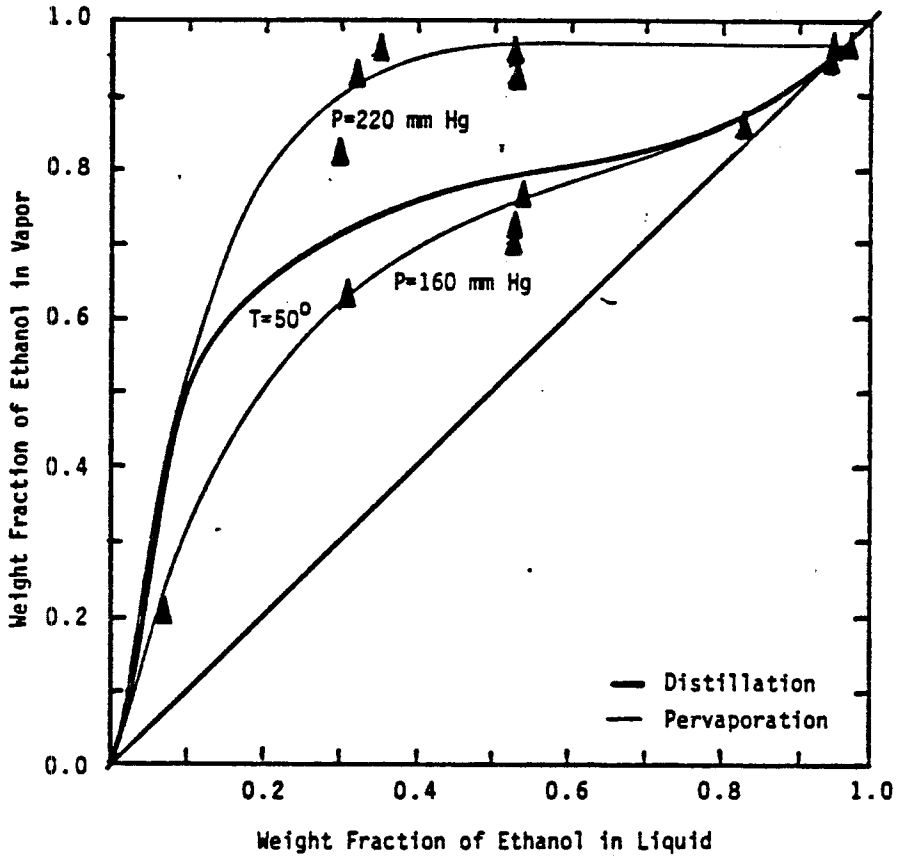

Figure 8.3 Comparison of Separation by Vacuum Distillation with the Results of Pervaporation with GE MEM-101 Membrane.

The data collected at the two different pressures on the vacuum side of the membrane indicate a flux dependence on absolute pressure as expected. The lower the absolute pressure, then the higher the flux. In addition, the absolute pressure may also affect the controlling mechanism of the separation. At an absolute pressure of 160 mm Hg the flux and the concentrate appeared to depend on the concentration of the feed. At an absolute pressure of 220 mm Hg, the ethanol flux and the permeate concentration did not vary within the error associated with this work. The permeate flux was also sensitive to temperature as noted by the lack of flux at 40°C, a low rate at 50°C and a ten fold increase at 60°C.

8.9 DESIGN AND ECONOMICS

In order to determine the economic advantages or disadvantages of pervaporation in ethanol dehydration, the energy and capital requirements of this process was compared to an azeotropic distillation process. The combination of membrane, feed and operating conditions which had the best separation was choosen for this evaluation. From the available experimental data, the GE MEM-101 was choosen to be evaluated in a hypothetical and optimistic actual case.

8.9.1 PROCESS DESCRIPTION

The first process, a hypothetical GE pervaporation unit, will accept a low concentration feed from a beer still and produce a 98.5 wt% ethanol product and a waste stream with only trace ethanol losses. A conceptual flow diagram of this process is in Figure 8.4

The second option was based on the most optimistic data from the GE MEM-101 experiments. This conceptual process consists of a beer still to remove dissolved solids from the fermentation beer and a distillation column to partially concentrate the feed before it is fed to the pervaporation unit. The concentrate from the pervaporation unit is recycled back to the concentrator column. The permeate, 96.4 wt% ethanol, then may be dried further by an adsorption process (9), to make it of comparable value. A conceptual flow diagram is in Figure 8.5

The azeotropic distillation consists of a beer still, a binary distillation column and a azeotropic column which uses penetane as the water entrainer (10). The process flow diagram is shown in Figure 8.6

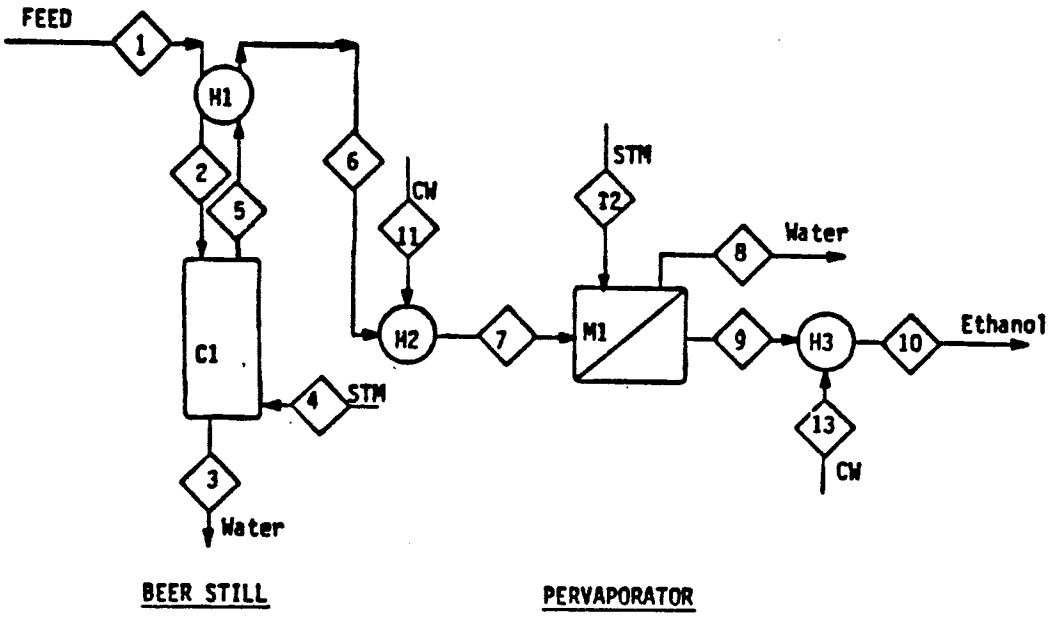

Figure 8.4 Conceptual Flow Diagram for Ethanol Recovery by a Hypothetical Pervaporation Unit.

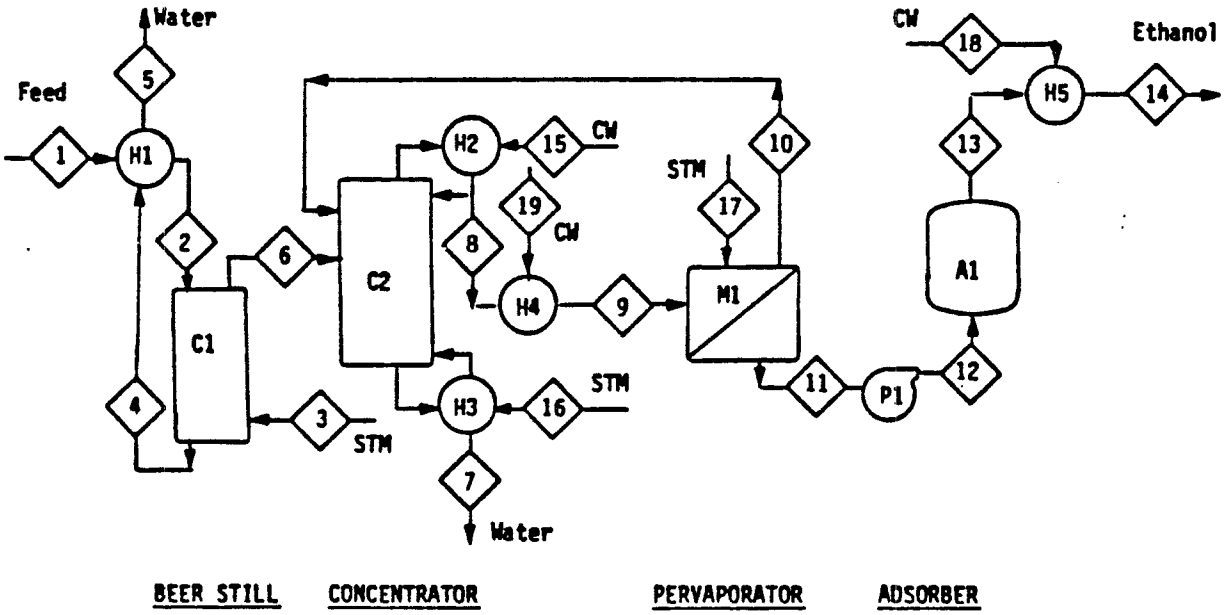

Figure 8.5 Conceptual Flow Diagram for Ethanol Recovery by Pervaporation and Adsorption.

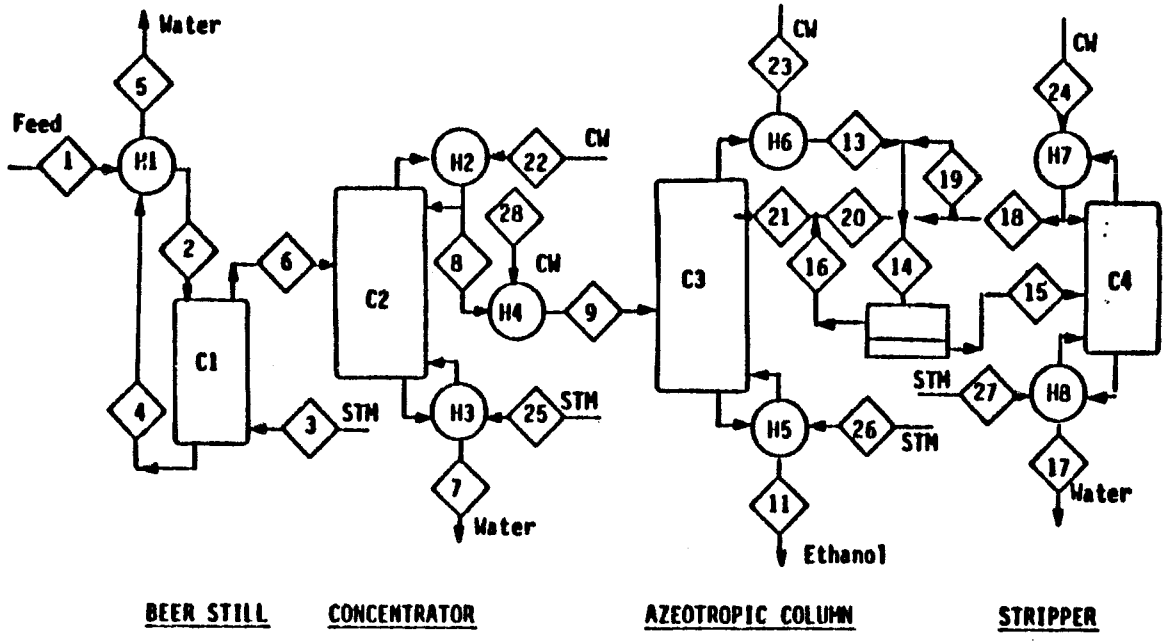

Figure B.6 Conceptual Flow Diagram for Ethanol Recovery by Azeotropic Distillation

8.9.2 DESIGN

Each of the three processes was designed to produce 1040 pounds per hour of ethanol product from a citrus molasses fermentation beer. The material and energy balances were performed by SimSci's Process Model (11) computerized simulator. The distillation columns used in any of the three processes were simulated by Process's Rigorous Distillation operation. This program performs tray and tray equilibrium calculations to obtain the material and energy balances.

The membrane units were simulated by Process's Component Separator program. This program will separate a feed into two products of specified composition by use of material balances. This is adequate for the membrane process simulation when experimental or hypothetical data are available as input for the permeate composition. When this data is not available, prediction of the permeate concentration and flux may be determined theoretically. The energy requirements for the pervaporation units were calculated with Process's Heat Exchanger program.

The area for the membrane unit is determined by:

$$A = \frac{Q}{J_{ave}} \qquad (8.7)$$

J_{ave} is the average flux through the mebrane and Q is the mass flow rate.

The average flux which is needed to calculate the membrane unit area can be obtained from the experimental data or theoretically when the permeability of the membrane and concentration profiles in the membrane unit are known. See Eq. 8.4. For these cases, the experimental average value of 0.022lb/hr ft^2 was used.

For the purposes of comparison, the installed cost for the membrane unit was assumed to be \$100/ft^2. The cost for the membrane unit was derived from conversations with reverse osmosis venders and literature values (1,12,13,14) corrected to 1984 dollars. The costs of commercial large scale pervaporation units was not available, but it was assumed that the equipment costs would be similar to those of large scale reverse osmosis equipment.

The other major pieces of equipment was sized and costed by usual methods (15).

8.9.3 RESULTS OF FEASIBILITY DESIGN CALCULATIONS

The installed costs for the three processes are summarized in Tables 8.4-8.6. As can be seen from these tables, the capital investment for the membrane processes is approximately four times greater than the investment for the distillation process. The major equipment cost appears in the purchase of the membrane unit which accounts for almost 80% of the total capital investment. The influence of membrane cost on the projects return on investment is discussed later.

Table 8.4 Estimated Installed Equipment Costs for the Hypothetical Pervaporation Unit.

ITEM	INSTALLED COSTS
Membrane Unit (49,500 ft^2 at \$1000/ft^2	\$4,950,000
Beer Still (2.5 ft O x 12 ft, cs)	21,000
Beer Still Internals	4,000
Heat Exchangers	
H1 (155 ft^2, cs)	17,000
H2 (196 ft^2, cs)	18,000
H3 (70 ft^2, cs)	14,000
Fermentation System	768,000
Plant Storage	162,000
TOTAL EQUIPMENT INVESTMENT	\$5,954,000

M&S Index = 773.2

Table 8.6 Estimated Installed Equipment Costs for the Azeotropic Distillation Process

ITEM	INSTALLED COSTS
Ethanol Concentrator	\$ 396,000
Azeotropic Purification	138,000
Fermentation System	768,000
Plant Storage	162,000
TOTAL EQUIPMENT INVESTMENT	\$1,464,000

M&S Index = 773.2

Table 8.5 Estimated Installed Equipment Costs for the Pervaporation Unit and Adsorption System.

ITEM	INSTALLED COSTS
Membrane Unit (49,500 ft^2) at \$100/ft^2	\$4,950,000
Beer Still (2.5 ft O x 12 ft, cs)	21,000
Beet Still Internals	4,000
Concentrator Column (3.0 ft O x 40 ft, cs)	42,000
Concentrator Internals	8,000
Heat Exchangers	
H1 (626 ft^2, cs)	30,000
H2 (7 ft^2, cs)	10,000
H3 (70 ft^2, cs)	14,000
H4 (290 ft^2, cs)	18,000
H5 (30 ft^2, cs)	11,000
Adsorption Columns (4) (2.0 ft O x 30 ft, cs)	100,000
Adsorption Column Internals	12,000
Fermentation System	768,000
Plant Storage	162,000
TOTAL EQUIPMENT INVESTMENT	\$6,152,000

M&S Index 773.2

Tables 8.7-8.9 compare production costs, energy requirements, and profitability of the three processes. From this analysis it appears that the azeotropic distillation, even though its energy requirements were relatively higher than the membrane processes, has the greatest possibility of being profitable. The relatively low capital investment and proven technology give it an economic advantage over the membrane processes.

Table 8.7

Estimated Annual Gross Profits for 98.99% Ethanol Production

	Option I	Option II	Distillation
ANNUAL COSTS			
Molasses	$ 991,000	991,000	991,000
Solvent	---	---	4,000
Cooling Water	9,100	12,900	13,500
Steam	175,500	196,700	240,000
Electricity	3,000	3,000	3,000
Labor	100,000	100,000	100,000
Nutrients	10,000	10,000	10,000
Fixed Costs*	1,985,000	2,051,000	146,000
TOTAL COSTS	$ 3,273,600	3,364,600	1,507,500
ANNUAL SALES			
Dry Ethanol	$ 1,525,000	1,525,000	1,525,000
By-Product	575,000	575,000	575,000
TOTAL SALES	$ 2,100,000	2,100,000	2,100,000
GROSS PROFIT	$-1,173,600	-1,264,600	592,500

*33.3% for Option I & II, 10% for the Distillation

The two membrane processes show losses at this time due to their higher fixed costs and similar operating costs. A reduction in either or both of these costs would improve the membrane process's profitability. The differences in the estimated operating costs between the membrane processes and the distillation are in the energy requirements and additional solvent for the azeotropic distillation. Since the membrane processes do not require solvent, a savings is already realized in this area. The present energy requirements for the membrane processes are nearly as high as the azeotropic distillation. Therefore, the energy consumption needs evaluation for possible areas of reduction such as economizers and less energy intensive pretreatment steps.

The energy intensive step in option I, the hypothetical pervaporation unit, is the beer still which removes the dissolved solids from the fermentation beer. The beer still is equipped with an economizer which preheats the feed with the exiting vapor. This saves approximately 4000 BTU/gal and reduces cooling water consumption. If a pretreatment process is available which could remove the dissolved solids without a phase change, the hypothetical pervaporation unit would greatly reduce the energy requirements for dehydrating ethanol. Reverse osmosis could be the solution. From literature reports (16) reverse osmosis can effectively reduce the dissolved solids concentration and not appreciabily alter the ethanol water ratio of the feed.

The beer still is also the energy intensive step in option II. In this process, as in the azeotropic distillation, the economizer preheats the beer still feed with the hot bottoms stream. This saves approximately 4000 BTU/gal and does not increase the reboiler duty of the concentration column. The replacement of the beer still by a process which removes the dissolved solids would also lower the energy requirements of this process. The total energy savings would not be as great as in option I unless the replacement process could effectively concentrate the feed stream also.

The fixed costs for the membrane processes were estimated at 33.3% of the capital investment, which reflects a 3 year life expectancy instead of a 10 year life. To reduce this cost, the membrane life expectancy assumption could be increased to 10 years as for the azeotropic distillation. But without data on the membrane life expectancy, 3 years in an optimistic estimate.

The influence of membrane costs and a 3 year life expectancy on the projects return on investment in shown in Figure 8.7. It can be seen that if the costs per unit area is lowered, or if the flux per unit area is increased, the pervaporation process cannot compete economically with the distillation. The estimated short life of the equipment and its high capital cost are economic disadvantages which can be overcome with improvements in the membrane.

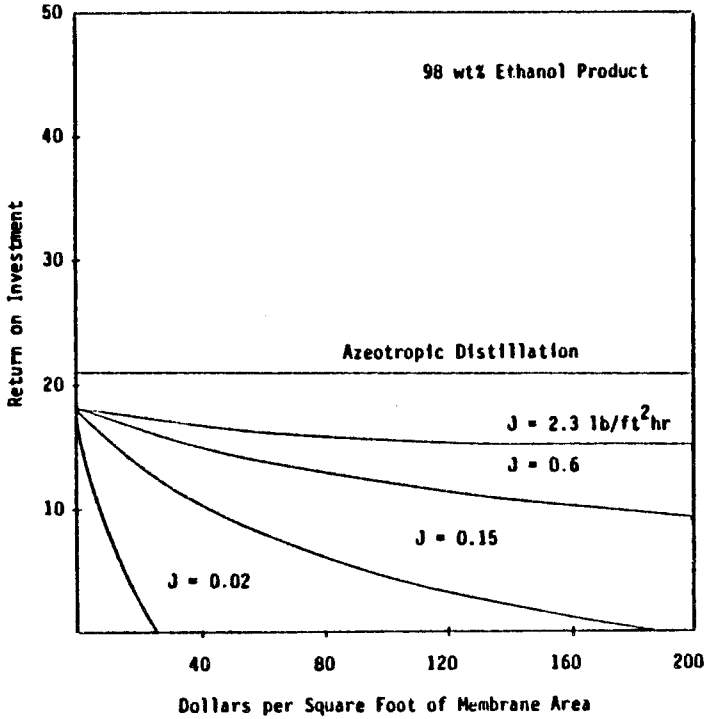

Figure 8.7. Variation for the Return on Investment for Option I with Membrane Unit Costs at Different Average Flux Rates and a Constant Selectivity. (3 Year Life Expectancy)

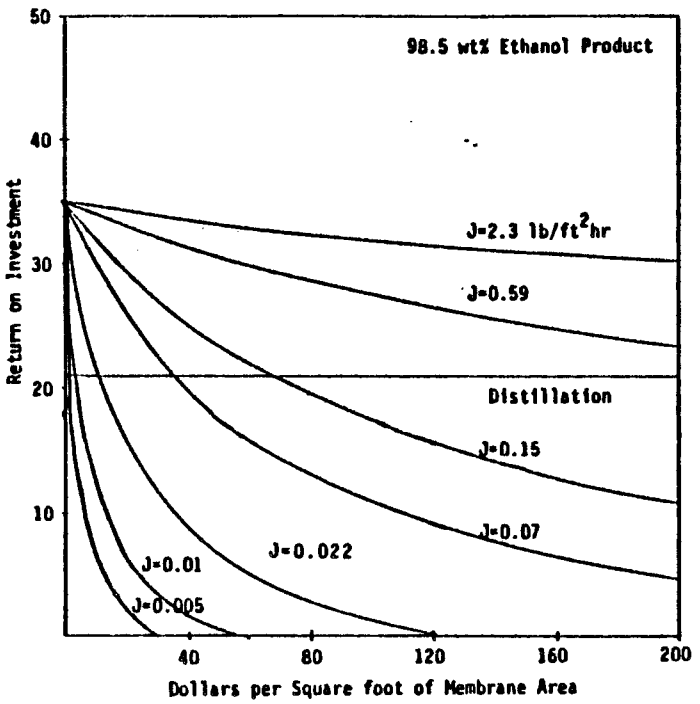

Figure 8.8. Variation for the Return on Investment for Option I with Membrane Unit Costs at Different Averages Flux Rates and a Constant Selectivity. (10 Year Life Expectancy)

Figure 8.8 shows the influence of membrane costs on the rate of return when a 10 year life expectancy is assumed. As can be seen in the figure, the longer life expectancy improves the economics for the membrane processes. If the costs per unit area is lowered, or if the flux per unit area is increased, then the pervaporation process can compete economically with the distillation. For the same production rates, the ROI for the distillation and extraction processes was about 21%. To obtain this return with membrane costs at $100 per ft2, option I needs a flux of .25 pounds per square foot per hour or at an average flux of .022 pounds per square foot per hour the costs of the membrane unit would be approximately $10 per square foot. If the flux can be increased above 0.5 pounds per square foot per hour, then the cost of the membrane does not cause the ROI to fall below the 20% mark even at prices as high as $200 ft^2.

8.10 CONCLUSIONS

The inovative nature of these processes along with the low return on investment will defer investment into such large ventures. The cost of the membrane unit is the major equipment expenditure, but has a potential to decrease as technology improves. The technological improvements may appear as increased flux, greater selectivity or inexpensive membrane manufacturing techniques. Thus membrane processes have the possibility of becoming practical unit operations in the future.

Of the membranes examined, pervaporation with the GE MEM-101 membrane resulted in the best separation of ethanol, and it may be a practical alternative to distillation for recovering ethanol from a 50 wt% feed of ethanol and water in some cases. The economics of the process suggests a need for improvements in the membrane flux and selectivity before it can compete with conventional methods. Also, technological improvements in the manufacturing of the membrane unit which decrease its costs would benefit the ecomonic outlook of the process.

Pervaporation with cellulose acetate films also had good results for recovering the ethanol from organic solvents. The flux and selectivity need improvement before this process can become practical.

8.11 References

1. Choo, C.Y. and Sanders, B.H., "Latest Advances in Membrane Permeation," Petroleum Refiner, 39, 6:133-138 (1960).

2. Binning, R.C., Lee, R.J., Jennings, J.F., and Martin, E.C., "Separation of Liquid Mixtures by Permeation," Ind. and Eng. Chem., 53:45-50 (1961).

3. Choo, C.Y., "Advances in Petroleum Chemistry," Vol. 16, Ch 2, Interscience, NY (1962).

4. Ballweg, A.H., Bruschke, H.E.A., Schneider, W.H., Tusel, G.F., "Pervaporation Membranes - An Economical Method to Replace Conventional Dehydration and Rectification Columns in Ethanol Distilleries", Proc. Fifth International Alcohol Fuel Technology Symposium, GFT Engineering for Industrial Plants, D6650, Homburg, Saar GFR. (1982).

5. Sweeny, R.F. and Rose, A., "Factors Determining Rates and Separation in Barrier Membrane Permeation", I&EC Prod. Res. Dev., 4, 4:248-251 (1965).

6. Schissel, P., "FY 1982 Annual Progress Report for the Membrane Research Subtask, Alcohol-Fuels Program", SERI/PR--255-1776, Golden, CO, Solar Research Institute, (1983).

7. Larkin, J.A., and Pemberton, R.C., "Thermodynamic Properties of Mixtures of Water and Ethanol Between 298.15 and 383.15 K", NPL Report Chem. 43, (Jan. 1976).

8. Lee, C.H., "Theory of Revserse Osmosis and Some Other Membrane Permeation Operations," J. Appl. Polymer Science, 19:83-95 (1975).

9. Bienkowsk, P.R., Voloch, M., Landish, M.R. and Tsao, G.T., "Nonisothermal Adsorption of Water Vapor on Corn," 1983 Winter Meeting, American Society of Agricultural Engineers.

10. Black, C. "Distillation Modeling of Ethanol Recovery and Dehydration Processes For Ethanol and Gasohol," Chemical Engineering Progress, 9:78-85 (1980).

11. Process Simulation Program," Simulation Sciences, Inc. Houston, TX

12. "Summary of Progress on the Development of Ethanol - Selective Membranes at the Southern Research Institute", (Subcontract XB-1-9189-3).

13. Beaton, N.C., "Applications and Economics of Ultrafiltration", I. Chem. E. Symposium Series No. 51 59-70.

14. Sherwood, T.K., Brian, P.L.T., and Fisher, R.E., "Desalination by Reverse Osmosis," I & EC Fund., 6, 1:2-12 (1967).

15. Peters, M.S. and Timmerhaus, K.D., "Plant Design and Economics for Chemical Engineers," 3rd. Edition, McGraw Hill NYC (1980).

16. Matsuura, T. and Sourirajan, S., "Characterization of Membrane Material, Specification of Membranes, and Predictability of Membrane Performance in Reverse Osmosis," Ind Eng. Chem Process Des Dev., 17:419-428 (1978).

CHAPTER 9

RECIPROCATING PLATE COLUMN
(W. Y. Tawfik)

9.1 Empirical Correlations for the Reciprocating Plate Column

The proposed process in this work deals with the recovery of ethanol from diluted aqueous solutions (1/2 - 7 wt % ethanol). Literature reviews (1-3), however, indicated that the present correlations of extractors' performances (4, 5, 6-12, 13-23, 24-28) do not apply to the case of very dilute solutes in the feed, especially in the presence of surfactants.

In this study, the Karr reciprocating plate column was chosen mainly due to its ability to handle solids and high ratios of continuous to dispersed phase. The availability of experimental data by Karr (27) on a 3-ft diameter column was an additional advantage for the development of a more generalized reciprocating plate column model.

Previous HETS correlations for the reciprocating plate column were developed by Eckles (5) and Bensalem (4). Eckles measured the performance of the extraction column in terms of the percentage extracted of the solute. He also measured the high equivalent to theoretical stages for the Isopar-M-ETOH-Water system. Subsequently, Eckles correlated those performance measures for the case of mass transfer from dispersed phase to continuous phase.

Bensalem (4) correlated hydrodynamic parameters as well as performance measures for acetic acid-toluene-water systems as functions of operating variables such as the reciprocation, frequency, amplitude, velocities of dispersed and continuous phases, and the hold up of the dispersed phase in the column. Those studies have been very helpful to this work in providing the hydrodynamic correlations as well as the experimental data that was used in the present models.

The mass transfer of a solute between two immiscible liquid phases can be expressed in terms of flux by:

$$N_A = K_x(x-x^*) = K_y(y^* - y) \qquad (9.1)$$

If the flow of both liquid phases is considered as a plug flow, and the superficial velocities of both phases have only a one-dimensional vector in the direction of flow of each phase within a length of dz of the column, Eqn. 9.1 was given in differential form as:

$$dN_A = K_x a(x-x^*)dz = K_y a(y^*-y)dz \qquad (9.2)$$

where:

N_A = mass flux of solute, gm/cm^{2}sec

x = weight of solute in X-phase

y = weight of solute in Y-phase

K_i = mass transfer coefficient in phase i, gm/cm^{2}sec

a = interfacial area per unit volume, 1/cm

When the flow pattern deviates from ideality and both phases flow partially in the opposite directions, a back flow model is then considered and the mass balance about an incremental height of the column is given by:

$$U_x\{(1+\alpha_{xi-1}) - (1+2\alpha_x)x_i + \alpha_x x_{i+1}\} = N_A \Delta Z a \qquad (9.3)$$

or

$$-U_y\{(-\alpha_y y_{i-1}) + (1+2\alpha_y)y_i - (1+\alpha_y)y_{i+1}\} = N_A \Delta Z a \qquad (9.4)$$

where:

U_i = velocity of phase i, cm/sec

α_i = back mixing ratio of phase i

The previous mass transfer models lead to different equations of the height of the transfer unit. When the plug flow model is considered, the HTU, or y-phase, is given by:

$$(HTU_y)_m = H_c / \{{}_{y_{n+1}}\int^{y_1} dy/(y^*-y)\} \qquad (9.5)$$

When both operating and equilibrium lines can be approximated to straight lines, Eqn. 9.5 becomes:

$$(HTU_y)_p = H_c / \{(y_1-y_{n+1})/(y^*-y)_{lm}\} \qquad (9.6)$$

where:

H_c = height of the column

where $(y^*-y)_{lm}$ is the logarithmic mean between y_1 and y_{n+1}.

For the back flow model, Misek and Rod (29) gave a general solution to Eqns. 9.3 and 9.4, with the analogy to the stagewise extractors:

$$HTU_y = H_c / \{(y_1-y_{n+1})/\Sigma(y_i^*-y_i)\} \qquad (9.7)$$

When the analogy with stage-wise contactors is made, and where the operating and equilibrium lines are approximated to be straight lines, the number equivalent to a theoretical stage was given by:

$$NETS = \log[(1/u)(1-1/\epsilon) + 1/\epsilon] / \log \epsilon \quad (9.8)$$

where

$$U = [x_n - (y_{n+1}/D_{en})] / [x_o - (y_{n+1}/D_{en})] \quad (9.9)$$

and

$$\epsilon = [(D_{en}D_{eo})^{0.5} E'] / R' \quad (9.10)$$

where:

D_{ei} = distribution coefficient of solute at position i

E' = extract mass flow rate, gm/sec

R' = raffinate mass flow rate, gm/sec

subscripts o, n denote the top and bottom positions of the column

The height equivalent to theoretical stages can be given by:

$$HETS = H_c / NETS \quad (9.11)$$

The heights equivalent to theoretical stage were chosen in this work as a good measure for the performance of a Karr reciprocating plate column. The dependence of HETS on the operating variables and the physical properties of the two phases of the extraction system are summarized in Figures 9.1 through 9.4.

Previous studies (6-12, 13-23, 30-42) on similar columns (pulsed column and rotating disk column) suggested that the HETS is a function of the following variables:

$$HETS = f_1(D, E, U_T, AF, \Delta\rho g, \rho_c, \mu_c, \sigma) \quad (9.12)$$

where:

D = column diameter, cm

E = extraction factor in weight basis

U_T = total throughput, cm^3/cm^2 sec

A = amplitude of reciprocation, cm

F = frequency of reciprocation, 1/sec

$\Delta\rho$ = density difference, gm/cm^3

ρ_c = continuous phase density, gm/cm^3

σ = interfacial tension, dyne/cm

μ_c = continuous phase viscosity, gm/cm sec

g = 981 cm/sec^2

Assuming an exponential form for the previous function,

$$HETS = c_0 D^a E^b U_T^c (AF)^d \Delta\rho g^e \rho_c^h \sigma^i \mu_c^j \qquad (9.13)$$

Using the Buckingham Pi theorum (43), a dimensionless analysis of Eqn. 9.13 leads to the following dimensionless relationships:

$$HETS/D = c_0 E^b (D\Delta\rho g/\rho_c U_T^2)^c (\mu_c/D\rho_c U_T)^d (\sigma/D\rho_c U_T^2)^h (AF/U_T)^i \qquad (9.14)$$

The experimental values available for the continuous phase viscosity exhibited very little variation ($0.9 < \mu_c < 1.1$ cp). Therefore, another function for HETS for low continuous phase viscosity was proposed in the following form:

$$HETS = f_2(D, E, U_T, AF/H, \Delta\rho g, \rho_c, \sigma) \qquad (9.15)$$

where H = the plate spacing, cm.

Similar dimensionless analysis led to the following correlation:

$$HETS/D = c_0 E^b (D\Delta\rho g/\rho_c U_T^2)^e (AFD/HU_T)^d (\sigma/D\rho_c U_T^2)^i \qquad (9.16)$$

Non-linear least square analysis indicated that the term E^b is statistically insignificant. It was found that the replacement of D in the middle term of Eqn. 9.16 with a dummy variable representing the length dimension would lead to a better correlation. The mean plate thickness (t_m) was chosen to replace the column diameter (D) in the middle group. This choice, however, was arbitrary and was made because t_m changes very little in different columns.

The experimental data from this work were combined with data by Karr et al. (44, 33) for 3-ft and 1-in diameter columns respectively. A non-linear least square program (45) was used to minimize the objective function:

$$S = \Sigma[(HETS/D)_{obs\,j} - (HETS/D)_{calc\,j}]^2 \quad , j = 1,2,....,NPTS \qquad (9.17)$$

For low viscosity systems ($\mu_c < 1.1$ cp), the best correlation was found to be:

$$HETS/D = 1.03(D\Delta\rho g/\rho_c U_T^2)^{-0.075} (AFt_m/HU_T)^{-1.30} (\sigma/D\rho_c U_T^2)^{0.625} \qquad (9.18)$$

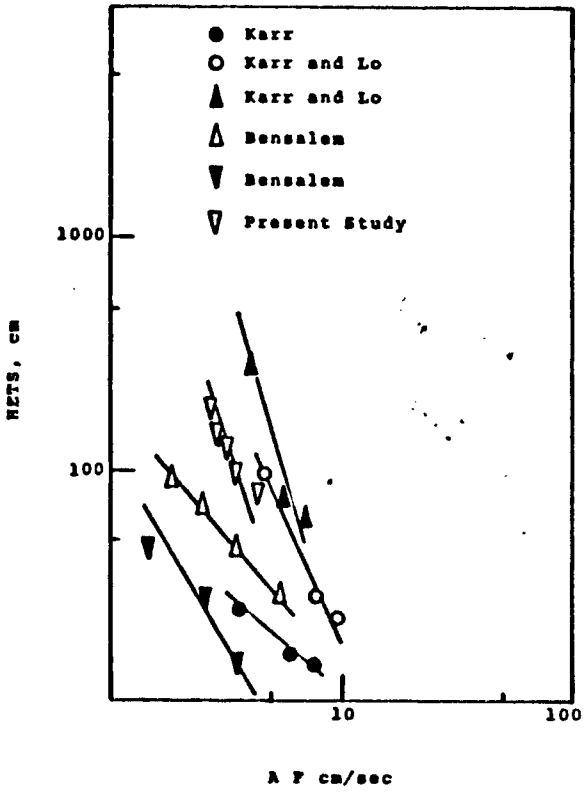

Fig. 9.1 Effect of Reciprocation Speed on HETS

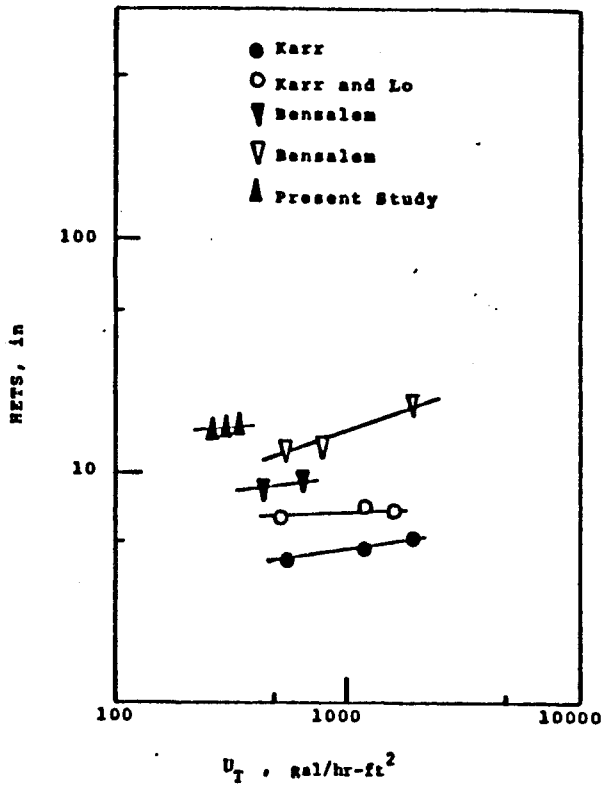

Fig. 9.2 Effect Of U_T On HETS

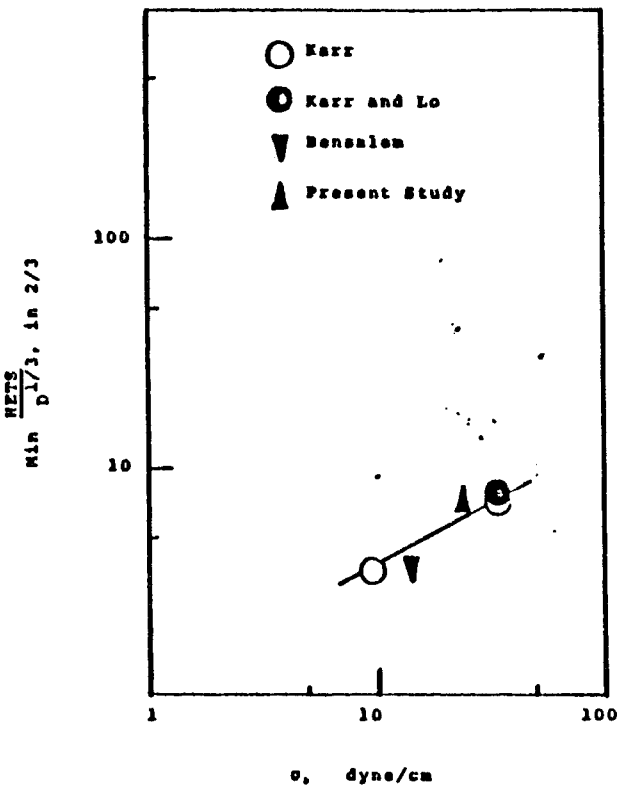

Fig. 9.3 Effect Of Surface Tension On HETS

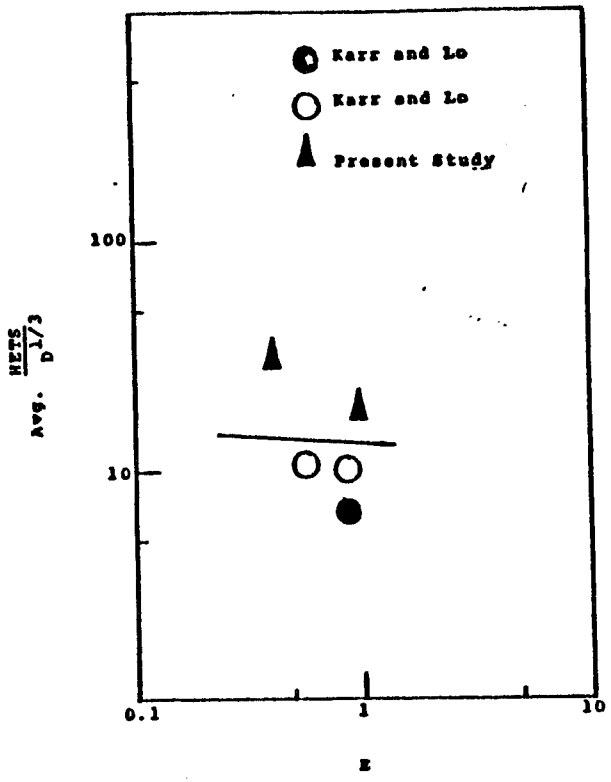

Fig. 9.4 Effect Of Extraction Factor On HETS

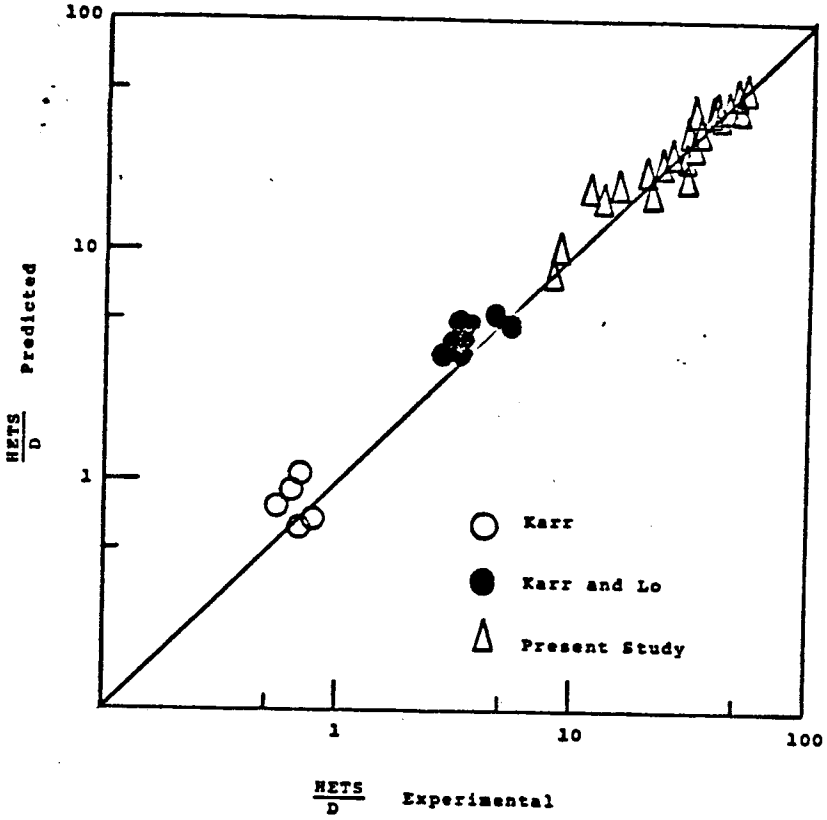

Fig. 9.5 Experimentally Measured $\frac{HETS}{D}$ Versus Predicted From Eqn. 5.53

with an average standard deviation of ±16.4%. The correlation is restricted to:

$$10 < \sigma < 40 \text{ dyne/cm}$$

and operating conditions below the flooding point.

Equation 9.18 can be rearranged in the following form:

$$HETS = 1.03D^{0.3}(\Delta\rho g)^{-0.075}\rho_c^{-0.55}(AF)^{-1.30}\, U_T^{0.20}\sigma^{0.625}(t_m/H)^{-1.3} \qquad (9.19)$$

The exponent of AF agrees reasonably well with the experimental data from Karr (33), Karr and Lo (44), and Bensalem (4) which have an average exponent of -1.28. The experimental data of different investigators (4, 44, 46, 33) suggests an average exponent for U_T of 0.1986, which agrees reasonably well with the value from Eqn. 9.19 of 0.2.

Henley and Seader (34) suggested a value of 0.645 for the exponent of the interfacial tension and 0.333 for the column diameter. These values agree with those obtained from Eqn. 9.19 of 0.625 and 0.3 for the interfacial tension and column diameter exponents, respectively.

The experimental values of HETS/D is plotted against the calculated values from Eqn. 9.18 in Figure 9.5. The deviation of the experimental values from those calculated using Eqn. 9.18 appears randomly distributed along the 45° line.

9.2 References

1. Lo, Baird and Hansen, Handbook of Solvent Extraction, Wiley, (1983).

2. P. A. Schwieitzer (ed.), Handbook of Separation Techniques for Chemical Engineers, McGraw Hill, (1974).

3. L. Alder, Liquid Liquid Extraction, Elsevier, (1975).

4. A.K. Bensalem, "Hydrodynamics and Mass Transfer in a Reciprocating Plate Extraction Column", DTC thesis, Swiss Federal Institute of Technology, Zirich, (1985).

5. A.J. Eckles, "Modeling of Ethanol Extraction in the Karr Reciprocating Plate Column", M.S. thesis, School of Chem. Eng., Georgia Institute of Technology, (1984).

6. L. D. Smoot and A. L. Babb, "Mass Transfer Studies in a Pulsed Extraction Column", I. & E. C. Fund., vol. 1, no. 2, (1962), pps. 93-103.

7. L. D. Smoot, B. W. Mar, and A. L. Babb, "Flooding Characteristics and Separation Efficiencies of Pulsed

Sieve-Plate Extraction Columns", Ind. Eng. Chem., vol. 51, no. 9, (1959), pps. 1005-1009.

8. B. W. Mar and L. A. Babb, "Longitudinal Mixing in a Pulsed Sieve-Plate Extraction Column", Ind. Eng. Chem., vol. 51, no. 9, (1959), pps. 1009-1018.

9. Richard H. Bell and Albert L. Babb, "Holdup and Axial Distribution of Holdup in a Pulsed Sieve-Plate Solvent Extraction Column", I. & E. C. Proc. Des. and Dev., vol. 8, no. 3, (1969), pps. 392-400.

10. Richard L. Bell, The Effect of Interfacial Tension on the Holdup of Pulsed Sieve-Plate Solvent Extraction Columns, Ph.D. thesis, University of Washington, Seattle, WA., (1964).

11. D. H. Logsdail and J. D. Thornton, "Mass Transfer in a Pulsed Plate Column", Trans. Instn. Chem. Eng., vol. 35, (1957), pps. 331-335.

12. H. L. Toor and J. M. Marchello, AIChE J., vol. 4, (1958), pps. 97-101.

13. E. Y. Kung and R. B. Beckman, "Dispersed-Phase Holdup in a Rotating Disk Extraction Column", AIChE J., vol. 7, no. 2, (1961), pps. 319-324.

14. Hiromichi Fumoto, Eric Zimmer, Ryohei Kiyose and Erich R. Merz, "A Study of Pulse Columns for Thorium Fuel Reprocessing", Nuclear Tech., vol. 58, (1982), pps. 447-464.

15. V. Kemanghorn, G. Murattet, and H. Angelino, "Study of Dispersion in a Pulsed Perforated-Plate Column", Proceedings of ISEC, The Canadian Inst. of Mining and Metallurgy, vol. 1, (1979); pg. 429.

16. V. Kemanghorn, J. Molinier, and H. Angelino, "Influence of Mass Transfer Direction on Efficiency of a PSE-Column", Chem. Eng. Sci., vol. 33, (1978), pg. 501.

17. S. D. Kim and M. H. I. Baird, "Axial Dispersion in a RPE-Column", Can. J. Chem. Eng., vol. 54, (1976), pg. 81.

18. Ibid, "Effect of Hole Size on Hydrodyamics of RPE-Columns", Can. J. Chem. Eng., vol. 54, (1976), p. 235.

19. A. N. Kolmogoroff, "Dissipation of Energy in the Locally Isotropic Turbulence", Comptes Rend. Acad. Sci., URSS, vol. 32, (1941), pg. 19.

20. I. Komasawa and H. Ingham, "Effect of System Properties on the Performance of Extraction Columns - Oldshue-Rushton Column", Chem. Eng. Sci., vol. 33, (1978), pg. 479.

21. W. J. Korchinski, R. Al-Husseini and C. H. Young, "Extraction Column Mass Transfer Parameters from Concentration Profiles", Proceedings of ISEC, Denver, (1983), pg. 106.

22. A. Kumar, "Hydrodynamics and Mass Trasfer Studies in a Khuni-Column", Ph.D. thesis in preparation at TCL, ETH-Zurich, (1985).

23. A. Kumar, D. K. Vohra, and S. Hartland, "Sedimentation of Droplet Dispersions in Counter-Current Spray Columns", Can. J. Chem. Eng., vol. 58, (1980), pg. 154.

24. S. Malanowski, "Experimental Methods for Vapor-Liquid Equilibrium, Part I. Circulation Methods.", Fluid Phase Equilibria, vol. 8, (1982), pps. 197-219.

25. C. Berro, M. Rogalski, and A. Peneloux, "A New Ebulliometric Technique", Fluid Phase Equilibria, vol. 8, (1981), pps. 55-73.

26. A.H.P.Skelland, private communication to W. Y. Tawfik, December, 1985.

27. D.S. Abrams and J.M. Prausnitz, AIChE J., vol. 21, (1975), pg. 116.

28. M.S. Peters and K.D. Timmerhaus, Plant Design and Economics for Chemical Engineers, 3rd Edition, McGraw Hill, (1980).

29. Process Simulation Program Version III by Simulation Sciences, Inc., (1984).

30. H. Groothius and F.J. Zuiderweg, "Coalescence Rates in a Continuous-Flow Dispersed Phase System", Chem. Eng. Sci., vol. 19, (1964), pg. 63.

31. W. J. Howarth, "Coalescence of Drops in a Turbulent Flow Field", Chem .Eng. Sci., vol. 19, (1964), pg. 33.

32. Robert E. Treybal, Liquid Extraction, 3rd Edition, (1982).

33. Andrew E. Karr, "Performance of a Reciprocating-Plate Column", AIChE J., vol. 15, no. 2, (1959), pps. 232-239.

34. Ernest J. Henley and J. D. Seader, Equilibrium Stage Separation Operations in Chemical Engineering, John Wiley

and Sons, Inc., New York, N.Y., (1981), pps. 516-522.

35. Edward S. Taylor, Dimensional Analysis for Engineers, Clarendon Press, Oxford, (1974).

36. A. H. P. Skelland and N. Chadha, "Selection of Dispersed Phase in Spray or Plate Extractions", Ind. Eng. Chem. Proc. Des. Dev., vol. 20, no. 2, (1981), pps. 232-239.

37. A. H. P. Skelland, Diffusional Mass Transfer, Wiley, Chpt. 7, (1980).

38. C. A. Plank, J. D. Olson, H. R. Null, O. L. Muthu, and B. D. Smith, Fluid Phase Equilibria, vol. 6, (1981), pps. 39-59.

39. M. M. Abbott and H. C. Van Ness, "An Extension of Barker's Method for Reduction of VLE Data", Fluid Phase Equilibria, vol. 1, (1977), pg. 3.

40. T. Ohta, J. Koyabu, and I. Naguata, Fluid Phase Equilibria, vol. 7, (1981), pps. 56-73.

41. Wilson,1964. VLE XI. "A New Expression for Excess Energy of Mixing", J. Am. Chem. Soc., vol. 86, (1964), pps. 127-130.

42. T. F. Anderson, and J. M. Prausnitz, Ind. Eng. Chem. Process Des. Dev., vol. 17, (1975), pps. 552-561.

43. M. Shoaei and D.W. Tedder, "Design Calculations for Multicomponent Distillation by and Improved Shortcut Method", Chem. Eng. R&D, (in press).

44. A.E. Karr and T.C. Lo, "Performance and Scale Up of Reciprocating Plate Extraction Column", Proc. of ISEC, Society of Chem. Ind., London, vol. 218, (1971).

45. D.W. Marquardt, "An Algorithm for Least Squares Estimation of Non-Linear Parameters", J. Soc. Ind. Appl. Math., vol. 11, no. 2, (1962), pg. 431.

46. T.C. Lo and A. E. Karr, "Development of a Laboratory Scale Reciprocating Plate Extraction Column", Ind. Eng. Chem. Proc. Des. Dev., vol. 11, no. 4, (1972).

CHAPTER 10

SEED PROCESS OPTIMIZATION STUDIES
(Wahid Y. Tawfik)

The Process Simulation Program (1) was developed by Simulation Sciences, Inc., in Fullerton, California, and is available on the ChE VAX system at the Georgia Institute of Technology. The Process Simulation Program is a comprehensive simulation system, combining the data resources of a large chemical component library and extensive thermodynamic properties prediction methods with advanced and flexible unit operations calculation techniques.

Preliminary studies using two solvent systems (Isopar-M and tridecyl alcohol) and three different feed concentrations (0.57, 1.90 and 5.15 wt % ethanol on the feed) were used to predict the energy requirement for the integrated process. Figure 2.2 summarizes the energy required to recover 99% of the ethanol in the feed with quality of 196-198 proof.

The process simulation program could not be used easily for optimization purposes. (For example, the theoretical stages cannot be treated as optimization variables in PROCESS.) However, it was valuable in testing the feasibility of the integrated process. The extraction column was simulated using a series of three-phase flash units, each representing a theoretical stage. The extractive distillation and the solvent regeneration unit were simulated as a series of two-phase flash units with the appropriate selection of the feed stages and the appropriate reboilers and condensers. The thermodynamic models used here were UNIFAC which was in the thermo library of the program and UNIQUAC with the experimental interaction parameters developed earlier by this study.

10.1 Optimization and Economic Analysis

The optimization program that was used in the study was RUNOPT, which was developed by D.W. Tedder (2) for multivariate optimization. This program is not as accurate as PROCESS, but it is much faster and oriented toward process synthesis and optimization of distillation processes. Further modification by Tedder, Tawfik and Poehlein (3) allowed the RUNOPT program to handle solvent extraction and extractive distillation units. Moreover, two thermodynamic algorithms (UNIFAC and UNIQUAC) were added for the VLE calculations of the extractive distillation and the solvent regeneration columns. The distribution coefficient models developed earlier by this study were used for the LLE calculations of the solvent extraction column. The HETS correlation developed by this work was used to size the extraction column, using Eqn. 9.18.

Theoretical stages for the solvent extraction column were estimated using the Kremser equation. The liquid/liquid equilibrium for the solvent extraction column was determined using the distribution coefficient correlation (Eqn. 6.4).

The calculation of the minimum theoretical trays for the extractive distillation and solvent regeneration columns used the Fenske equation:

$$(X_{it}/X_{ib})(X_{jb}/X_{jt}) = (\alpha_{ij}')^{Nm} \qquad (10.1)$$

where the subscripts b and t refer to the composition nodes of the bottom and top of a given section of the column. Theoretical trays were estimated using an extended Gilliland correlation developed by Shoaei and Tedder (4, 5). Actual trays were estimated using an efficiency correlation cited by Peters and Timmerhaus (6).

The UNIQUAC liquid activity coefficient model was used to calculate the K-values for the extractive distillation and the solvent regeneration columns. The interaction parameters for the UNIQUAC model are tabulated in Table 7.3.

RUNOPT as developed by D.W. Tedder is a modular sequential program. The overall process under optimization is set up using the node composition technique. Sequential types of calculations take place by assigning the composition of nodes in strategic locations. The SEED process was set up in this work in fourteen nodes as shown in Fig. 10.1 consisting of three main unit operation parts: solvent extraction, extractive distillation and vacuum distillation. The design equations used by RUNOPT are described in detail elsewhere (7).

Newton's Search Technique was used in this work to optimize nonlinear objective functions with linear constraints. The venture analysis could be justified in that maximizing the net profit would result in a zero rate of return of investment (ROI) at I_1 . When a minimum incremental ROI is specified at investment level I_2, a difference in capital investments (I_1 - I_2) is then available for alternative investments with greater-than-zero ROI. When the venture profit is maximized the venture cost is then minimized. The venture profit is given by:

$$VP = NP - i_m f(\underline{r},\underline{I}) \qquad (10.2)$$

The objective function in this work was taken as the venture cost, which is given by:

$$VC = C + gI - (C\text{-}eI_s\text{-}dI_D\text{-}II_L)t + i_m f(\underline{r},\underline{I}) \qquad (10.3)$$

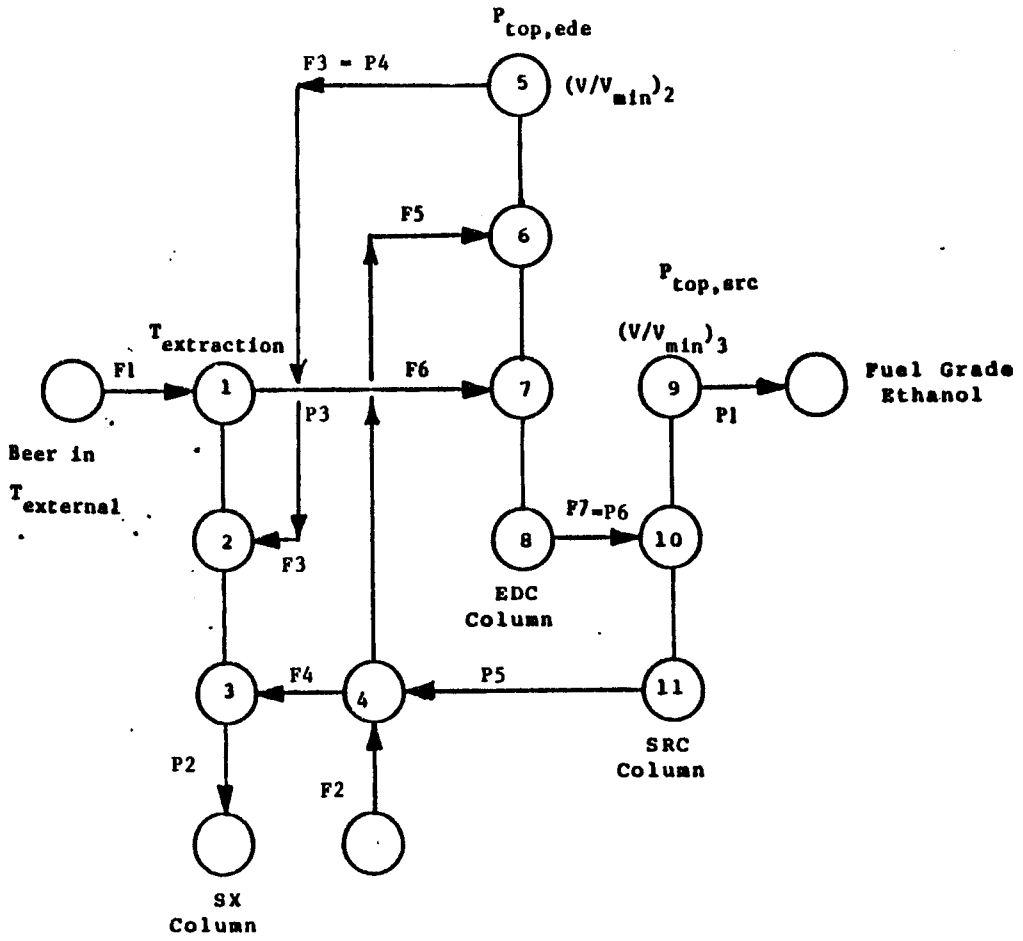

Fig. 10.1 Description Of The GIT Process Through Composition Node Model

where

i_m = Minimum rate of investment

$f(\underline{r},\underline{I})$ = Function of the risk and investment

I_s = Start-up costs

I_D = Depreciation costs

I_L = Land investment

I = total investment

g = Capital recovery, annuity or sinking fund based on the actual plant life

The following is a list of the linear constraints for the optimization of the integrated process.

$$T_{external} = 95°F$$

$$100°F \leq T_{extraction} \leq 160°F$$

$$2\ PSI \leq Press_{top\ EDC} \leq 14.7\ PSI$$

$$-0.9 \leq FVAP_{F5} \leq 1.0$$

$$-0.1 \leq FVAP_{F6} \leq 1.0$$

$$0.05 \leq F5/F4\ Ratio \leq 2.0$$

$$1.01 \leq (V/Vmin)_2 \leq 2.0$$

$$0.01 \leq P4/P1\ Ratio \leq 2.0$$

$$0.5\ PSI \leq Press_{top\ SRC} \leq 14.7\ PSI$$

$$-0.1 \leq FVAP_{F7} \leq 2.0$$

$$1.01 \leq (V/Vmin)_3 \leq 2.0$$

$$0.0 \leq \varphi_m \leq 1.0$$

$$0.01 \leq FEQ \leq 0.99$$

where:

$T_{external}$ = external temperature

$T_{extraction}$ = extraction column temperature

$Press_{top\ EDC}$ = pressure at top of extractive distillation column

$FVAP_{Fi}$ = fraction of vaporization of feed i

F5/F4 Ratio = feed 5 to feed 4 ratio

$(V/Vmin)_i$ = ratio of vapor rate to minimum vapor rate for the ith column

P4/P1 Ratio = product 4 to product 1 ratio

$Press_{top\ SRC}$ = pressure at top of solvent regeneration column

φ_m = volume fraction of the modifier

FEQ = fractional approach to equilibrium in LLE column

The upper and lower bounds of the previous constraints were based on the physical restrictions suggested by the experimental runs as well as the Process Simulation programs.

The blended solvent system (Isopar-M,tridecyl alcohol) was used here to demonstrate the optimization between two types of solvents. Since tridecyl alcohol is considered a recovery solvent, it has the advantage of higher distribution coefficients over the Isopar-M system. On the other hand, the Isopar-M solvent system has a much higher selectivity than the tridecyl alcohol system.

The optimization analysis indicated, however, that the optimum solvent blend would be achieved at 100% tridecyl alcohol. This result suggests that the effect of solvent loading is much more important than the effect of the relative volatility of water to ethanol in the extractive distillation column. Higher ethanol loading leads to smaller diameter extractive distillation columns and solvent regeneration columns. Moreover, the use of a recovery solvent leads to a smaller number of transfer units in the extraction column and, therefore, reduced height.

The economic analyses of the integrated process (Fig. 2.1) based on RUNOPT for five different ethanol concentrations in the feed (0.5, 2.0, 3.5, 5.0, 10 wt % ethanol in the feed) are summarized in Tables 10.1 through 10.10.

The resulting energy requirements to recover 99% of the ethanol in the feed with quality of 197 proof per gallon of the product were plotted against the percentage of ethanol in the feed in Fig. 10.2.

The cost of ethanol recovery using the solvent extraction process is plotted against the ethanol concentration in the feed in Fig. 10.3.

The economic analysis in this work was based on 100 million liters of ethanol per year, 7920 hours per year, M&S index of 781.7 and 99% recovery for comparison purposes.

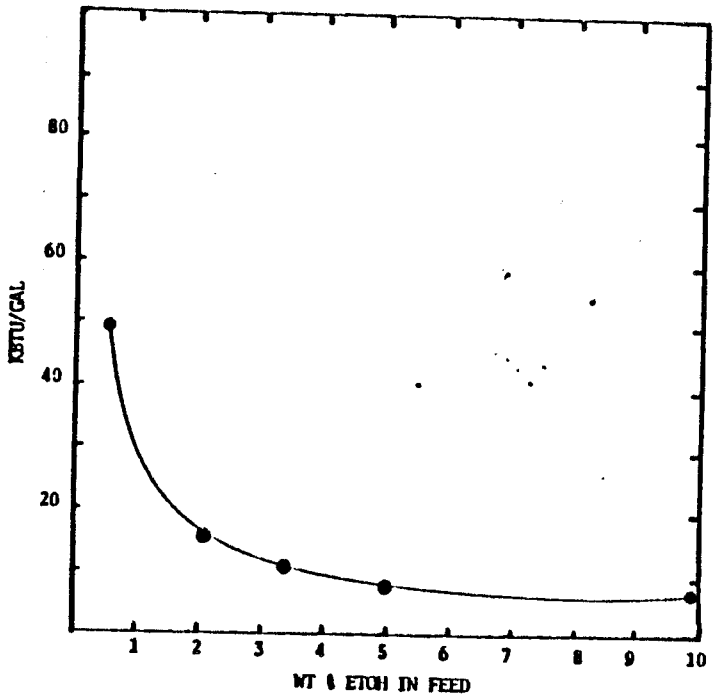

Figure 10.2 Energy Requirements for Ethanol Recovery based on RUNOPT

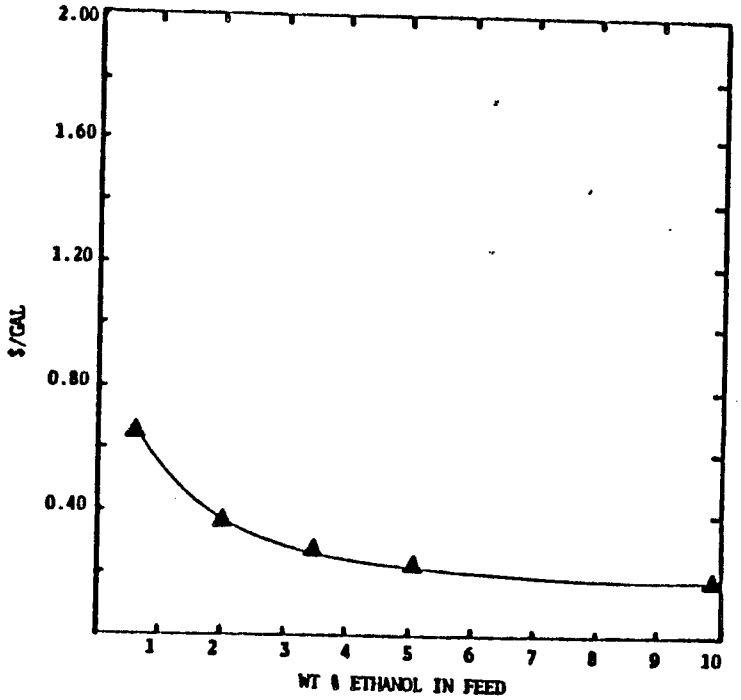

Fig. 10.3 Ethanol Production Cost Based on SEED Process

Table 10.1 Total Capital Investment for Ethanol Recovery ½% Case

Item	Module Cost ($1000)
Battery Limits Equipment	$ 6292.3
Offsite Costs	1258.5
Totals	7550.8
Contingency & Fees - 18%	1359.1
Total Installed Cost (TIC)	8909.9
Working Capital - 15% TIC	1336.5
Total Capital Investment (TCI)	$10246.4

Table 10.2 Manufacturing Costs for Ethanol Recovery - ½% Case
Basis: 100 million L Ethanol/yr ($1000) ($1000)

Fixed Costs		
TCI Finance Charge - 5 years at 12%		$ 2842.5
Taxes & Insurance - 5% of TIC		445.5
Maintenance - 5% of TIC		445.5
Subtotal		3733.5
Utilities		
Electricity ($0.06/kw-hr)		
Natural Gas ($6.47/million BTU)		
Water ($2.00/1000 gal)		
Subtotal		7106.9
Labor		
(2 workers/shift at $12/worker-hr)		630.7
Overhead		
(50% of Labor and Maintenance		450.4
Annual Manufacturing Cost:		$11921.5
$/L Ethanol:	0.12	
$/Gal. Ethanol:	0.45	
Ethanol Selling Price (30% ROI before taxes)		
$/L Ethanol:	0.16	
$/Gal. Ethanol	0.59	

Table 10.3 Total Capital Investment for Ethanol Recovery 2% Case

Item	Module Cost ($1000)
Battery Limits Equipment	$3912.1
Offsite Costs	782.4
Totals	4694.5
Contingency & Fees - 18%	845.0
Total Installed Cost (TIC)	5539.5
Working Capital - 15% TIC	830.9
Total Capital Investment (TCI)	$6370.4

Table 10.4 Manufacturing Costs for Ethanol Recovery - 2% Case
Basis: 100 million L Ethanol/yr ($1000) ($1000)

Fixed Costs		
TCI Finance Charge - 5 years @ 12%		$1767.2
Taxes & Insurance - 5% of TIC		276.9
Maintenance - 5% of TIC		276.9
Subtotal		2321.0
Utilities		
Electricity ($0.06/kw-hr)		
Natural Gas ($6.47/million BTU)		
Water ($2.00/1000 gal)		
Subtotal		3476.4
Labor		
(2 workers/shift at $12/worker-hr)		630.7
Overhead		
(50% of Labor and Maintenance)		450.1
Annual Manufacturing Cost:		$6878.2
$/L Ethanol:	0.069	
$/Gal Ethanol:	0.261	
Ethanol Selling Price (30% ROI before taxes)		
$/L Ethanol:	0.09	
$/Gal Ethanol:	0.34	

Table 10.5 Total Capital Investment for Ethanol Recovery 3.5% Case

	Module Cost ($1000)
Battery Limits Equipment	$3363.1
Offsite Costs	605.4
Totals	3968.5
Contingency & Fees - 18%	714.3
Total Installed Cost (TIC)	4682.8
Working Capital - 15% TIC	702.4
Total Capital Investment (TCI)	$5383.2

Table 10.6 Manufacturing Costs for Ethanol Recovery - 3.5% Case
Basis: 100 million L Ethanol/yr ($1000) ($1000)

Fixed Costs		
TCI Finance Charge - 5 years at 12%		$1493.9
Taxes & Insurance - 5% of TIC		234.1
Maintenance - 5% of TIC		234.1
Subtotal		1962.1
Utilities		
Electricity ($0.06/kw-hr)		
Natural Gas ($6.47/million BTU)		
Water ($2.00/1000 gal)		
Subtotal		2670.9
Labor		
(2 workers/shift at $12/worker-hr)		630.7
Overhead		
(50% of Labor and Maintenance)		450.4
Annual Manufacturing Cost:		$5714.1
$/L Ethanol:	0.057	
$/Gal. Ethanol:	0.22	
Ethanol Selling Price (30% ROI before taxes)		
$/L Ethanol:	0.07	
$/Gal. Ethanol:	0.28	

Table 10.7 Total Capital Investment for Ethanol Recovery 5% Case

	Module Case ($1000)
Battery Limits Equipment	$2497.1
Offsite Costs	495.8
Totals	2992.9
Contingency & Fees - 18%	538.7
Total Installed Cost (TIC)	3531.6
Working Capital - 15% TIC	529.7
Total Capital Investment (TIC)	$4061.3

Table 10.8 Manufacturing Costs for Ethanol Recovery - 5% Case
Basis: 100 million L Ethanol/yr ($1000) ($1000)

Fixed Costs		
TCI Finance Charge - 5 years at 12%		$1126.7
Taxes & Insurance - 5% of TIC		176.6
Maintenance - 5% of TIC		176.6
Subtotal		1479.9
Utilities		
Electricity ($0.06/kw-hr)		
Natural Gas ($6.47/million BTU)		
Water ($2.00/1000 gal)		
Subtotal		2497.1
Labor		
(2 workers/shift at $12/worker-hr)		630.7
Overhead		
(50% of Labor and Maintenance)		450.4
Annual Manufacturing Cost:		$5058.1
$/L Ethanol:	0.051	
$/Gal. Ethanol:	0.192	
Ethanol Selling Price (30% ROI before taxes)		
$/L Ethanol:	0.066	
$/Gal. Ethanol:	0.249	

Table 10.9 Total Capital Investment for Ethanol Recovery 10% Case

Item	Module Case ($1000)
Battery Limits Equipment	$1423.3
Offsite Costs	284.66
Totals	1707.96
Contingency & Fees - 18%	307.43
Total Installed Cost (TIC)	2015.39
Working Capital - 15% TIC	302.31
Total Capital Investment (TCI)	$2317.7

Table 10.10 Manufacturing Costs for Ethanol Recovery - 10% Case
Basis: 100 million L Ethanol/yr ($1000) ($1000)

Fixed Costs		
TCI Finance Charge - 5 years at 12%		$ 642.95
Taxes & Insurance - 5% of TIC		100.77
Maintenance - 5% of TIC		100.77
Subtotal		844.49
Utilities		
Electricity ($0.06/kw-hr)		
Natural Gas ($6.47/million BTU)		
Water ($2.00/1000 gal)		
Subtotal		1871.42
Labor		
(2 workers/shift at $12/worker-hr)		630.7
Overhead		
(50% of Labor and Maintenance)		450.4
Annual Manufacturing Cost:		$3797.01
$/L Ethanol:	0.038	
$/Gal. Ethanol:	0.14	
Ethanol Selling Price (30% ROI before taxes)		
$/L Ethanol:	0.05	
$/Gal Ethanol:	0.19	

This optimization explicitly considered the economic effects of solvent selectivity versus that of solvent loading. Since solvents with higher loadings exhibit lower selectivities, these two factors are in competition with each other. It was learned that selectivity is less important for the SEED process than is solvent capacity in reducing costs. That is, the cost of removing more water in the EDC column is less than the cost of recirculating larger solvent rates throughout the system. The RUNOPT model went to an optimal solvent blend consisting of 100 vol% tridecyl alcohol. Therefore, future studies should focus on the use of modifiers with even larger capacities and lower selectivities than tridecyl alcohol (e.g. tridecyl acetate or diols).

10.2 References

1. Process Simulation Program Version III by Simulation Sciences, Inc., (1984).

2. D.W. Tedder, "The Heuristic Synthesis and Topology of Optimal Distillation Networks", Ph.D. Thesis, Chemical Engineering, University of Wisconsin, Madison, Wisconsin, (1975).

3. D.W. Tedder, Y. W. Tawfik, and S.R. Poehlein, "Ethanol Recovery from Low Grade Fermentates by Solvent Extraction and Extractive Distillation: The SEED Process", Fourth Symp. ofSeparation Science, (1985).

4. M. Shoaei and D.W. Tedder, "Design Calculations for Multicomponent Distillation by and Improved Shortcut Method", Chem. Eng. R&D, (in press).

5. M. Shoaei, "An Improved Method for Design Calculations in a Multicomponent Distillation Column", M.S. Thesis, School of Chemical Engineering, Georgia Institute o Technology, Atlanta, Georgia, (1983).

6. M.S. Peters and K.D. Timmerhaus, Plant Design and Economics for Chemical Engineers, 3rd Edition, McGraw Hill, (1980).

7. D.W. Tedder, Chemical Process Synthesis, Design and Optimization, A ChE Course Notes, Georgia Institute of Technology, (1985).

A P P E N D I X A

VLE Data

P : Vapor pressure , mm Hg
T : Temperature , K
Y_i: Mole fraction of component i in the vapor phase
X_i: mole fraction of component i in the liquid phase

Table A1 Experimental Ethanol Vapor Pressures

T(C)	P(mm Hg)
25.0	59.20
30.0	78.62
50.0	221.30
70.0	542.30

Table A2 Experimental Tridecyl Alcohol Vapor Pressures

T(C)	P(mm Hg)
192.5	92.5
196.5	121.5
210.5	200.0
214.5	247.5
223.5	317.5
235.5	457.7
239.5	496.5
251.6	736.5

Table A3 Experimental Diisopropyl Ketone Vapor Pressures

T(C)	P(mm Hg)
104.0	158.0
122.8	286.9
132.0	410.6
138.5	505.9
155.5	742.9
167.5	760.0

Table A4 Experimental Isopar-M Initial Boiling Point Vapor Pressure

T(C)	P(mm Hg)
121.0	40.7
158.6	134.3
175.4	208.3
187.2	280.3
200.7	391.4

Table A5 Experimental Tri-n-butyl Phosphate Vapor Pressures

T(C)	P(mm Hg)
182.0	44.5
189.0	61.6
233.0	165.4
257.2	391.4

Table A6 Experimental Vapor Pressure Data for Methyl Ester, CE-1218

T(C)	P(mm Hg)
132.8	125.2
144.8	167.5
170.3	310.0
212.8	450.0
224.8	535.5
255.8	740.0

Table A7 Experimental 2-ethylhexanol Vapor Pressures

T(C)	P(mm Hg)
150.2	270.0
159.5	371.1
169.2	501.2
172.2	543.7
182.2	740.2

Table A8 Experimental Tridecyl Acetate Vapor Pressures

T(C)	P(mm Hg)
210.7	190.1
223.8	272.1
242.8	447.1
259.3	739.1

Table A9 Isoboric Ethanol Water VLE at 380 MM Hg

T(C)	X_1	X_2	Y_1	Y_2
81.15	0.0037	0.9963	0.0290	0.9710
69.65	0.0959	0.9041	0.4440	0.5560
68.75	0.0976	0.9024	0.4655	0.6345
64.25	0.3086	0.6914	0.6211	0.3789
64.05	0.4145	0.5855	0.6674	0.3326
63.65	0.6041	0.3959	0.6889	0.3111
61.05	0.6550	0.3450	0.7200	0.2800
63.05	0.9411	0.0589	0.9599	0.0401

Table A10 Isobaric Ethanol TDOH VLE at 380 mm Hg

T(C)	X_1	X_2	Y_1	Y_2
179.35	0.2528	0.7472	0.7211	0.2789
110.85	0.2500	0.7500	0.9184	0.0816
80.25	0.4570	0.6430	0.9351	0.0649
60.65	0.6420	0.3580	0.9452	0.0548
59.85	0.8098	0.1902	0.9487	0.0513
59.65	0.8754	0.1246	0.9558	0.0442
59.55	0.5404	0.4596	0.9386	0.0614

Table A11 Isobaric Ethanol Isopar-M VLE at 380 mm Hg

T(C)	X_1	X_2	Y_1	Y_2
168.0	0.0081	0.9919	0.5810	0.4190
134.0	0.0227	0.9773	0.7999	0.2001
93.0	0.0429	0.9571	0.9431	0.0569
66.7	0.0643	0.9357	0.9680	0.0320
63.0	0.4539	0.5461	0.9928	0.0072
61.1	0.7217	0.2783	0.9855	0.0145
61.9	0.7805	0.2195	0.9885	0.0115
60.3	0.8265	0.1735	0.9850	0.0150
63.5	0.8313	0.1687	0.9872	0.0128
60.0	0.8687	0.1313	0.9866	0.0134
62.0	0.9128	0.0872	0.9954	0.0046
62.1	0.9884	0.0116	0.9970	0.0030
61.7	0.9992	0.0008	0.9992	0.0008

Table A12 Isobaric Isopar-M TDOH VLE at 188 mm Hg

T(C)	X_1	X_2	Y_1	Y_2
177.1	0.1529	0.8471	0.5672	0.4328
168.2	0.4416	0.5584	0.7302	0.2698
164.7	0.3753	0.6247	0.7423	0.2577
163.2	0.5076	0.4924	0.7663	0.2337
160.9	0.4702	0.5298	0.8012	0.1988
158.5	0.4722	0.5278	0.7829	0.2171
155.8	0.5839	0.4161	0.8012	0.1988
152.0	0.6689	0.3311	0.8103	0.1897
151.1	0.6879	0.3121	0.8338	0.1662
149.0	0.8275	0.1725	0.8356	0.1644

APPENDIX B

LLE Data

X_{ei} : Initial wt. fraction of ethanol in aqueous solution

X_e : Weight fraction of ethanol in equilibrated aqueous phase

X_D : Weight fraction of dextrose in equilibrated aqueous phase

D_i : Distribution coefficient of component i in wt. basis

Y_i : weight fraction of component i in equilibrated organic phase

Table B1 The Measured Ethanol and Water Distribution Coefficients using 2-Ethyl Hexanol as a Solvent

X_{ei} [a]	X_e [b]	T [c]	D_e	D_w
0.34	0.06	85	0.85	0.042
0.42	0.07	85	0.99	0.052
0.34	0.07	60	0.81	0.041
0.42	0.08	60	0.88	0.047
0.09	0.02	23	0.49	0.025
0.34	0.09	23	0.57	0.030
0.42	0.13	23	0.71	0.032
0.58	0.28	23	0.77	0.092
0.77	0.45	23	1.02	0.500

a Xei is weight fractions

b Xe is weight fraction

c T in ^{o}C

Table B2 The Measured Ethanol and Water Distribution Coefficient Using Isopar-L as a Solvent

X_{ei} [a]	X_e [b]	T [c]	D_e	D_w
0.69	0.67	20	0.017	0.0008
0.78	0.77	20	0.019	0.001
0.88	0.86	20	0.039	0.004
0.46	0.435	25	0.019	0.000[illegible]
0.88	0.86	25	[illegible].035	0.004
0.69	0.635	60	0.039	0.006
0.46	0.41	66	0.042	0.0006
0.88	0.83	66	0.071	[illegible].005
0.46	0.36	85	0.062	0.0006
0.69	0.[illegible]9	85	0.061	0.0036
0.88	0.5[illegible]	85	0.099	0.0039

[a] Xei is weight fractions

[b] Xe is weight fractions

[c] T in ^{o}C

Table B3 The Measured Ethanol and Water Distribution Coefficients Using Dimethyl Heptanone as a Solvent

X_{ei} [a]	X_e [b]	T [c]	D_e	D_w
0.24	0.11	25	0.21	0.0081
0.29	0.12	25	0.24	0.009
0.34	0.14	25	0.25	0.009
0.42	0.15	25	0.29	0.01
0.50	0.31	30	0.35	0.03
0.24	0.06	70	0.46	0.011
0.29	0.10	70	0.79	0.03
0.09	0.01	80	1.3	0.036
0.5	0.1 0	80	1.6	0.042

[a] X_{ei} is weight fraction

[b] X_e is weight fraction

[c] T in ^oC

Table B4 The Measured Ethanol and Water Distribution Coefficients using 20% Tridecyl Alcohol in Norpar-12

X_{ei} [a]	X_e [b]	T [c]	D_e	D_w
0.017	0.11	24	0.12	0.0071
0.34	0.21	24	0.16	0.0096
0.58	0.26	24	0.25	0.0164
0.17	0.04	70	0.34	0.0119
0.34	0.11	70	0.38	0.0162
0.58	0.18	70	0.49	0.0211

[a] Xei is weight fraction

[b] Xe is weight fraction

[c] T in ^{o}C

Table B5

The Experimental values of ethanol and water distribution coefficients for TDOH/Isopar M system in presence of dextrose

D_e[a]	D_w[a]	x_e[b]	x_D[b]	ϕ_T[c]	100/T
0.089	0.0016	0.072	0.205	0.1	0.342
0.061	0.0018	0.198	0.215	0.1	0.342
0.082	0.0034	0.354	0.212	0.1	0.342
0.781	0.0174	0.031	0.217	0.4	0.342
0.567	0.0183	0.098	0.234	0.4	0.342
0.648	0.0312	0.217	0.231	0.4	0.342
0.270	0.006	0.029	0.201	0.2	0.332
0.180	0.0052	0.105	0.226	0.2	0.332
0.210	0.0097	0.218	0.261	0.2	0.332
0.208	0.0029	0.032	0.214	0.1	0.291
0.21	0.0039	0.105	0.245	0.1	0.291
0.32	0.0058	0.195	0.240	0.1	0.291
0.378	0.0019	0.0091	0.491	0.1	0.291
0.188	0.0056	0.053	0.424	0.1	0.291
0.321	0.0088	0.146	0.474	0.1	0.291
1.98	0.031	0.003	0.225	0.4	0.291
0.97	0.058	0.032	0.244	0.4	0.291
1.54	0.062	0.141	0.235	0.4	0.291

[a] Weight fraction ratio

[b] Weight fraction

[c] Volume fraction before mixing with diluent

Table B6

The experimental values of ethanol and water distribution coefficients for TBP/Isopar M system in presence of dextrose

D_e	D_w	X_e	X_D	ϕ_T	100/T
0.0791	0.0018	0.051	0.195	0.05	0.332
0.0442	0.0016	0.194	0.182	0.05	0.332
0.0524	0.0039	0.330	0.21	0.05	0.332
0.103	0.0023	0.0386	0.357	0.05	0.332
0.089	0.0031	0.1110	0.411	0.05	0.332
0.0982	0.0044	0.2153	0.396	0.05	0.332
0.1079	0.0048	0.206	0.421	0.05	0.332
0.175	0.0059	0.079	0.442	0.05	0.292
0.210	0.0022	0.158	0.474	0.05	0.292
0.314	0.0013	0.022	0.441	0.05	0.292
0.685	0.0202	0.0196	0.216	0.5	0.332
0.470	0.0224	0.085	0.225	0.5	0.332
0.505	0.0351	0.178	0.276	0.5	0.332
1.591	0.0236	0.0054	0.400	0.5	0.332
0.52	0.021	0.059	0.449	0.5	0.332
0.923	0.0409	0.1011	0.424	0.5	0.332
0.665	0.029	0.0932	0.503	0.5	0.332
0.264	0.0059	0.0329	0.203	0.2	0.332
0.153	0.00522	0.127	0.202	0.2	0.332
0.179	0.0102	0.236	0.245	0.2	0.332
0.374	0.00644	0.024	0.366	0.2	0.332
0.290	0.0067	0.0766	0.4301	0.2	0.332
0.251	0.0096	0.205	0.232	0.2	0.3332
0.291	0.0103	0.128	0.473	0.2	0.332
3.23	0.0222	0.0021	0.478	0.5	0.292
1.45	0.028	0.0168	0.519	0.5	0.292
1.868	0.039	0.0289	0.604	0.5	0.292

Table B7

The experimental values of ethanol and water distribution coefficents for Methyl ester system in presence of dextrose

D_e	D_w	X_e	X_D	100/T
0.1055	0.0024	0.07	0.0	0.3413
0.1075	0.0025	0.117	0.0	0.3413
0.2223	0.0034	0.147	0.0	0.3413
0.1663	0.0037	0.278	0.0	0.3413
0.1416	0.0049	0.30	0.0	0.3413
0.145	0.0023	0.062	0.0519	0.3413
0.164	0.0029	0.099	0.0536	0.3413
0,.2358	0.0041	0.1365	0.0593	0.3413
0.1944	0.0049	0.2119	0.063	0.3413
0.1345	0.0049	0.279	0.062	0.3413
0.1597	0.002	0.0828	0.2118	0.3413
0.175	0.0033	0.1401	0.2215	0.3413
0.169	0.0047	0.1997	0.233	0.3413
0.1001	0.0048	0.2681	0.233	0.3413
0.3118	0.00145	0.045	0.0	0.2915
0.5088	0.0023	0.087	0.0	0.2915
0.5529	0.0035	0.133	0.0	0.2915
0.1825	0.004	0.225	0.0	0.2915
0.339	0.0029	0.043	0.0534	0.2915
0.2128	0.0029	0.089	0.054	0.2915
0.273	0.0037	0.126	0.0667	0.2915
0.34	0.0038	0.154	0.0667	0.2915
0.248	0.0039	0.209	0.0669	0.2915
0.2754	0.0037	0.065	0.2164	0.2915
0.4045	0.0045	0.0919	0.2344	0.2915
0.265	0.0047	0.1629	0.2422	0.2915
0.677	0.0059	0.1035	0.276	0.2915

Table B8 Mutual Solubility Data for Ethanol/water/2-ethyl-hexanol System

X_e	X_w	X_s	Y_e	Y_w	Y_s	T
0.024	0.9755	0.005	0.0169	0.0261	0.9570	293
0.050	0.9490	0.001	0.0350	0.0280	0.9370	293
0.097	0.9000	0.003	0.0520	0.0295	0.9185	293
0.232	0.7600	0.008	0.1660	0.0516	0.7824	293
0.283	0.7060	0.011	0.2170	0.0652	0.7178	293
0.408	0.4990	0.093	0.4140	0.2710	0.3150	293
0.053	0.9450	0.002	0.0480	0.0290	0.9230	343
0.060	0.9350	0.005	0.0510	0.0390	0.9100	343
0.067	0.9230	0.010	0.0610	0.0440	0.8950	343
0.072	0.9080	0.020	0.0710	0.0490	0.880	343
0.205	0.7350	0.060	0.1950	0.1410	0.6640	343

* X_i, Y_i are mass fractions.

Table B9

Mutual solubility data for
Ethanol/Water/Isopar M system at 298°K

* X_e	X_w	X_s	Y_e	Y_w	Y_s
0.320	0.6798	0.0002	0.0093	0.0004	0.9903
0.435	0.5645	0.0005	0.0113	0.0009	0.9878
0.664	0.331	0.005	0.0130	0.0010	0.9850
0.775	0.204	0.021	0.0208	0.0011	0.9781
0.787	0.1854	0.0276	0.0252	0.0012	0.9736
0.830	0.115	0.055	0.0341	0.0013	0.9646

*x_i, y_i are mass fractions

Table B10

Mutual solubility data for
Ethanol/water/Methyl Ester System

* X_e	X_w	X_s	Y_e	Y_w	Y_s	T
0.070	0.9292	0.0008	0.0073	0.0017	0.991	294
0.1170	0.8811	0.0009	0.0120	0.0018	0.9862	294
0.147	0.8517	0.0013	0.0216	0.0023	0.9761	294
0.276	0.721	0.003	0.0297	0.0026	0.9677	294
0.310	0.6885	0.005	0.0425	0.0034	0.9541	294
0.045	0.9542	0.0008	0.0145	0.0012	0.9843	338
0.095	0.9045	0.0015	0.0189	0.0014	0.9797	338
0.136	0.8620	0.002	0.0417	0.0021	0.9562	338
0.220	0.7760	0.004	0.0437	0.0028	0.9535	338
0.233	0.762	0.005	0.0635	0.0031	0.9334	338

* X_i, Y_i are mass fractions

A P P E N D I X C

Reciprocating Plate Extraction Column Data

Table C1 Data on 1" Reciprocating Plate Extraction Column

Run No.	Reciprocation Speed, cm/sec	Feed Rates, cc/min.		Conc. of Solute, wt% in the Aq. Phase		HETS, cm
		Org.	Aq.	in	out	
1	4.0	92.0	6.2	50.94	25.92	133.3
2	4.0	89.2	6.2	50.94	25.43	131.4
3	4.1	102.5	6.2	50.94	24.21	128.5
4	4.8	84.3	6.2	52.71	16.19	88.5
5	4.2	92.8	5.8	50.60	23.54	125.0
6	4.3	82.8	5.7	50.70	20.76	111.8
7	4.1	70.3	5.7	48.90	23.21	127.6
8	4.0	74.7	5.7	48.90	24.41	133.3
9	4.1	101.4	5.8	48.90	23.41	129.5
10	4.4	132.3	5.8	49.78	18.52	104.0
11	4.8	115.5	5.8	50.55	16.45	89.1
12	4.5	133.5	5.8	50.55	17.63	96.3
13	5.0	105.6	5.8	50.84	16.02	82.2
14	4.3	98.5	5.8	50.84	24.06	128.6
15	4.6	99.2	5.8	50.84	17.51	96.7
16	4.5	99.6	5.8	50.84	18.98	104.0
17	4.5	93.9	5.8	50.84	19.21	101.6
18	4.5	122.3	2.2	50.39	19.03	100.6
19	4.5	121.8	2.2	50.56	19.62	105.9
20	8.3	111.3	2.2	50.41	11.04	13.36
21	7.9	130.4	2.2	50.08	11.81	13.33
22	7.5	130.8	1.9	50.66	10.71	29.5

1" spacing between plate
Temperature range: $45<T<74^{\circ}C$

Solute : Ethanol
Solvent: Isopar-M

Table C2 Data on 3' Reciprocating Plate Extraction Column

Agitator Speed, SPM	Feed Rates, GPM		Conc. of Solute, wt%				HETS
	Organic	Aqueous	Org. in	Org. out	Aq. in	Aq. out	inches
197	47.5	3.58	0.04	1.54	26.81	10.19	26.5
186	47.6	3.58	0.309	1.529	25.93	13.11	20.45
150	47.0	3.58	0.257	1.823	29.49	12.287	22.86
121	47.0	3.58	0.395	1.722	28.5	14.424	28.44
182	47.0	3.58	0.329	1.810	29.43	13.835	27.43

Xylene-acetic acid-Water system (water dispersed-Xylene extraction)
Karr & Lo, 1976

Table C3 Data on 1" Reciprocating Plate Extraction Column

Agitator Speed	Feed Rates, GPH/ft^2 hr		Conc. of Solute, wt%				HETS
	Org	Aq.	Org. in	Org. out	Aq. in	Aq. out	in.
360	249.0	323.0	0	14.545	18.705	5.715	3.1
345	249.0	323.0	0	14.295	18.75	5.43	3.3
320	249	323.0	0	14.32	18.735	5.80	3.5
401	456.5	456.5	0	12.15	17.05	2.91	2.8
393	446.0	479.0	0	12.53	17.04	4.01	3.1
312	446.0	482.0	0	12.46	17.5	5.58	4.4
322	446.0	482.0	0	11.67	15.78	4.64	3.3
311	674	761	0	11.335	15.59	5.95	5.2

MIBK-Acatic acid-Water system (water dispersed-MIBK extraction)
Karr & Lo, 1972

Document Control Page	1. SERI Report No. SERI/STR-321-3126	2. NTIS Accession No.	3. Recipient's Accession No.

4. Title and Subtitle
Fuel Grade Ethanol by Solvent Extraction, Final Subcontract Report

5. Publication Date
June 1987

6.

7. Author(s)
D. W. Tedder

8. Performing Organization Rept. No.

9. Performing Organization Name and Address
Georgia Institute of Technology
Chemical Process Design Institute
School of Chemical Engineering
Atlanta, GA 30332-0100

10. Project/Task/Work Unit No.
5260.10

11. Contract (C) or Grant (G) No.
(C) XX-4-04076-01
(G)

12. Sponsoring Organization Name and Address
Solar Energy Research Institute
A Division of Midwest Research Institute
1617 Cole Boulevard
Golden, CO 8040103393

13. Type of Report & Period Covered
Technical Report

14.

15. Supplementary Notes
Technical Monitor: John Wright

16. Abstract (Limit: 200 words)

This report summarizes final results for ethanol recovery by solvent extraction and extractive distillation (SEED), discusses the comparative economics of the two processes, and summarizes the economic analyses for the combined process. Although the use of the SEED process for the recovery of ethanol enhances the economics of gasohol production using fermentation, the benefits are not yet sufficient for entry into the current market. The process was found to be technically feasible.

17. Document Analysis

a. Descriptors Feasibility studies, ethanol, ethanol fuels, solvent extraction, distillation, gasohol

b. Identifiers/Open-Ended Terms

c. UC Categories

18. Availability Statement
National Technical Information Service
U.S. Department of Commerce
5285 Port Royal Road
Springfield, Virginia 22161

19. No. of Pages
158

20. Price
A08

Form No. 0069 (3-25-82)